HIGH PERFORMANCE PLANAR POWER DIVIDERS AND RING RESONATORS

KUNNTHPHONG SRISATHIT

A THESIS SUBMITTED IN PARTIAL FULFILLMENT
OF THE REQUIREMENTS FOR THE DEGREE OF
DOCTOR OF ENGINEERING IN ELECTRICAL ENGINEERING
FACULTY OF ENGINEERING
KING MONGKUT'S INSTITUTE OF TECHNOLOGY LADKRABANG
2012

KMITL-2012-EN-D-018-10

หัวข้อวิทยานิพนธ์	ตัวแบ่งกำลังงานและรีโซเนเตอร์วงแหวนโครงสร้างระนาบที่ให้สมรรถนะสูง
นักศึกษา	นายกันต์พงษ์ ศรีสถิตย์
รหัสประจำตัว	49060021
ปริญญา	วิศวกรรมศาสตรดุษฎีบัณฑิต
สาขาวิชา	วิศวกรรมไฟฟ้า
พ.ศ.	2555
อาจารย์ที่ปรึกษาวิทยานิพนธ์	ศาสตราจารย์ ดร. วัลลภ สุระกำพลธร
อาจารย์ที่ปรึกษาวิทยานิพนธ์ร่วม	ศาสตราจารย์ ดร. อภิศักดิ์ วรพิเชฐ

บทคัดย่อ

การเติบโตอย่างมากของตลาดไร้สายได้กระตุ้นความสนใจอย่างเป็นประวัติการณ์ทางด้านสมรรถนะของอุปกรณ์ ให้เหมาะกับราคาและขนาดทางกายภาพที่เล็กลง อุปกรณ์พาสซีฟ อาทิเช่น ตัวแบ่ง/รวมกำลังงานและวงจรกรอง จัดเป็นอุปกรณ์ที่มีศักยภาพในการปรับปรุงสมรรถนะของวงจรและระบบสื่อสารได้ อุปกรณ์พาสซีฟเหล่านี้ ล้วนเป็นอุปกรณ์พื้นฐานทางด้านความถี่วิทยุ/ไมโครเวฟ ที่มักใช้ในเครื่องส่งและเครื่องรับ การปรับปรุงสมรรถนะของอุปกรณ์พาสซีฟวิธีการหนึ่ง คือ การกำจัดผลตอบสนองแบบซ้ำคาบที่เกิดขึ้นจากการใช้สายส่งเป็นส่วนประกอบ

วิทยานิพนธ์นี้ เน้นการออกแบบและวิเคราะห์อุปกรณ์พาสซีฟดังกล่าว โดยแบ่งการนำเสนอออกเป็นสามหัวข้อหลัก ประกอบด้วย ตัวแบ่งกำลังงาน วงจรกรองผ่านแถบวงแหวนแบบสองโหมดและแบบสามโหมด ตัวแบ่งกำลังงานที่มีเฟสเดียวกันและเฟสต่างกัน 90 องศา จัดเป็นตัวแบ่งกำลังงานพื้นฐานที่มีการใช้งานกันอย่างแพร่หลายในวงจรความถี่วิทยุ/ไมโครเวฟ ในหัวข้อแรกนี้จะเป็นการศึกษาสายส่งรูปตัวทีเพื่อนำไปใช้กับตัวแบ่งกำลังงานโครงสร้างพื้นฐาน การที่สตับปลายเปิดซึ่งเป็นส่วนหนึ่งของสายส่งรูปตัวทีประพฤติตัวเสมือนวงจรรีโซแนนซ์อนุกรมนั้น จะสามารถกำจัดความถี่ที่ไม่ต้องการได้อย่างสมบูรณ์

หัวข้อที่สองจะเป็นการนำเสนอสองแนวทางการออกแบบการรบกวนโหมด เพื่อใช้กับรีโซเนเตอร์วงแหวนโครงสร้างที่มีสตับต่ออนุกรม อย่างไรก็ดี ความต้องการสตับซึ่งมีอิมพีแดนซ์คุณลักษณะต่ำหรือสูงมากเพื่อการออกแบบเฉพาะงาน ได้ทำให้สตับมีขนาดที่กว้างมากหรือแคบมาก ความไม่ต่อเนื่องซึ่งเกิดขึ้น ณ รอยต่อระหว่างวงแหวนกับสตับหรือการเชื่อมต่อที่บริเวณรอยต่อได้ส่งผลกระทบต่อความถี่ศูนย์กลางของวงแหวน การรบกวนโหมดโครงสร้างใหม่ซึ่งอยู่ในรูปสายส่งโครงสร้างขวามือและซ้ายมือภายใต้อัตราส่วนอิมพีแดนซ์ที่เหมาะสมได้ถูกนำเสนอเพื่อหลีกเลี่ยงปัญหาที่เกิดขึ้นดังกล่าวโดยให้สามารถสร้างขึ้นได้จริงในทางปฏิบัติ ดังนั้น ความด้อยสมรรถนะของวงจรกรองที่เป็นผลมาจากความไม่ต่อเนื่อง ณ บริเวณรอยต่อจะสามารถละเลยได้

ส่วนหัวข้อสุดท้ายในวิทยานิพนธ์นี้ จะนำเสนอเกี่ยวกับรีโซเนเตอร์วงแหวนไมโครสตริปแบบสามโหมด เพื่อนำไปออกแบบเป็นวงจรกรองผ่านแถบความถี่กว้าง โครงสร้างรีโซเนเตอร์ที่นำเสนอเป็นการดัดแปลงรีโซเนเตอร์วงแหวนโครงสร้างพื้นฐานแบบโหมดเดี่ยว การแทนตัวเชื่อมต่อปลายเปิด 1 คู่ที่ต่อใช้งานร่วมกับสตับปลายเปิด เข้าไปแทนสายส่งหนึ่งในรีโซเนเตอร์โครงสร้างพื้นฐานจะทำให้ได้รีโซเนเตอร์แบบสามโหมด เนื่องจากรีโซเนเตอร์ที่นำเสนอเกิดรีโซแนนซ์ขึ้นสามตำแหน่ง กล่าวคือ

เกิดขึ้น ณ ความถี่ศูนย์กลาง 1 ตำแหน่งและเกิดขึ้นอีก 2 ตำแหน่งใกล้ๆ ขอบผลตอบสนองของแถบผ่าน เมื่อนำไปสร้างวงจรกรองผ่านแถบจะทำให้ช่วงแถบผ่านมีผลตอบสนองที่ราบเรียบ การที่รีโซเนเตอร์ที่นำเสนอให้โพลลดทอนใกล้ขอบแถบผ่านนั้น ทำให้ได้วงจรกรองผ่านแถบที่มีความชันสูงมาก นอกจากนี้ การที่สัญญาณซึ่งป้อนให้กับวงจรกรองทางอินพุตถูกบังคับให้สัญญาณส่วนใหญ่ในช่วงแถบผ่านเดินทางในสายส่ง ดังนั้น การสูญเสียที่เกิดขึ้นในตัวเชื่อมต่อจึงมีค่าต่ำสุด นั่นเอง การวิเคราะห์รีโซเนแตอร์วงแหวนแบบสามโหมดในเชิงทฤษฎี พร้อมทั้งตัวอย่างการออกแบบวงจรกรองวงแหวนผ่านแถบต้นแบบได้ถูกนำเสนอ โดยผลลัพธ์ที่ได้จากการจำลองสมรรถนะและผลการวัดวงจรกรองต้นแบบมีความสอดคล้องกับผลการทำนายทางทฤษฎีเป็นอย่างดี ส่วนสมรรถนะนอกช่วงแถบผ่านของวงจรกรองโดยเฉพาะโครงสร้างที่ต่อเรียงกันสามารถปรับปรุงได้ ด้วยการใช้เทคนิคการกดแบบหลายความถี่

Thesis Title	High Performance Planar Power Dividers and Ring Resonators
Student	Mr. Kunnthphong Srisathit
Student ID.	49060021
Degree	Doctor of Engineering
Program	Electrical Engineering
Year	2012
Thesis Advisor	Prof. Dr. Wanlop Surakampontorn
Thesis Co-Advisor	Prof. Dr. Apisak Worapishet

ABSTRACT

The tremendous growth of the wireless market has spurred unprecedented interest in the performance of RF devices with affordable cost and small physical size. Passive devices such as power dividers/combiners and filters have potential to enhance the performance of the communication circuits and systems. These devices are key RF/microwave building blocks and they are usually employed in transmitters and receivers. One approach to improving performances of the devices, as well as the other passive devices, is to reject the periodic response associated with the transmission line in the structure.

This work focuses on the design and analysis of such passive devices. There are three main topics which are investigated including power dividers and dual-mode and triple-mode ring bandpass filters. Among various power dividers, the *in-phase* and *quadrature-phase* are the most fundamental components in RF/microwave circuit and are employed extensively in a variety of applications. In particular, the investigation of the first topic is based on the conventional structure of power divider with the use of an equivalent T-shaped transmission line. Since the open-ended stub associated with T-shaped line behaves like a series resonance, the complete rejection of unwanted frequency can be obtained.

The second topic is an investigation of two possible designs of ring's perturbation in series stub configuration to achieve dual-mode response. However, when the small or high characteristic impedance is required for specification design, the width of its perturbation is too wide or too narrow.

The discontinuity at the junction between the ring and its perturbation can affect the center frequency of the ring. To avoid this problem, whether due to the physical dimension or the associated coupling at discontinuities of the ring and its perturbation, the new perturbation in the forms of the symmetrical *right-* and *left-*handed transmission lines under the proper impedance ratios has been proposed for a physically realizable perturbation where the performance degradation of the filter induced by step discontinuity is neglected.

The last topic described in this dissertation is a triple-mode microstrip ring resonator core for the design of wideband bandpass filters. It is a modification of the conventional single-mode ring resonator with a pair of open-ended coupled lines and a shunt open stub for a transmission-line path of the ring substituted to form a triple-mode resonator. Since the triple-mode resonator possesses three resonances, one at the center frequency and the other two near the edges of the passband, a flat passband response can be achieved when it is employed to implement a bandpass filter. The resonator also exhibits attenuation poles close to the edges of the passband, thereby offering sharp rejection in the bandpass filter response. Moreover, since the signal applied at the input port is effectively forced to travel mainly through the transmission line path over the passband frequency, the loss incurred by the coupled lines is minimized. Extensive theoretical analysis of the triple-mode ring and design example of the bandpass filter prototypes based on the ring structure are given. The prototype filters's performance is validated through both simulations and experiments, where good agreement with the theoretical prediction is observed. The out-of-band performance, particularly in the cascaded filter, can be improved with multi-frequency suppression technique.

ACKNOWLEDGEMENTS

I would like to express my deep and sincere gratitude to all who made this work possible. I am especially grateful to Prof. Wanlop Surakampontorn for his constant support and guidance throughout my D.Eng. studies at King Mongkut's Institute of Technology Ladkrabang (KMITL). His broad vision, together with his remarkable knowledge of our field of research, has proved to be invaluable in defining my research direction. I cannot forget how he encouraged and supported me while I was lying in bed for long time due to a disease treatment. He has been a great instructor, advisor, and teacher. I extend my sincere thank to Prof. Apisak Worapishet for sharing the time, discussions, and proof-reading for this entire dissertation. He was an advisor in M.Eng. degree and introduced me to my advisor, and, until now, he is my associate advisor from the Mahanakorn University of Technology (MUT).

I would like to thank Assoc. Prof. Dr. Mitchai Chongcheawchamnan served as an Associate Dean Academic of Faculty of Engineering at Prince of Songkla University, for the opportunity to work with him and for helping to improve the knowledge base and gain my experiences in microwave planar devices and systems. I had many grants under his management, and many research works published in IEE (now IET) and IEEE societies also under his technical support, which became extremely helpful in my research. Although we do not work together anymore, I would also like to thank you once again.

I would like to thank Assoc. Prof. Dr. Varakorn Kasemsuwan, Assoc. Prof. Dr. Apinunt Thanachayanont, and Assist. Prof. Dr. Kasin Vichienchom for being part of my seminar committees. I also want to give special thanks to Assoc. Prof. Dr. Sompol Kosulvit, Assoc. Prof. Dr. Chuwong Phongcharoenpanich, Assoc. Prof. Dr. Suripon Somkuarnpanit, and Assoc. Prof. Dr. Pipat Prommee for devote their time to serving on my qualifying exam. Without these courses, my work would not have been possible. I also thank Prof. Ikuo Awai from Kyoto University, Kyoto, Japan, for his valuable comments on the perturbation in dual-mode ring resonator during my presentation at the APMC-2007. Additionally, I would also like to thank the Editors-in-Chief of IEEE Microwave Theory and Techniques Society of Prof. Dylan Williams and Prof. Amir Mortazawi, that they said

"... I have always thought that dual-mode filters were very elegant, and I am glad to see work on this extension of the dual-mode approach."

This is an encouragement to me for creating the qualitative research in the future.

I am especially indebted to Assoc. Prof. Dr. Kiattisak Kumwachara and Assoc. Prof. Dr. Worapong Tangsrirat, they served as the instructor of the MVLSI Laboratory at KMITL for their continue support and encouragement. I am also indebted to all the past members of our Laboratory – Assist. Prof. Dr. Chaiwat Chongkulstitchai, Dr. Chalermpan Fongsamut, Dr. Boonchai Boonchu, Dr. Amorn Jiraseree-amornkun, Dr. Khanittha Kaewdang, Dr. Ittipat Roopkom, Mr. Dulpardon Pulsub, and Mr. Klanarong Noulkaew – were fund to work with and discussions during the research meetings. I also want to acknowledge the help of our secretary Miss Supanuch Oon-ob for making sure that our day-to-day operations run smoothly. Additionally, I would like to give special thanks to Prof. Monai Krairiksh at KMITL and Assist. Prof. Dr. Chaiwat Chongkulstitchai at RMUTR for allowing me to use their network analyzers.

I want to thank my colleagues and friends. In particular, I would like to thank Dr. Sawat Bunnjaweht for his brilliance in areas of practical microwave engineering during my experiments and proof-reading in some conference papers. He is my good teacher and friend. I would also like to thank Dr. Apichan Kanjanavapastit for proof-reading this entire dissertation at the first time. I would like to thank my native speaker, Mr. Dave Benson who served as the Director of English Language Center at MUT, for reading the manuscript of the journal publication very carefully and pointing out many errors and misspellings. Never to forget is Mr. Piyavit Jadpum, my student and friend, for his tremendous help in the fabrication expertise and measurement work of the prototypes in the first year of my doctoral course. Special thanks to Mr. Sumongkol Patisang and Mr. Jetwara Tangjit, also my students and friends, I spent some times and shared some ideas for a long vacation at Mae-Pim beach in Rayong province since we are victims during

Thai flood crisis in Nontaburi province. Thanks again for the delicious foods made by Patisang's mother during that time of the vacation.

I would also like to acknowledge the Thailand Research Fund (TRF) for their financial support through the Royal Golden Jubilee Ph.D Program under Grant number PHD/0010/2550. A partial support from the Commission on Higher Education under Research Group Program (CHE-RG) in Microelectronics for Communication managed by Prof. Surakampontorn, Ministry of Education, is also acknowledged. I am also grateful to the dissertation scholarship from the School of Graduate Studies. This work would not have been possible without the support from them.

Personally, my loving gratitude goes to Abbot of Wat Lam-Phak Chi, Luang Phor Yutthasarn, and my parents, Siripong and Arunnee Srisathit for providing opportunities, constant encouragement, and support to pursue this goal. I am also grateful to my senior sisters, Aussadaporn Kawee and Jittanan Srisuwan, and my junior brother, Kantapoat Srisathit, for trust me in the long study. Their unconditional love has been the greatest energy to me. Finally, my greatest thanks are due to my girlfriend, Saranya Vitayakerkkai, for her unwavering love, patience, and reassurance me to go forward during difficult times.

TABLE OF CONTENTS

LIST OF TABLES

Table **Page**

LIST OF FIGURES

CHAPTER 1

INTRODUCTION

A plethora of new applications for novel RF/microwave subsystems is being introduced as new communication and security systems, radar, surveillance, and positioning services are becoming available. The objective of these communication systems is to transmit information from one place to another through wireless network without interruption and clear reproduction at the receiver. This chapter first provides an overview of some wireless communication systems and further discusses the distortion presented in the systems. The motivation of this dissertation is to investigate the possibility and new techniques to achive high performance power divider/combiner and ring resonator in planar structure. Finally, the chapter shows the organization of the dissertation.

1.1 Background

During the last few decades, the requirement of high data rate to transfer data between data terminals and other portable wireless devices has increased significantly due to the popularity of internet and other computer, and mobile phone networks. This implies that the systems now support not only voice communications but also data services. Figure 1.1 shows an illustration of some popular systems for wireless communications.

For modern digital wireless communications, the quadrature modulation methods, i.e., M-PSK, M-QAM, have become more common in communication systems and standards since they offer superior spectral efficiency when compared to the frequency and phase modulation methods [1]. Typically, the quadrature modulations employ both the amplitude and phase to carry the information, and are often implemented using baseband quadrature signals. They also require a linear power amplification [2-3] at transmission. Unfortunately, the limitation of battery capacity and dc power ability impose primary restrictions on the power consumption of mobile handsets and base station power amplifiers [4-7]. Such systems were notoriously sensitive to distortion.

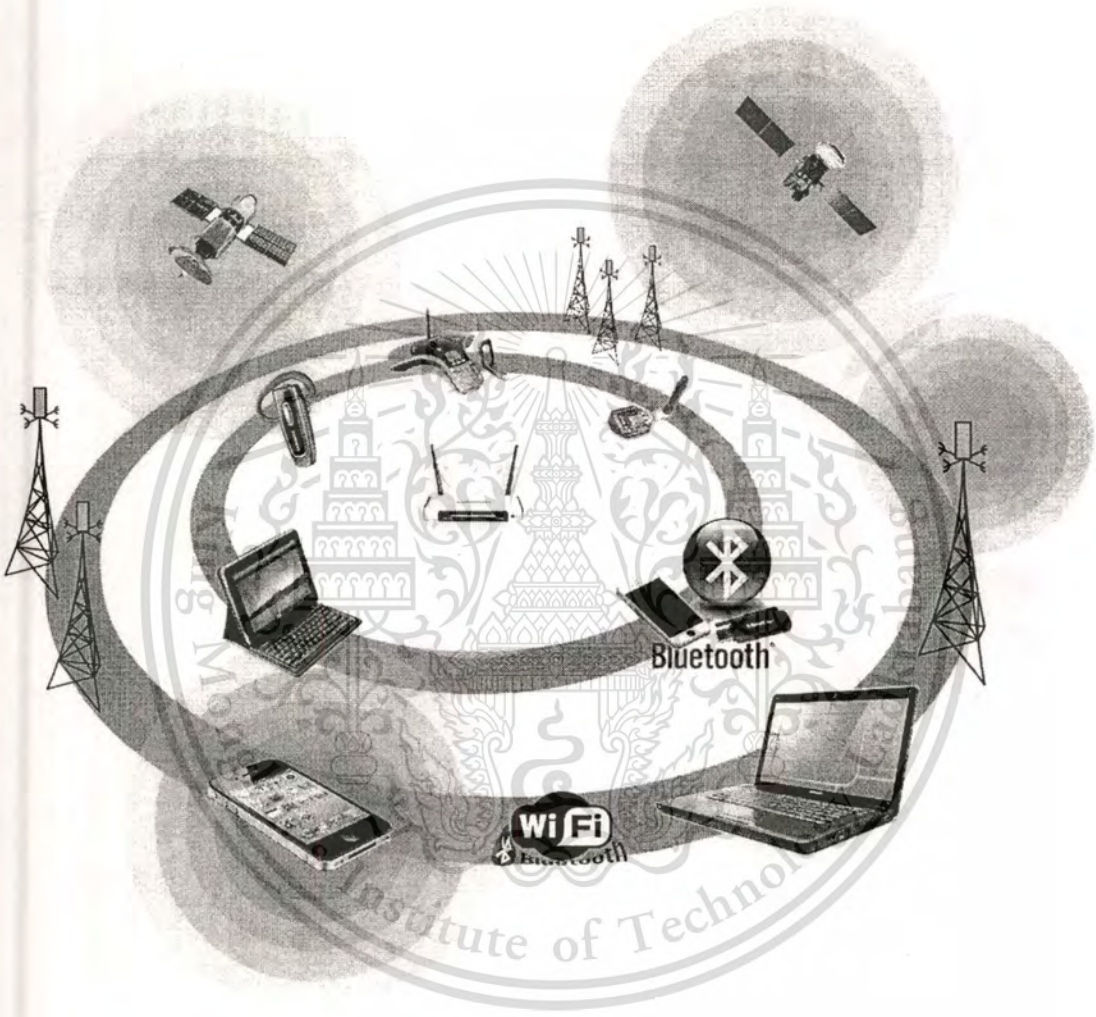

Figure 1.1 An example of wireless communication applications.

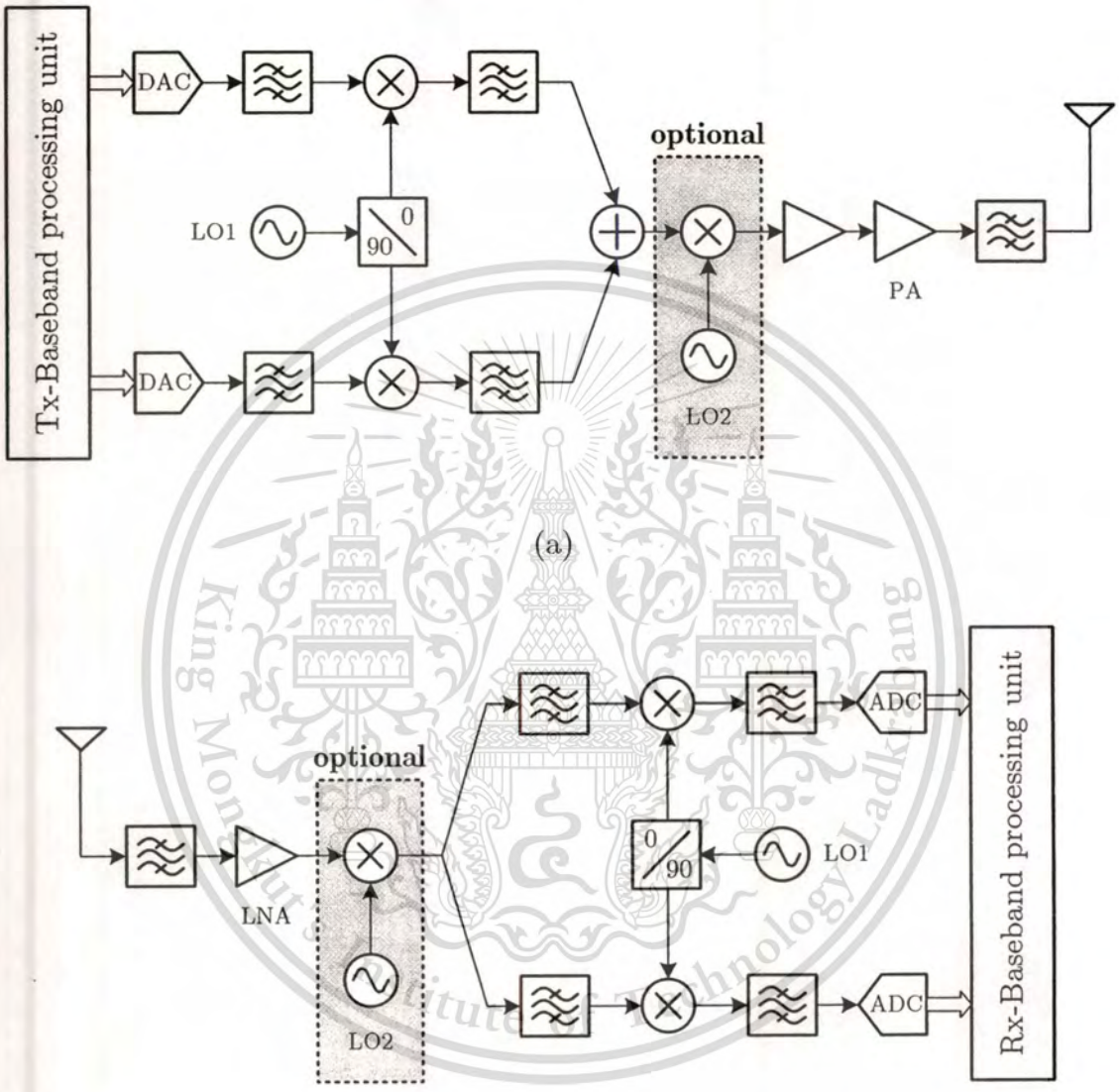

Figure 1.2 Block diagram of a general wireless communications for (a) transmitter and (b) receiver.

Figure 1.2 shows the block diagram of a general wireless communications with transmitter and receiver. Today, the baseband signal processing is usually performed digitally. Therefore, the digital-to-analog converter (D/A) is required. With the use of reconstruction filters, the unwanted signals are removed after the conversion, before sending to the transmitter. The quadrature modulation will be employed, depending on the modulation method, for providing the baseband signal in quadrature form with simultaneous conversion into an intermediate frequency (IF) or directly to a radio frequency (RF) and combination of these signals into one single signal. After that the signal is amplified with a power amplifier for transmission and is then converted from a guided electromagnetic wave on a transmission line to a plane wave propagating in free space.

Since a practical transmitter has nonlinear characteristics like any power amplifiers, it can qualitatively modify spectra and generate new ones, usually named as *spectral regrowth* [8]. The major cause of distortion presented in the system is linear and nonlinear distortions. Linear distortion or *harmonic distortion* can be manifested at the output as the extra frequency components appearing at integral multiples of an input frequency [9-10]. When *nonlinear device* is incorporated in the circuits such as the mixer [11] and the transmission power amplifier, the *nonlinear distortion* will be appeared at the output. This output frequencies are linear combinatons of the fundamental signal and all harmonics presented at the input signals. These distortions can degrade the performance of many communication systems [2, 8]. For example, signal transmitted with excessive intermodulation distortion can interfere with other transmission. Focusing on the receiving system, it must also be distortion-free, especially in the preamplifier stages to prevent crosstalk between adjacent channels by pressing information carried on one channel onto another channel. Therefore, distortions are a great deal of attention in microwave and wireless systems.

1.2 Motivation for the Dissertation

In line with the development of power amplifiers with high efficiency and high linearity has been introduced to ameliorate the nonlinear distortion [4-6], the high-performance passive devices have also been developed [12-15] where they are employed in the systems. Wilkinson power divider and Quadrature hybrid coupler are key components in microwave and millimeter-wave applications [16-24] such as power amplifiers, mixers, oscillators, beamforming arrays and so on. They are easy to implement depending on the type of transmission line being used, however, their responses exhibit the periodic characteristic in frequency. However, most research works such as lumped elements [25-28], three-dimensional structure [16], stepped-impedance coupled resonator [14], and two- and three-section transmission lines, concentrate upon acquiring the miniaturized size and make it suitable for dual-band [29] and tri-band applications [30]. However, for a power divider, the suppression of harmonic signals that could interfere with other equipments was rarely developed.

In this work, an extension of the concept of the T-shaped transmission line [31] to Wilkinson divider and Quadrature hybrid coupler for compact size and the n-th harmonic suppression is developed beyond the classical design. Moreover, the design equations are given and also shown that an unwanted harmonic frequency is related to the length of stub in an equivalent T-shaped transmission line. The proposed devices can also be applied at the operating frequency from the 1 to 2 GHz range right up to the millimeter-wave region.

An indispensable passive device employing in the RF front-ends of modern wireless communication systems is the bandpass filter. Various resonators based narrowband filter were introduced in the form of parallel coupled line resonator [32], hairpin resonator [33], and dual-behavior resonator [34]. Among the filter designs, the narrowband filter based on the dual-mode ring resonator is simple structure and easy to integrate with other planar circuits. It has many attractive features, including low radiation loss, high-Q factor, and compact size [35-41]. Two degenerated modes are excited by using asymmetric feedlines [35] or a perturbation with different schemes [36-41].

With regard to the practical implementation for a perturbation, we propose two new perturbation schemes based on the *right-* and *left-*handed

transmission lines with symmetrical structure for the small and high impedance ratios, respectively. For conventional perturbation, when the small impedance ratio is required as presented in [42], it is difficult to realize in practice to obtain the original center frequency since it introduces an extra-capacitance at the step transition due to the physical layout. On the other hand, when high impedance ratio is applied in the structure, it exhibits poor rejection performance since the structure does not provide attenuation pole on both side of the passband. These problems can be alleviated when the perturbation based on the proposed structure is employed in the ring resonator.

Another important concern in designing bandpass filter is a wide fractional passband based on ring resonator. Recently, many works have shown that dual-mode ring resonators are not only appropriate for the design of narrowband bandpass filters [35-42] but also for the development of wideband filters [43-45]. However, the dual-mode filter does not provide enough flat passband because it has only two passband resonance frequencies. Therefore, this work investigates a triple-mode ring resonator core and its applications to bandpass filter. This concept has been further implemented in designing 1.0 GHz bandpass filter that helps improve a flat passband response and sharp rejection. Some techniques are also introduced to enhance spurious response. Analysis is verified by the comparison of simulation results to *S*-parameter measurements.

1.3 Organization of Dissertation

This dissertation is concerned with improving performances of microwave devices and ring resonator bandpass filters, in planar structure implementation. The dissertation is divided into four main chapters as follows.

Chapter 2 presents the fundamental concepts of microwave power divider, particularly *in*-phase and *quadrature*-phase dividers. Some applications for the use of power divider are explained. Furthermore, a conventional and an equivalent T-shaped transmission lines are discussed and compared to show the feasibility of both transmission lines. In addition, two layouts of power dividers using the T-shaped transmission line are discussed in detail, and their fabrication and measurement are presented.

In Chapter 3, we discuss the principal operation and arrangements of dual-mode ring resonator. Various perturbations, at the plane of symmetry, of ring resonators with a dual-mode characteristic for discussion are the series stub, shunt stub, series-capacitance, and shunt-capacitance perturbations to show the advantages and drawbacks of each approach. The practical feeding lines including coupling and direct structures are also described to achieve low insertion loss and constant passband characteristic. The next section presents two kinds of an artificial transmission line to diminish the limitation of the perturbation approach. This dual-mode ring is analyzed, demonstrated, and verified with the measurement results that emphasize the success of the approach for implementing the dual-mode ring bandpass either a very low or very high characteristic impedance of the series stub.

Chapter 4 focuses on the design and implementation of triple-mode ring resonator for wideband bandpass filter in a planar structure. The chapter starts by a review of different configurations of dual-mode ring filters. Subsequently, the difficulty in implementing a triple-mode ring resonator in planar structure is explained. In addition, practical design issues in the planar triple-mode ring resonator including configuration, characteristic, analysis method using the basic of two-port network and even- and odd-mode excitation, graphical consideration, and physical interpretation are described to support the triple-mode ring filter for a wideband response. Measurement results are provided to ensure the performance of the design in overcoming the insertion loss with flat passband and sharp rejection response. Two techniques, the inter-digital coupled line and the T-shaped transmission line as described in chapter 2, are applied to a cascaded single-ring resonator filter for multi-frequency suppression.

Finally, Chapter 5 draws conclusions from the results and provides ideas for future research which are relevant to this dissertation.

CHAPTER 2

COMPACT POWER DIVIDER WITH HARMONIC SUPPRESSION

In this chapter, the projects motivations are briefly introduced in Section 2.1. The material presented in Section 2.2 provides the background of 3-dB power dividers/combiners with *in-phase* and *quadrature-phase* that is necessary to understand the operating mechanism and characteristic, and the design of conventional power dividers. An application example for power divider with quadrature-phase is also illustrated in this Section. In Section 2.3, an overview of transmission line is described and an equivalent T-shaped line used in this dissertation is then discussed in detail. Finally, two devices such as Wilkinson power divider (in-phase) and Quadrature hybrid coupler (quadrature-phase) in planar structure realized on an FR-4 material are investigated in Section 2.4 and 2.5, respectively. Section 2.6 summarizes the chapter with conclusion.

2.1 Introduction

In RF and microwave communication systems, power dividers sometimes called "*power combiners*" are the indispensable signal-processing devices. They are passive microwave devices used for splitting and combining of signal power. Mixers, balanced amplifiers, feedforward linear power amplifiers, transposed gain amplifiers as an oscillation sustaining amplifier, vector modulators, unbalanced-to-balanced converters, phase shifters, and many other applications require dividers and combiners as a part of the whole circuit [3, 11, 46-48]. A Wilkinson divider is one of the very first techniques that adopts the idea of a power divider approach to solve in-phase power divider between the output ports. When the quadrature phase (90-deg) is required, Quadrature hybrid may be considered since its structure provides a 90-deg phase difference between two outputs. If these devices have symmetrical layout, an equal power division ratio (3-dB) can be obtained.

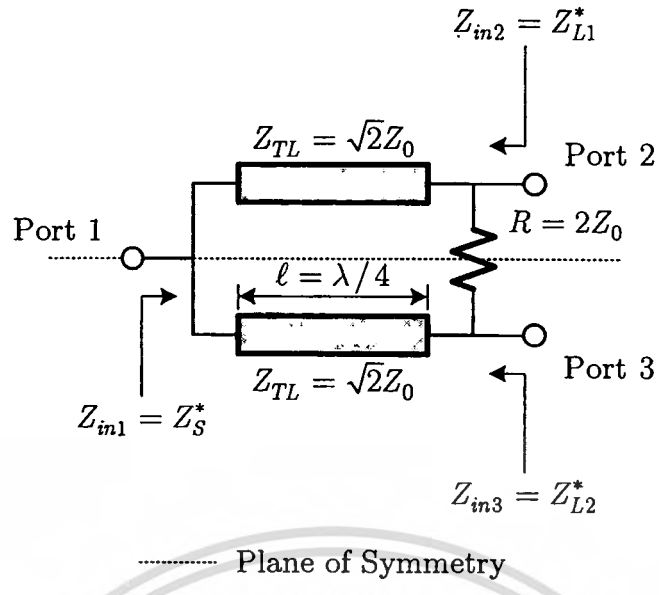

Figure 2.1 The Wilkinson power divider.

2.2 Basics of Planar Power Divider

To provide an insight into their principle operations and limitations, a qualitative discussion on scattering parameters of the power dividers based on the Wilkinson and Quadrature hybrid topologies is given in this section. The quasi-static TEM mode of operation is assumed for analyzing the lossless transmission line without discontinuity effects.

2.2.1 Wilkinson Power Divider

The Wilkinson power divider/combiner was first introduced in 1960 by Wilkinson E. J. in 1960 [49] as a method to divide an input signal into n equiphase equiamlitude output signals, whereas n is the number of output ports. On the other hand, it combines theses output signals into one on the opposite direction. For the case of an equal-splitting (3-dB), the structure is accomplished based on the quarter-wavelength transmission line pair and only one resistor as illustrated in Figure 2.1. These two transmission lines, connected in parallel at the port 1 (input port), have the characteristic impedance of Z_{TL1} and Z_{TL2}, respectively. A resistor R is connected between port 2 and 3 (output ports) to obtain independence and matching at theses output ports.

If port 1, 2, and 3 have the characteristic impedance of Z_S, Z_{L1}, and Z_{L2}, respectively, the characteristic impedance of each transmission line is found to be

$$Z_{TL1} = \sqrt{2Z_S Z_{L1}}\,, \tag{2.1}$$

and

$$Z_{TL2} = \sqrt{2Z_S Z_{L2}}\,. \tag{2.2}$$

The isolation resistor is then given by

$$R = 2\sqrt{Z_{L1} Z_{L2}}\,. \tag{2.3}$$

No power is dissipated by the resistance when matched loads are connected to the outputs, or, in other words, the input of the power divider is also matched when the condition for isolation between outputs is satisfied.

When all ports of Figure 2.1 are terminated with the characteristic impedance of Z_0, we can define two separate mode of excitation. These are the even-mode and odd-mode as depicted in the *top* and *bottom* rows, respectively, of Figure 2.2(a) to calculate S_{11}, S_{12} (or S_{21}), and S_{13} (or S_{31}). By using the principle of a two-port network as depicted in Figure 2.2(b), the scattering parameters of S_{22}, S_{23}, S_{32}, and S_{33} can be obtained. A Wilkinson power divider of a matched three-port network with lossless and reciprocal properties has the scattering matrix as

$$[S] = \frac{-1}{\sqrt{2}}\begin{bmatrix} 0 & j & j \\ j & 0 & 0 \\ j & 0 & 0 \end{bmatrix}. \tag{2.4}$$

The input port 1 would transmit half its power with equal magnitude and phase response to port 2 and 3. The system would be reciprocal, thus, port 2 and 3 would combine equal signal at port 1 so the power adds with no losses. The phase delay between port 1 and port 2/3 is $\pi/2$ radian. Therefore, this power divider may be *called* as 0° or *in-phase* power divider. The *S*-parameter magnitudes and phases are plotted in Figure 2.3(a) and (b), respectively.

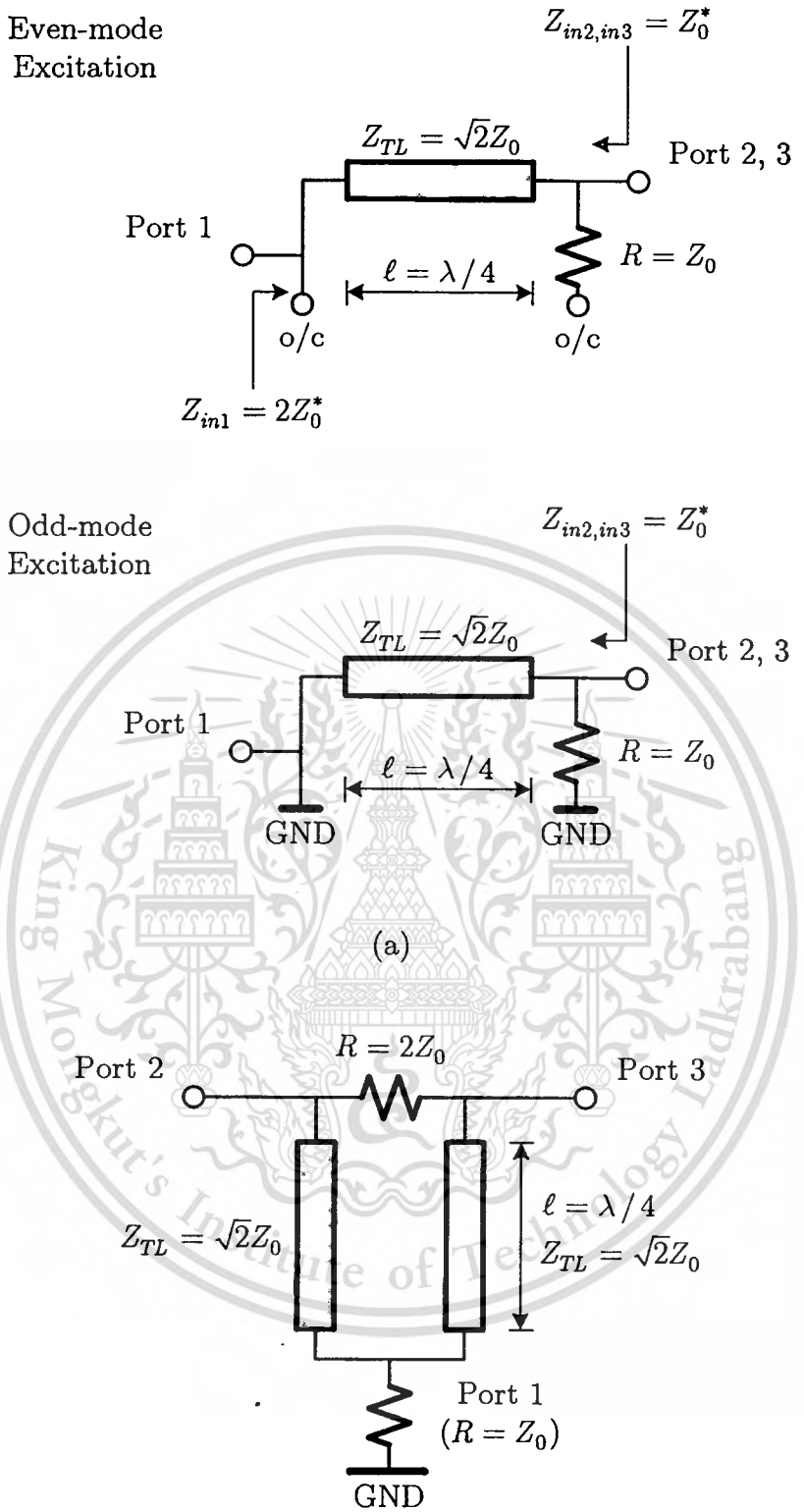

Figure 2.2 Analysis of the Wilkinson power divider to find (a) S_{11}, S_{12} (or S_{21}), and S_{13} (or S_{31}) by using even- and odd-mode excitations (b) S_{22}, S_{33}, and S_{23} (or S_{32}) by using the two-port network theorem.

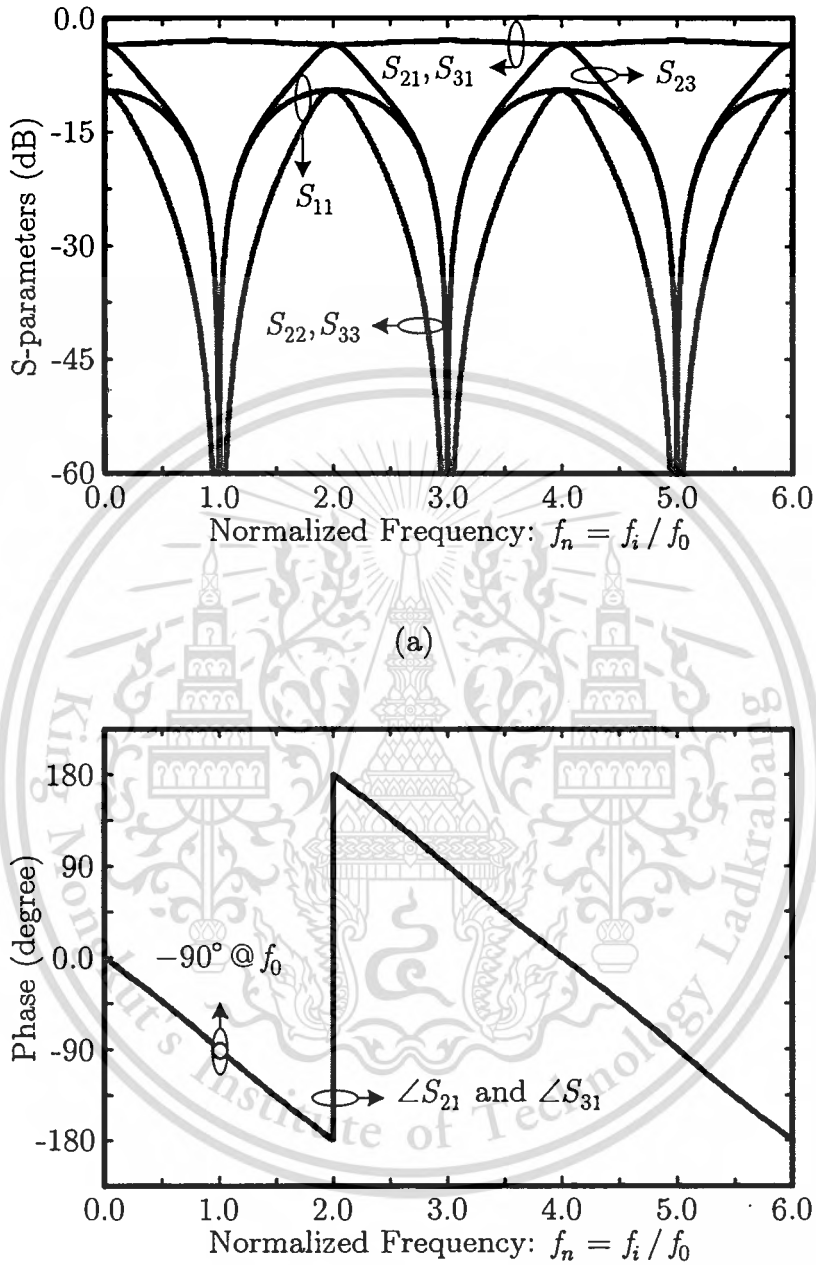

Figure 2.3 Frequency response of 3-dB three-port Wilkinson power divider. (a) Magnitude response of S_{11}, S_{21}, S_{31}, S_{22}, S_{33}, and S_{23}. (b) Phase response of S_{21} and S_{31}.

2.2.2 Quadrature Hybrid Coupler

The 90° Hybrid coupler is a four-port device known as the *quadrature hybrid* or *branch line coupler*. It is a directional coupler with a 90° phase difference in the outputs of the through and coupled arms. Any form of transmission line may be used. Figure 2.4 shows a Quadrature hybrid. It consists of two coupling- and main-lines. The lengths of them are quarter-wavelength transmission line section at the center frequency. The characteristic impedance of coupling-line and of main-line are Z_{TL1} and Z_{TL2}, respectively. The operation of the Quadrature hybrid may be analyzed using even-odd mode theory of Reed and Wheeler [50] similar to that used for the Wilkinson power divider.

With reference to Figure 2.4, port 1 is an input port whereas port 2 and 3 are direct port and coupled port, respectively. Both port 2 and 3 act as output ports. Port 4 is an isolated port. All ports are terminated with the characteristic impedance of Z_0. The basic operation of the Quadrature hybrid is described as follows under the perfectly matched condition only at its center frequency at which there is also complete isolation between port 1 and port 4. This implies that no power is coupled to port 4, or vice versa. With all ports matched, power entering at port 1 is evenly divided between port 2 and 3, with a 90° phase shift only at center frequency between these output ports. A Quadrature hybrid as shown in Figure 2.4 has two planes of symmetry, i.e., horizontal and vertical planes of symmetry.

To analyze the scattering parameters of the Quadrature hybrid, Figure 2.4 can be decomposed into the superposition of an even- and an odd-mode excitation without any change in its operation, [see horizontal plane of symmetry in Figure 2.5]. In the case of the even-mode excitation as indicated in Figure 2.5(a), the symmetrical plane acts as a perfect magnetic wall and this implies the open-circuited at the plane of symmetry. On the other hand, the symmetrical plane acts as a perfect electric wall under the odd-mode excitation. Thus, this plane represents the short-circuited as demonstrated in Figure 2.5(b). By using the two-network theorem, the design equations for a Quadrature hybrid are given as follow

$$C = 10\log\frac{1}{1-(Z_{TL1}/Z_0)^2}, \tag{2.5}$$

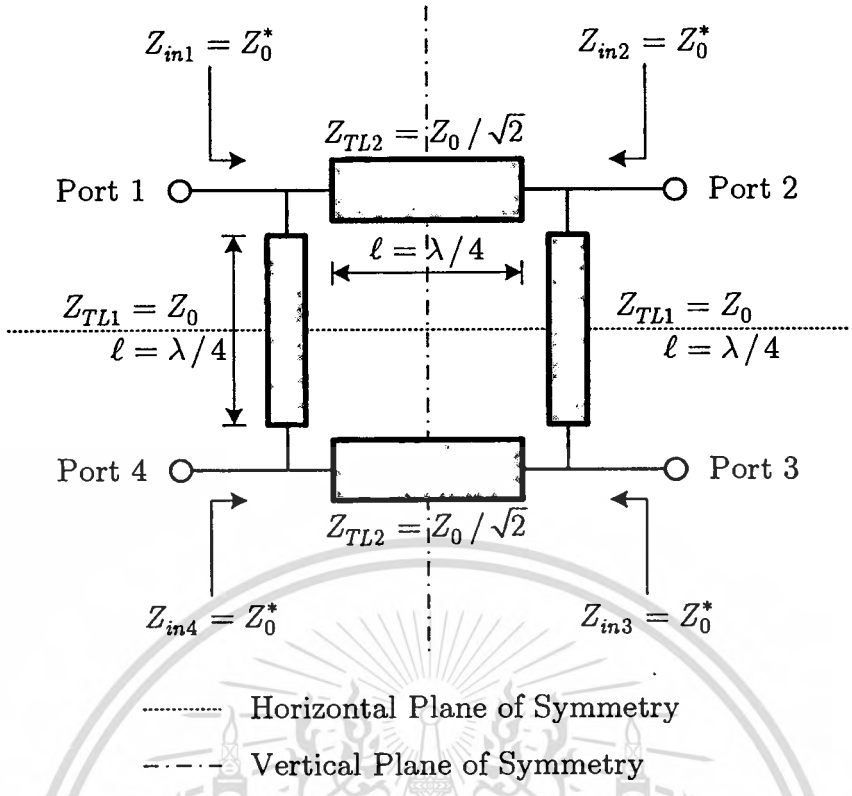

Figure 2.4 A schematic of Quadrature hybrid coupler.

$$Z_{TL2} = \frac{Z_{TL1}}{\sqrt{1-(Z_{TL1}/Z_0)^2}}, \tag{2.6}$$

where C is the coupling coefficient in decibels and Z_0 denotes the characteristic impedance of the connecting lines. For the 3-dB Quadrature hybrid, Z_{TL1} and Z_{TL2} are simplified to Z_0 and $Z_0/\sqrt{2}$, respectively. Under match condition, the scattering matrix can thus be expressed as

$$[S] = \frac{-1}{\sqrt{2}}\begin{bmatrix} 0 & j & 1 & 0 \\ j & 0 & 0 & 1 \\ 1 & 0 & 0 & j \\ 0 & 1 & j & 0 \end{bmatrix}. \tag{2.7}$$

This above scattering matrix was developed with a physical meaning that any port of the Quadrature hybrid can be used as the input port. The input and output ports are always opposite side. The isolated port will be the same side as the input port.

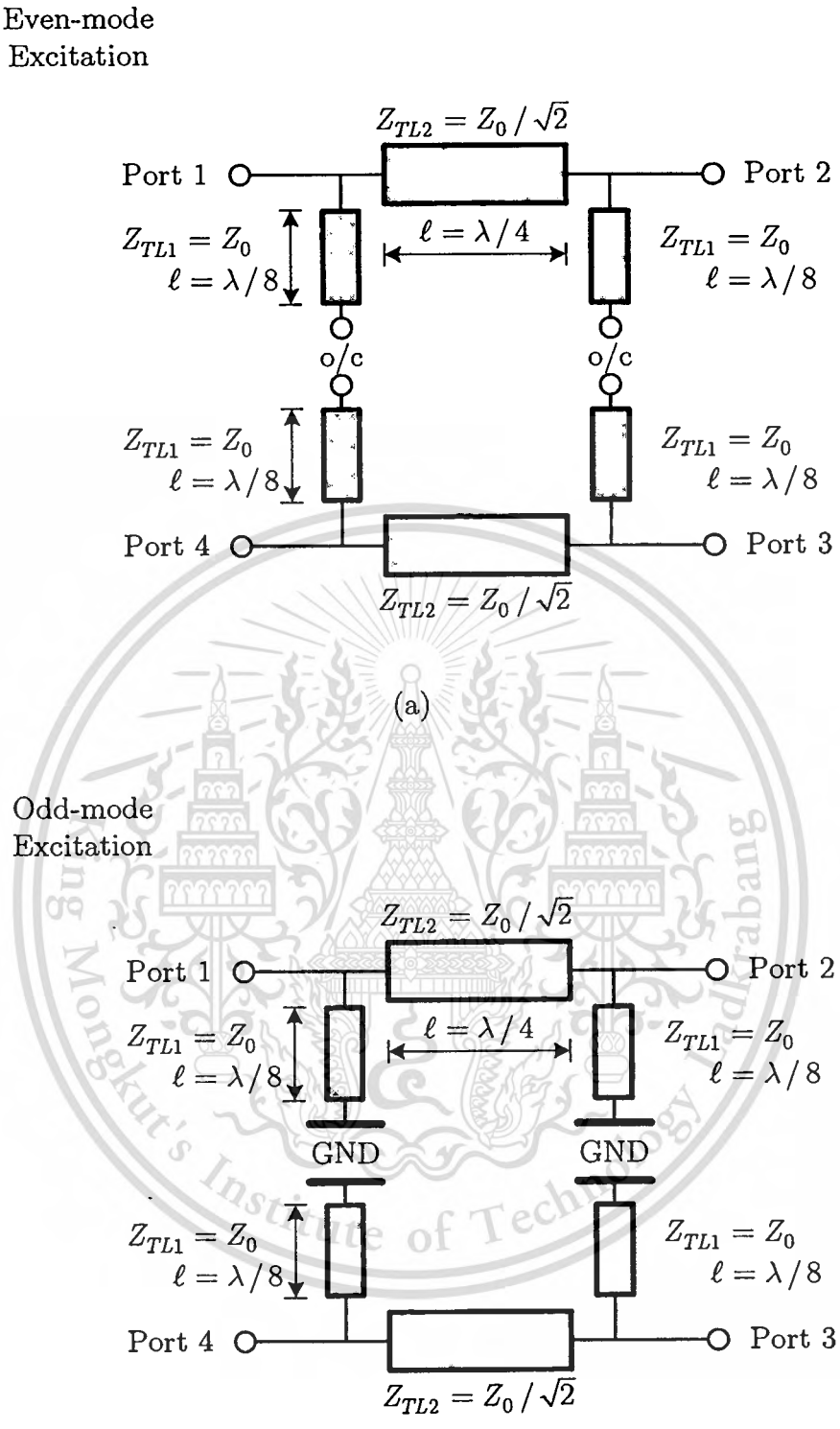

Figure 2.5 Analysis of the Quadrature hybrid along the horizontal plane of symmetry using (a) even-mode excitation and (b) odd-mode excitation.

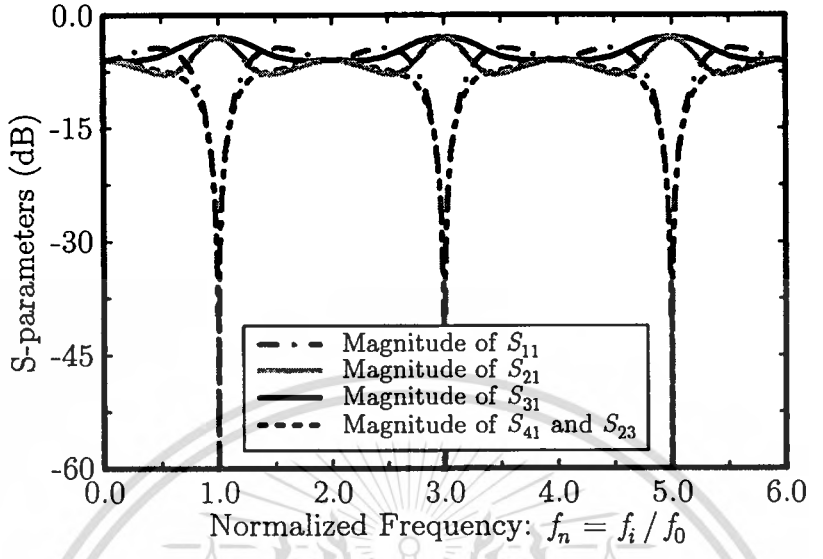

(a)

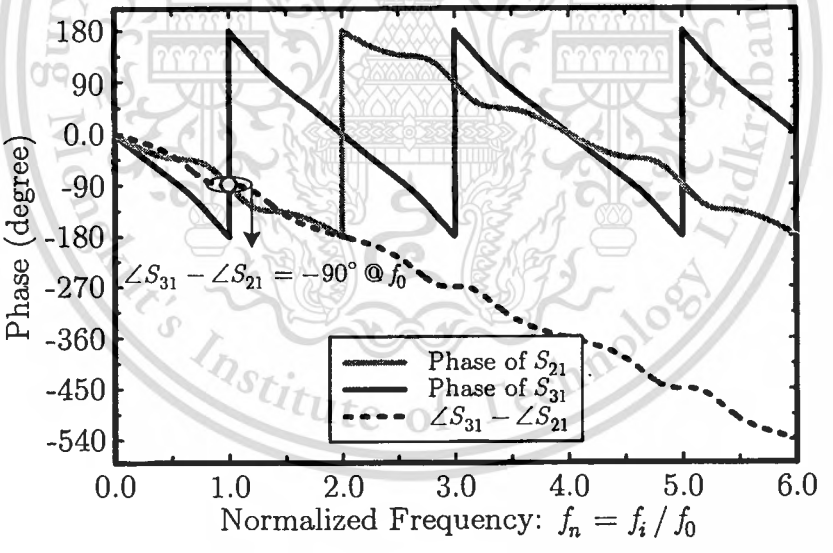

(b)

Figure 2.6 Calculated performances of 3-dB Quadrature hybrid based on an ideal transmission line. (a) Magnitude response of S_{11}, S_{21}, S_{31}, and S_{41}. (b) Phase response of S_{21}, S_{31}, and $\angle S_{31} - \angle S_{21}$.

The calculated frequency response of Quadrature hybrid is plotted in Figure 2.6. As indicated in Figure 2.6(a), the magnitude response as a function of the normalized frequency with the center frequency, i.e., $f_n = f_i / f_0$ displays perfect 3-dB power division in port 2 and 3 at $f_n = 1$, 3, and 5 by observing the S_{21} and S_{31}. The isolation between direct port and coupled port is indicated by observing the S_{23} in the figure. We also achieve perfect isolation and reflection at port 1 and 4 by observing the S_{41} and S_{11} at $f_n = 1$. However, all of these quantities degrade rapidly as frequency is moved away from f_0. Another point of view is the phase response as indicated in Figure 2.6(b). The relation of a quadrature phase between two output ports is satisfied only at $f_n = 1$.

2.2.3 Applications of Power Divider

The most common signal power divider application is for signal preparation for the inputs of mixers [11] that execute frequency translation. Mixers are used in communication transmitters and receivers. The four basic topologies of mixer are categorized as single-ended, single-balanced, double-balanced, and balanced quadrature types. A single-ended mixer is based on the nonlinear properties of a single diode or transistor. It suffers insufficient isolation between the radio frequency (RF), local oscillator (LO), and intermediate frequency (IF) ports. This results in frequency translation of all in-band spurious signals. A single-balanced mixer has the RF or LO divided into a differential signal to improve isolation between RF and LO and spurious rejection whereas a double-balanced mixer divide the RF and LO into balanced signals to improve isolation and second-order spurious rejection. A balanced quadrature mixer divides the RF and the LO signals are four arms into a differential quadrature signal obtaining sideband suppression or image rejection. The level of second-order spurious attenuation and sideband suppression is depended on the balance of signal.

Also, the Quadrature hybrid couplers are widely used in microwave circuits [46-47, 51] such as balanced amplifiers, balanced mixers, phase shifters, and circularly polarized patch antennas, because of their unique features. To introduce the application of Quadrature hybrid, the balanced amplifier with 3-dB couplers will be discussed in the following manner [47].

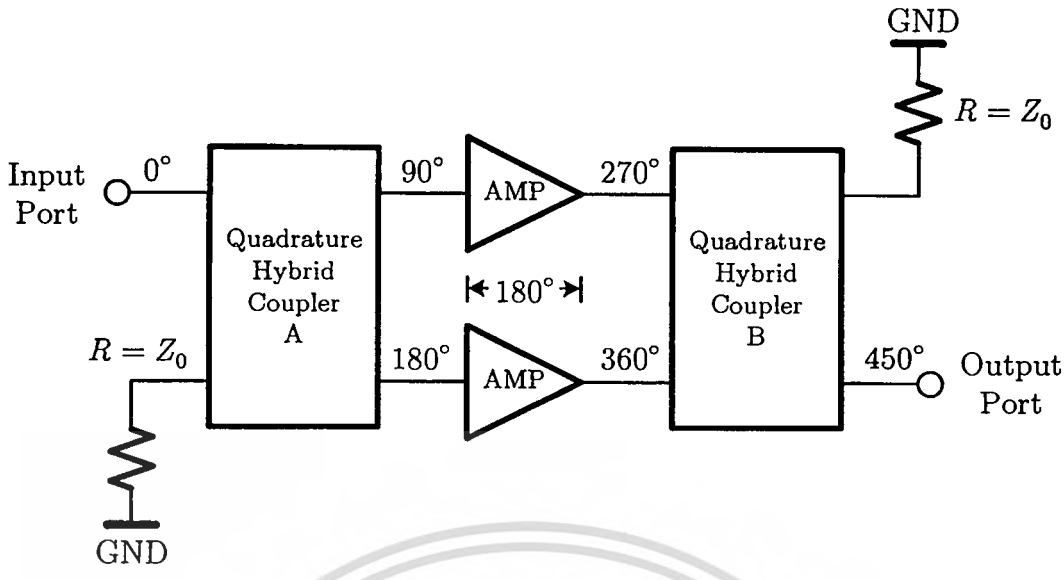

Figure 2.7 Schematic diagram of the classical balanced amplifier.

Considering the classical balanced amplifier using two Quadrature hybrid couplers and two identical single-ended amplifiers as shown in Figure 2.7. The output power of each individual amplifier is combined by an identical Quadrature hybrid that also offsets the initial phase difference. Note that the output power of each amplifier is added in phase thus achieving high output power levels, which would otherwise be impossible to obtain from single amplifier. In addition, the input and output reflection coefficients of the balanced amplifier are also improved since the reflected signals from the original amplifiers are added out-of-phase and in-phase at the input ports and termination ports, respectively. This implies that the reflected powers from individual amplifiers are absorbed in terminating resistor. This resistor must then be selected with a proper power rating. It is important to design the individual amplifiers as identical as possible for optimum performance.

2.3 Transmission Line Fundamentals

The following discussion provides an overview of transmission line fundamentals. In general, circuits and networks are made up of some components that perform operations on signals and on some others that only carry signals from one place to another with minimum distortion on the signals. These components that are responsible for transmission of signals are

called a *transmission line*. At microwave frequencies, the characterization of transmission lines plays a much more important role than their characterization at low frequencies. This is because the transmission lines are extremely short for low frequency circuits in terms of wavelength. On the other hand, they are no longer than short as compared to the wavelength at high frequencies. It is hence necessary to take into account of their influence on the signals passing through them.

In the case of all planar transmission lines, they are considered as stripline, microstrip line, coplanar waveguide, and their variants. Microstrip is the most popular for realizing microwave circuits. Since the separation between the conductor and ground plane in microstrip transmission line is very small compared to the wavelength, the mode of propagation on the line can be considered to be close to TEM mode. This mode is called a *quasi*-TEM mode [51].

2.3.1 Conventional Transmission Lines

2.3.1.1 Parameters of Interest

The schematic of a transmission line section along with the z-direction is shown in Figure 2.8 (*top row*). The parameters of interest for a quasi-TEM mode transmission line are its characteristic impedance Z_0 and propagation constant γ. In the case of an *infinitesimal segment* δz of this line, its equivalent circuit can be modeled as a lumped-element network in terms of line parameters *per unit length*, i.e., inductance (L), capacitance (C), resistance (R), and conductance (G), as depicted in Figure 2.8 (*bottom row*). Note that a finite length of transmission line can be indicated as a cascade of segments of Figure 2.8 (*bottom row*). The characteristic impedance Z_0 is defined as the ratio of voltage over current across the infinitesimal segment for either the *forward* wave or *reverse* wave considered alone, which is given by

$$\begin{aligned} Z_0 &= \frac{V^+}{I^+} = \frac{V^-}{I^-} \\ &= \sqrt{\frac{R + j\omega L}{G + j\omega C}}, \end{aligned} \tag{2.8}$$

where V^+, V^-, I^+, and I^- are the magnitude of the voltage and current waves,

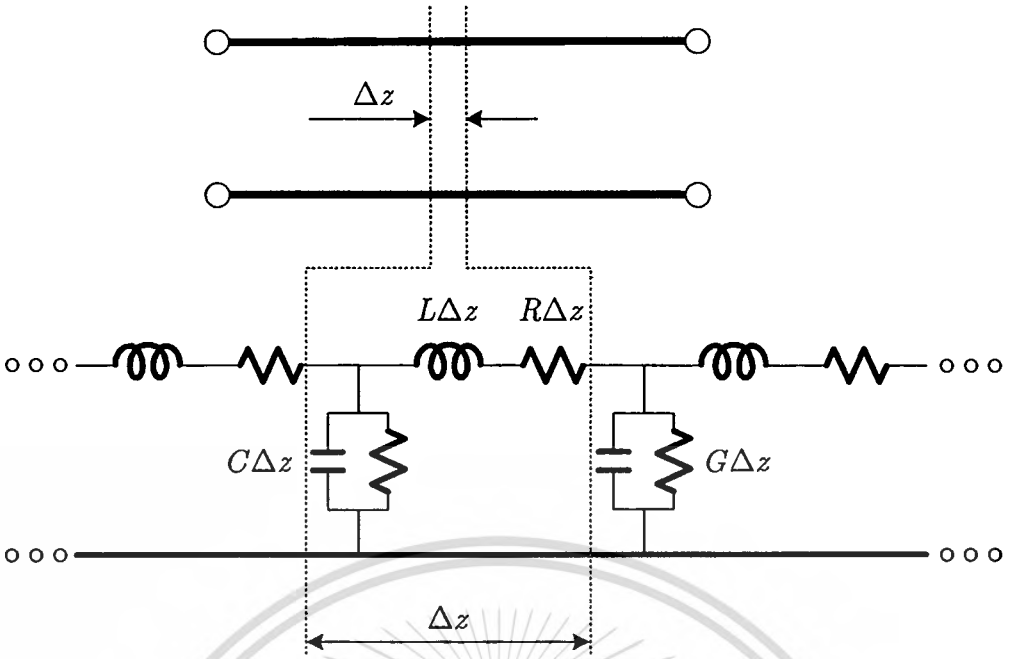

Figure 2.8 Lumped model of infinitesimal transmission line segment.

and the superscripts + and − refer to the forward and reverse waves, respectively.

For a lossy transmission line, the parameter γ is a complex propagation constant. In general, it can be decomposed into real and imaginary parts as

$$\gamma = \alpha + j\beta = \sqrt{(R + j\omega L)(G + j\omega C)}\,, \tag{2.9}$$

where the real part α denotes the loss in the line called the *attenuation constant* given in Nepers per meter (Np/m). The imaginary part β represents the responsibility for phase shift calling *phase constant* in radians per meter (rad/m).

For a lossless transmission line, the attenuation constant is neglected and set to zero. The characteristic impedance and propagation constant can be reduced to

$$Z_0 = \sqrt{\frac{L}{C}}\,, \tag{2.10}$$

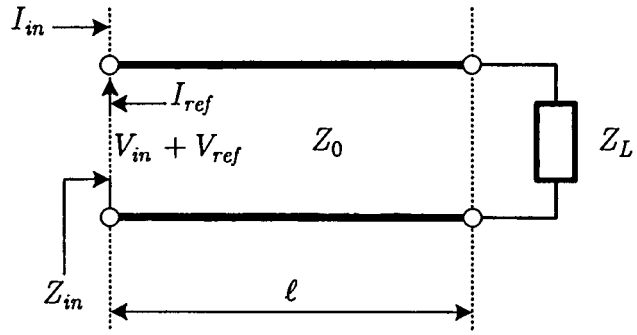

Figure 2.9 A transmission line terminated with a load impedance.

and

$$\gamma = j\beta\,. \tag{2.11}$$

These equations are for a transmission line under infinite conductivity of conductors, zero conductivity of dielectric materials, and no polarization loss.

2.3.1.2 Terminated Lossless Transmission Line

Figure 2.9 shows a lossless transmission line ($\gamma = j\beta$) with an arbitrary load impedance termination Z_L. The input impedance seen across a pair of terminals located at any point along the line is dependent on the length of the line between the terminal and the load, as well as the line parameters and termination, which is given by

$$Z_{in} = Z_0 \frac{Z_L + jZ_0 \tan\beta\ell}{Z_0 + jZ_L \tan\beta\ell}. \tag{2.12}$$

Note that this expression is periodic with ℓ. Of course, this behavior is strictly true only for lossless lines, but practical lines will behave similarly as long as the loss is negligible. Periodicity implies that one need consider the impedance behavior only over some finite section of line, i.e., a *half-*wavelength long.

Considering (2.12), this reveals that there is no reverse wave when the load termination $Z_L = Z_0$ is terminated at the end of a finite length. The input impedance is thus a constant which is equal to the terminating impedance, i.e., $Z_{in} = Z_L = Z_0$.

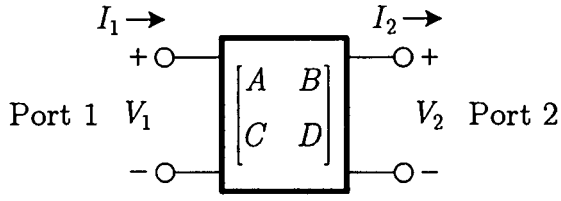

(a)

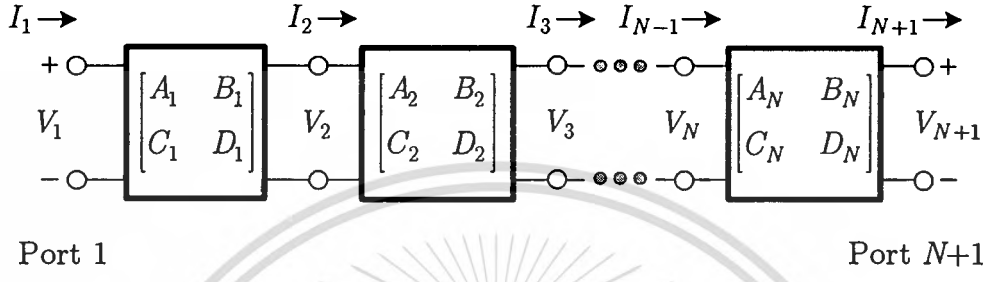

(b)

Figure 2.10 Definitions of voltages and currents for ABCD-matrix representation (a) a two-port network and (b) cascaded two-port network.

2.3.1.3 *ABCD*-Matrix of Transmission Line

A distinctive microwave subsystem consists of a cascade of two-port configurations such that the output of the first network is connected to the input of the next network. The matrix of overall cascaded network can easily be calculated by multiplying the *ABCD*-matrices of individual networks.

To introduce the *ABCD*-matrix, a general two-port network is depicted in Figure 2.10(a). The voltage and current at the input of the network are related to the voltage and current at the output by the following matrix

$$\begin{bmatrix} V_1 \\ I_1 \end{bmatrix} = \begin{bmatrix} A & B \\ C & D \end{bmatrix} \begin{bmatrix} V_2 \\ I_2 \end{bmatrix}. \tag{2.13}$$

The cascaded networks according to Figure 2.10(b) is given by

$$\begin{bmatrix} A_t & B_t \\ C_t & D_t \end{bmatrix} = \begin{bmatrix} A_1 & B_1 \\ C_1 & D_1 \end{bmatrix} \times \begin{bmatrix} A_2 & B_2 \\ C_2 & D_2 \end{bmatrix} \times \cdots \times \begin{bmatrix} A_N & B_N \\ C_N & D_N \end{bmatrix}, \tag{2.14}$$

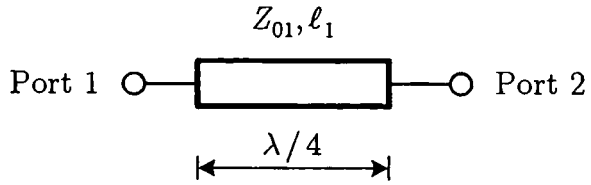

(a)

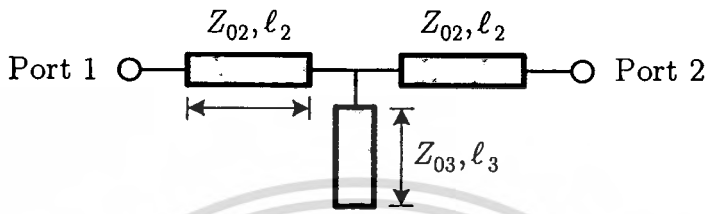

(b)

Figure 2.11 The structure of (a) conventional line and (b) T-shaped line

where N is the number of cascaded networks. This property is very useful in evaluating overall performance of the cascaded configurations.

Since the microwave circuits and subsystems employ the transmission lines as a part of the design, the $ABCD$-matrix of the transmission line will be considered. For a lossless transmission line section with the characteristic impedance of Z_{01} and the physical length of ℓ_1, the $ABCD$-matrix is expressed as

$$[M_1] = \begin{bmatrix} \cos(\beta\ell_1) & jZ_{01}\sin(\beta\ell_1) \\ jY_{01}\sin(\beta\ell_1) & \cos(\beta\ell_1) \end{bmatrix}, \tag{2.15}$$

where $Y_{01} = 1/Z_{01}$ is the characteristic admittance of the transmission line and $\beta = 2\pi/\lambda$ is the phase constant.

2.3.2 T-Shaped Transmission Line

In the conventional transmission line structure as shown in Figure 2.11(a), its T-shaped transmission line is illustrated in Figure 2.11(b) [31]. The T-shaped transmission line consists of two identical series transmission lines and a shunt open stub at the middle of two identical lines. The overall

ABCD-matrix can be used to characterize its performance. In the case of the series transmission line with the characteristic impedance of Z_{02} and the length of ℓ_2, the *ABCD*-matrix can be found as

$$[M_2] = \begin{bmatrix} \cos(\beta\ell_2) & jZ_{02}\sin(\beta\ell_2) \\ jY_{02}\sin(\beta\ell_2) & \cos(\beta\ell_2) \end{bmatrix}, \tag{2.16}$$

where $Y_{02} = 1/Z_{02}$ is the characteristic admittance of the series line. Since a shunt open stub has the characteristic impedance of Z_{03} and the physical length of ℓ_3, its *ABCD*-matrix of the shunt open stub also can be found as

$$[M_3] = \begin{bmatrix} 1 & 0 \\ jY_{03}\tan(\beta\ell_3) & 1 \end{bmatrix}, \tag{2.17}$$

where $Y_{03} = 1/Z_{03}$ is the characteristic admittance of the shunt stub. Note that the T-shaped transmission line is the cascade of three two-port networks. Therefore, the representation of *ABCD*-matrix for the T-shaped transmission line can be derived by multiplying of $[M_2]$, $[M_3]$, and $[M_2]$, respectively, as follows

$$\begin{aligned} [M_{\text{T-shaped}}] &= [M_2][M_3][M_2] \\ &= \begin{bmatrix} \cos(\beta\ell_2) & jZ_{02}\sin(\beta\ell_2) \\ jY_{02}\sin(\beta\ell_2) & \cos(\beta\ell_2) \end{bmatrix} \begin{bmatrix} 1 & 0 \\ jY_{03}\tan(\beta\ell_3) & 1 \end{bmatrix} \\ &\quad \begin{bmatrix} \cos(\beta\ell_2) & jZ_{02}\sin(\beta\ell_2) \\ jY_{02}\sin(\beta\ell_2) & \cos(\beta\ell_2) \end{bmatrix}. \end{aligned} \tag{2.18}$$

The equivalent circuit of the T-shaped transmission line behaves like a series resonance with the length of $\ell_3 = \lambda/4$ at a particular frequency. This implies that the utilization of T-shaped transmission line can rejected any frequency with respect to the length of the shunt stub. For example, if ℓ_3 is assigned to be $\lambda/8$ at the fundamental frequency, two-times of fundamental frequency ($2f_0$) can be suppressed. At this state, the *ABCD*-matrix of the stub in (2.17) can thus be reduced to

$$[M_3]_{\ell_3=\lambda/8} = \begin{bmatrix} 1 & 0 \\ jY_{03} & 1 \end{bmatrix}. \tag{2.19}$$

If the T-shaped transmission line model [see Figure 2.11(b)] is equivalent to the conventional transmission line [see Figure 2.11(a)], its *ABCD*-matrix will be equal to the *ABCD*-matrix of the conventional transmission line at the vicinity of center frequency. By inspecting the conventional transmission line with the impedance of Z_{01} and the length of $\ell_1 = \lambda/4$, the original *ABCD*-matrix as indicated in (2.15) can thus be reduced to

$$[M_1]_{\ell_1=\lambda/4} = \begin{bmatrix} 0 & jZ_{01} \\ jY_{01} & 0 \end{bmatrix}. \tag{2.20}$$

The analytical equations may be developed by first considering an unwanted harmonic frequency which is related to the length of ℓ_3. The relation between $\beta\ell_3$ and f_i is

$$\beta\ell_3 = \left(\frac{\pi}{2}\right)\left(\frac{f_0}{f_i}\right), \tag{2.21}$$

where f_i is the frequency-suppressed location beyond the fundamental frequency f_0 (i.e., $f_i > f_0$). Three unknown variables, i.e., Z_{02}, Z_{03}, and ℓ_2, can be solved by equating (2.18) and (2.20). The general design equations for Z_{02} and Z_{03} in terms of Z_{01}, ℓ_2, and ℓ_3 can be expressed by

$$Z_{02} = Z_{01}\cot(\beta\ell_2), \tag{2.22}$$

and

$$Z_{03} = Z_{01}\frac{\cot^2(\beta\ell_2)\tan(\beta\ell_3)}{1-2\sin^2(\beta\ell_2)}. \tag{2.23}$$

It should be noted that the length of ℓ_2 should be less than $\lambda/8$ to obtain such compact T-shaped transmission line.

Table 2.1 Summary of T-shaped transmission line parameters at differently attenuating frequency locations.

Parameters	Normalized attenuating frequency locations: $Z_{01} = 100\ \Omega$, $\beta\ell_1 = \pi/2$ rad				
	2.0	3.5	3.0	3.5	4.0
Z_{02} (Ω)	173.20				
$\beta\ell_2$ (rad)	$\pi/6$				
Z_{02} (Ω)	150	108.98	86.60	72.23	62.13
$\beta\ell_3$ (rad)	$\pi/4$	$\pi/5$	$\pi/6$	$\pi/7$	$\pi/8$

2.3.3 Comparative Properties of Transmission Lines

In order to show the benefits of T-shaped transmission line, let us compare a $\lambda/4$ conventional transmission line with a $\lambda/4$ T-shaped transmission line at the fundamental frequency. For the characteristic impedance of these transmission lines at $Z_0 = 100\Omega$, five cases of T-shaped transmission line with different attenuation are considered. Table 2.1 shows the calculated parameters, which are obtained from the developed design equations in (2.22) and (2.23). It should be noted that the shorter the electrical length of the stub, the higher the attenuating frequency location.

Figure 2.12 illustrates the transmission performances in magnitude and phase against normalized frequency ($f_n = f_i / f_0$) response of these transmission lines. No significant differences are observed in and around the center frequency, i.e., $f_n = 1$.

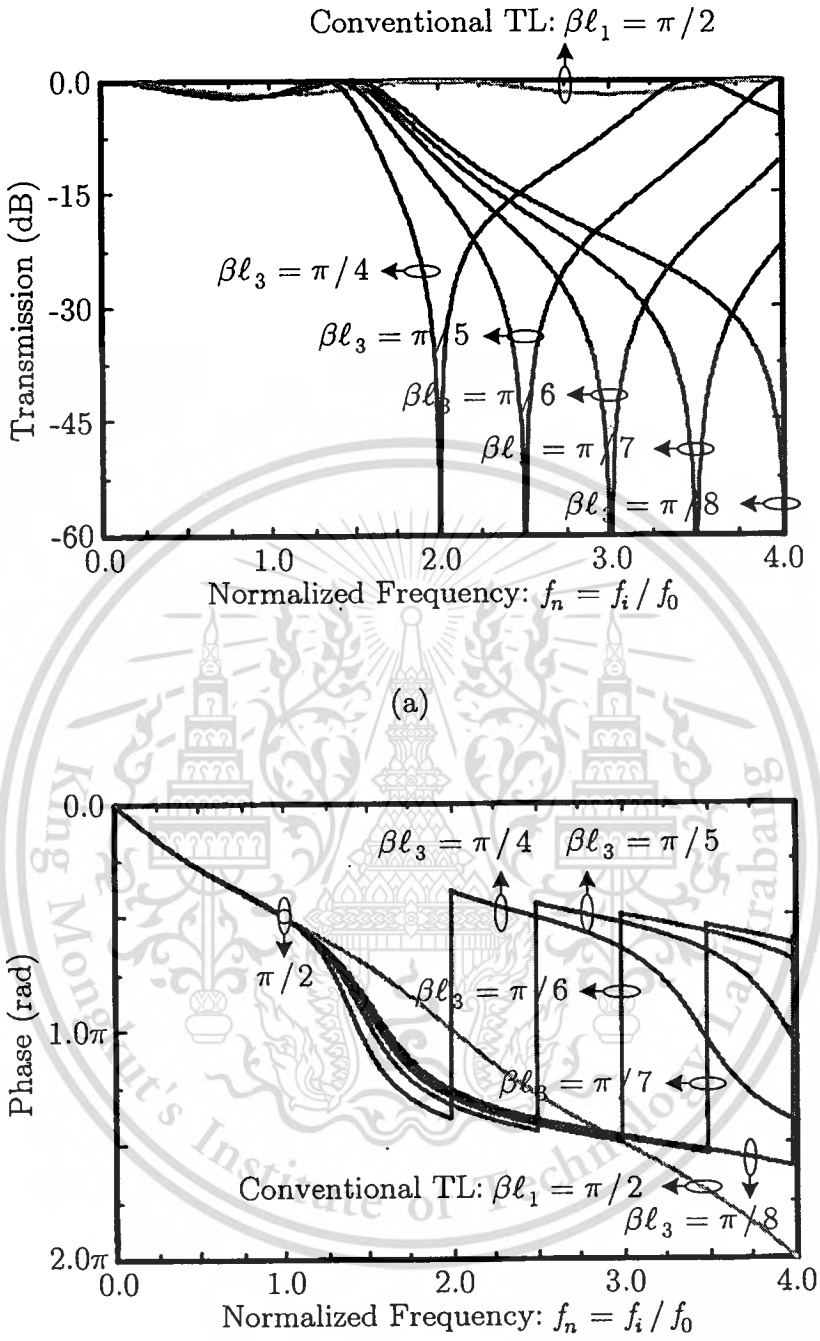

Figure 2.12 Simulated frequency response of T-shaped transmission line with $Z_0 = 100\ \Omega$ for $f_i/f_0 = 2$, 2.5, 3, 3.5, and 4. (a) Transmission response. (b) Phase response.

2.4 Compact Wilkinson Power Divider

Since a conventional Wilkinson power divider consists of two quarter-wavelength transmission lines, it is therefore large in size when operating in low frequency range. In addition, the spurious responses of this device at the harmonic frequencies may introduce undesired interference in various circumstances, which affects the performance of the circuit drastically, especially when the divider is applied in wireless systems.

2.4.1 Wilkinson Divider Considerations

In recent years, a miniaturized power divider using lumped elements has been proposed in [16]. This technique suffers from the low-Q factor problem. Another technique for miniaturization is to add capacitive loadings to a conventional microstrip line [52]. It is noted that, however, the size reduction of this design is rather limited. To eliminate the harmonic signals of a power divider, one can use an additional bandstop filter at the output ports to suppress the specific harmonic signals. However, this would also increase the passband insertion loss, cost, circuit size, and circuit complexity. Although, the defected ground structure (DGS) structure provides alternative way for miniaturization, the lack of an easily extracted equivalent circuit model of DGS makes this design in an unsystematic and troublesome approach [53]. Furthermore, the DGS requires a double-side fabrication that makes it difficult to maintain the repeatability. The slotted ground plane structure has been further implemented to microwave circuits for harmonic suppression. This structure, however, has a relatively limited ability to miniaturize the circuit size.

2.4.2 Wilkinson Divider's Planar Implementation

In this section, we will apply the T-shaped transmission line as previously mentioned in the section 2.3.2 to the conventional Wilkinson divider as described in section 2.2.1. The proposed Wilkinson power divider is therefore illustrated in Figure 2.13 [54].

The schematic of the proposed 3-dB Wilkinson without discontinuity can be shown in Figure 2.13(a). Typically, if all ports (port 1, port 2, and port 3) are matched with $Z_0 = 50\ \Omega$, the characteristic impedance of transmission

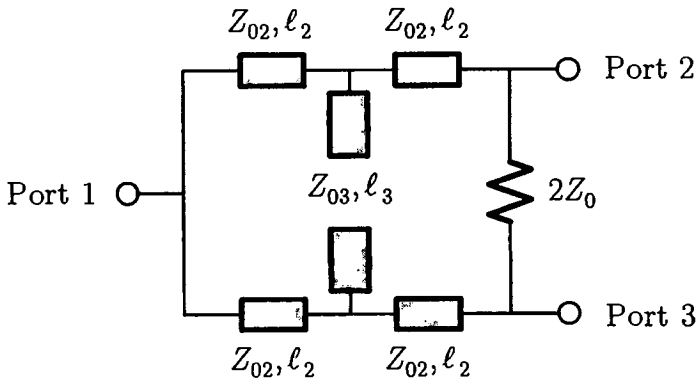

(a)

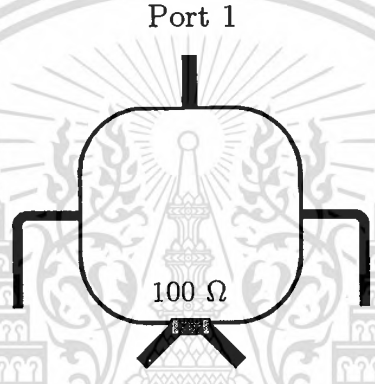

(b)

Figure 2.13 The proposed Wilkinson power divider (a) schematic and (b) layout.

lines are $Z_{01} = 70.7\ \Omega$ and an isolation resistor is $100\ \Omega$. In this case, we choose $\beta\ell_2 = \beta\ell_3 = \pi/6$ radian at $f_0 = 1$ GHz for miniaturizing the Wilkinson divider and suppressing third harmonic at 3 GHz, respectively. Using the equations in (2.21) to (2.23), the calculated characteristic impedance of Z_{02} and Z_{03} are $122.47\ \Omega$ and $61.24\ \Omega$, respectively.

The FR-4 substrate, as well as many other microwave substrates, has been selected to implement the proposed Wilkinson power divider in the planar structure. This FR-4 substrate has the substrate thickness of 0.8 mm, the relative dielectric constant of 4.55, the loss tangent of 0.02, and the copper metallization thickness of 18 μm. Based on the calculated parameters of the

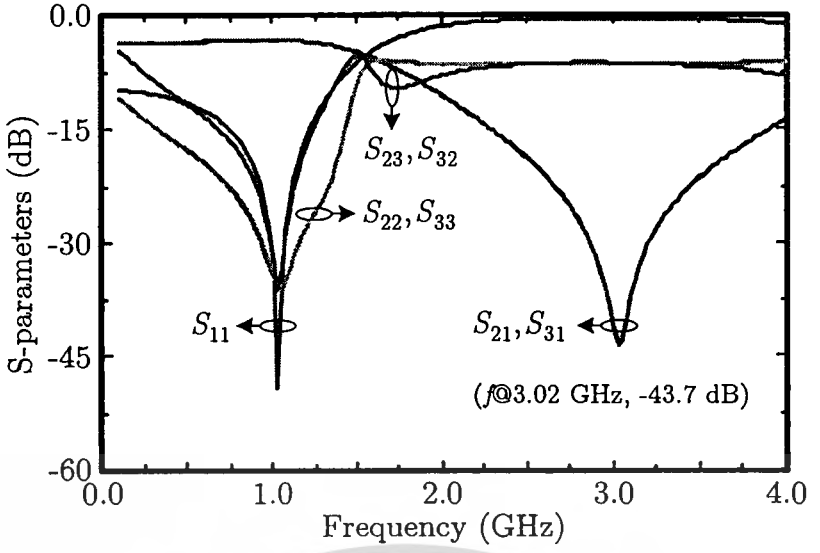

Figure 2.14 Simulated performances of the proposed Wilkinson power divider.

T-shaped line, the physical parameters such as width and length, are then synthesized by using LineCalc Tool in Agilent-ADS software. The final layout of Figure 2.13(a) is obtained as shown in Figure 2.13(b). It is noted that the bending form of open-stub and the curvature form of two transmission lines are chosen to achieve a more compact layout of T-shaped line. After creating the layout, it is then submitted for electromagnetic (EM) simulation with the help of a full-wave software for planar circuit produced by *SONNET™ Lite* [55]. The 0403 SMT resistor is used as a 100 Ω isolation resistor. The completed response can be obtained by using co-simulation between the data generated by EM simulator and the circuit level of an isolation resistor.

Figure 2.14 shows the EM-simulated results of the proposed Wilkinson divider. The simulated operating frequency is at 1.025 GHz. The simulated insertion losses (S_{21} and S_{31}) are less than -3.25 dB. An isolation between output ports (S_{23}) is greater than -35.83 dB at center frequency and less than -10 dB over 0.35 to 1.325 GHz. The reflection coefficient at the input (port 1) is better than -49.11 dB, whereas both output reflection coefficients are kept below -35.96 dB. Moreover, the amplitude imbalance and phase imbalance among the outputs are well balanced at less than 0.5 dB and 1 degree, respectively, over 0.1 to 4 GHz. The third harmonic frequency is deeply attenuated to below -43.7 dB.

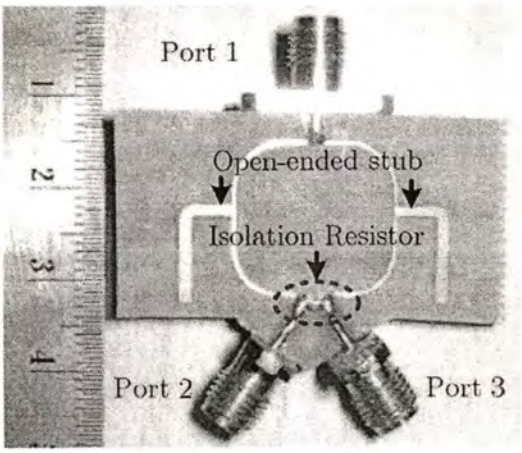

Figure 2.15 A photograph of the proposed Wilkinson power divider.

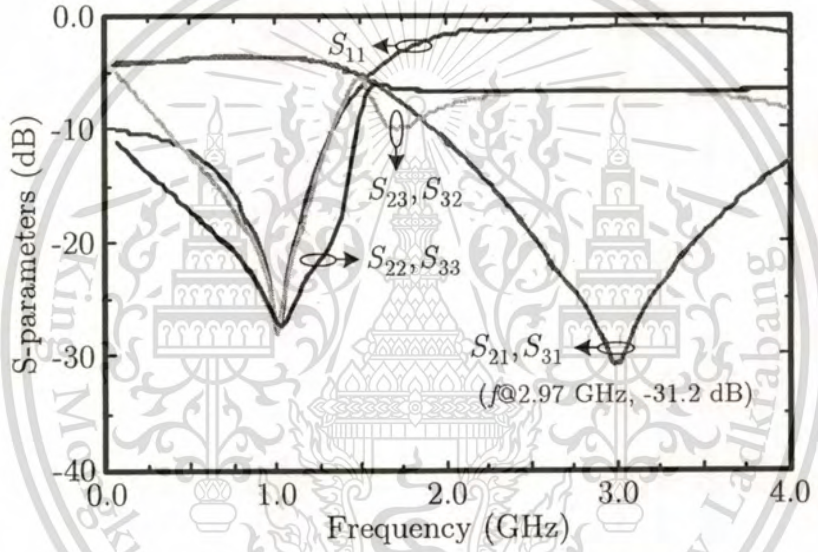

Figure 2.16 Measured magnitude performances of the proposed Wilkinson power divider.

2.4.3 Measurement Results

A photograph of the fabricated compact Wilkinson power divider is shown in Figure 2.15. The circuit size excluding three SMA-connectors is about 25 mm × 35 mm. Measurements are performed using an HP8510A vector network analyzer test system, which is calibrated using a standard two-port Short-Open-Load-Through (SOLT) calibration. Measured *S*-parameters for the compact Wilkinson power divider are shown in Figure 2.16.

A fairly good match between the simulated [cf. Figure 2.14] and measured [see Figure 2.16] is observed. The results match quite well up to 4 GHz. In Figure 2.16, the measured insertion losses are less than -3.48 dB at the operating frequency of 1.05 GHz, owing to mainly the conductor and tangent loss. The isolation and reflection coefficients are better than -10 dB at frequencies between 0.40 and 1.30 GHz, and better than -27.5 dB at operating frequency. Furthermore, the third harmonic frequency at 2.97 GHz is highly suppressed to below -31.2 dB. Note that the proposed structure provides not only a compact Wilkinson power divider, but also a spurious response suppression at the third harmonic frequency in the conventional Wilkinson divider.

2.5 Compact Quadrature Hybrid Coupler

The conventional Quadrature hybrid is composed of four sections. Each section is the quarter-wavelength transmission line with different characteristic impedances to provide the required performance. The major disadvantage of the Quadrature hybrid is that it occupies too large circuit area for microwave integrated circuits (MICs) and monolithic microwave integrated circuits (MMICs) applications. This results in a larger circuit area and a higher cost. Recently, wireless communication systems usually require smaller device size in order to satisfy circuit miniaturization and cost reduction. Thus, size reduction has become major design considerations for practical applications. Another important issue is the spurious response. This is due to the fact that the conventional transmission line in the Quadrature hybrid exhibits periodic response.

2.5.1 Quadrature Hybrid Considerations

Several design techniques have been reported to achieve the size reduction [18, 25, 28]. The straight forward approach is to replace transmission lines with lumped elements [28]. It is very effective for low frequencies, but quite inefficient at millimeter waves range due to the fact that capacitors are inaccurate in MMIC process and inductors are very lossy at high frequencies. Reduced-size Quadrature hybrid couplers were first demonstrated by Hirota et al. [18]. The technique used both lumped elements

and short high impedance lines to form an equivalent circuit of a section of transmission line. The coplanar waveguide (CPW) with metal-insulator-metal (MIM) capacitors has another issue to reduce circuit size [56]. In this case, air bridges, which are potentially expensive, are needed to eliminate slot-line mode excitation. A quasi-lumped element in microstrip configurations is another solution [57]. The Quadrature hybrid coupler without additional lumped elements and process on ground plane was described by the compensated spiral compact microstrip resonant cell (SCMRC) transmission lines [58]. The compensated SCMRC transmission line has considerable slow-wave effect for size reduction. The harmonic signals have been deeply suppressed due to the stop-band effect of SCMRC and open stub microstrip line resonator. However, this structure exhibits poor isolation performances. This technique can be used in various hybrid microwave integrated circuits (HMICs) and monolithic microwave integrated circuits (MMICs) without any additional process. However, this report does not give the design equations to achieve the desired performance.

2.5.2 Quadrature Hybrid's Planar Implementation

Figure 2.17(a) shows a conventional Quadrature hybrid. The characteristic impedances are $Z_{01}^{A} = 35.35\,\Omega$ and $Z_{01}^{B} = 50\,\Omega$. The lengths of each line, i.e., $\beta\ell_1^A$ and $\beta\ell_1^B$, are all $\pi/2$ radian. By applying the T-shaped transmission line, the proposed Quadrature hybrid having a compact size and harmonic rejection is shown in Figure 2.17(b) [54]. To obtain the electrical parameters, the ideal T-shaped transmission lines are also calculated by using the equations in (2.21) to (2.23).

Table 2.2 shows the calculated results for the proposed Quadrature hybrid at the center frequency in order to suppress the third harmonic frequency. At $\beta\ell_2^A = \beta\ell_3^A = \pi/6$ radian and $\beta\ell_2^B = \beta\ell_3^B = \pi/6$ radian, the overall electrical length of each T-shaped transmission line is about 33.3 % more compact than the conventional quarter-wavelength transmission line. When the center frequency = 2 GHz, the simulated results of the conventional Hybrid are shown in Figure 2.18(a). Those of the proposed Quadrature hybrid are also demonstrated in Figure 2.18(b).

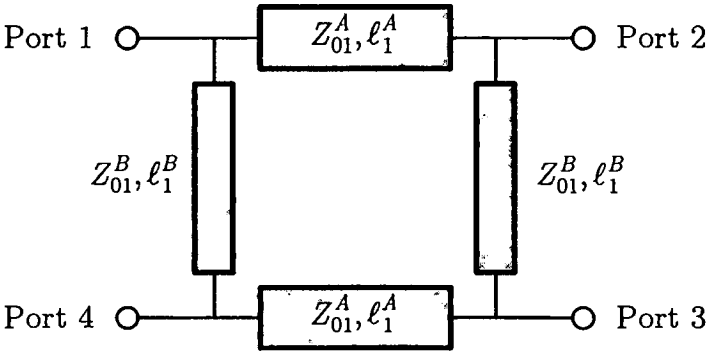

(a)

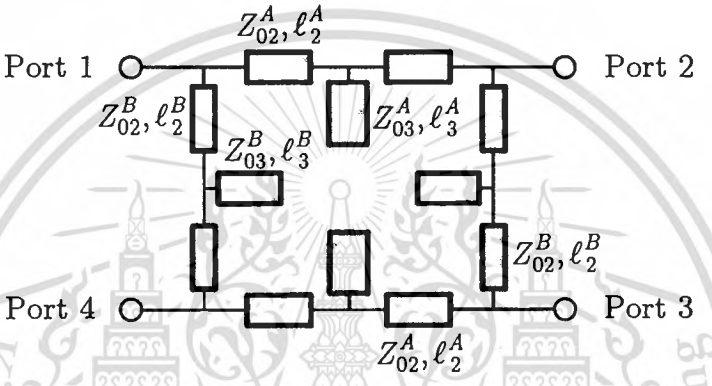

(b)

Figure 2.17 Schematics of the (a) conventional Quadrature hybrid and (b) proposed Quadrature hybrid couplers.

Table 2.2 Calculated results for the proposed Quadrature hybrid.

Conventional Parameters	Proposed Parameters
$Z_{01}^{A} = 50/\sqrt{2}\ \Omega$	$Z_{02}^{A} = 61.23\ \Omega$ $Z_{03}^{A} = 30.62\ \Omega$
$\beta\ell_1^{A} = \pi/2$ rad	$\beta\ell_2^{A} = \pi/6$ rad $\beta\ell_3^{A} = \pi/6$ rad
$Z_{01}^{B} = 50\ \Omega$	$Z_{02}^{B} = 86.60\ \Omega$ $Z_{03}^{B} = 43.30\ \Omega$
$\beta\ell_1^{B} = \pi/2$ rad	$\beta\ell_2^{B} = \pi/6$ rad $\beta\ell_3^{B} = \pi/6$ rad

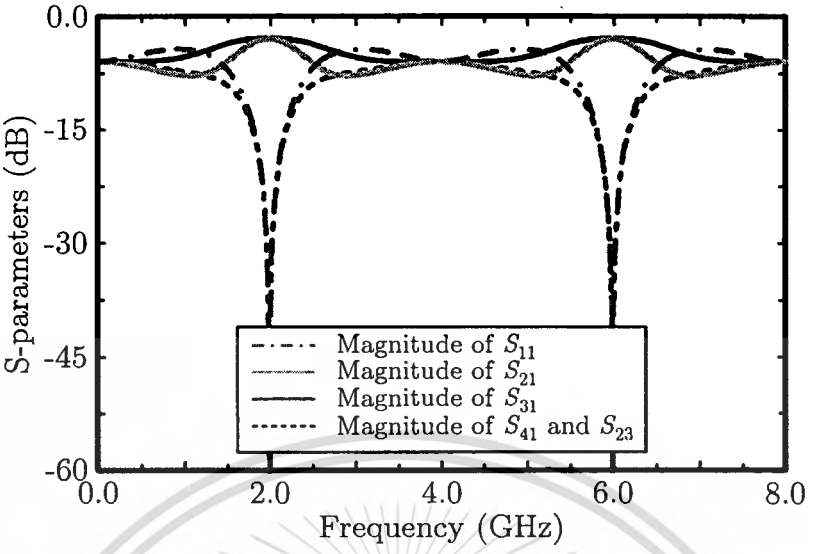

(a)

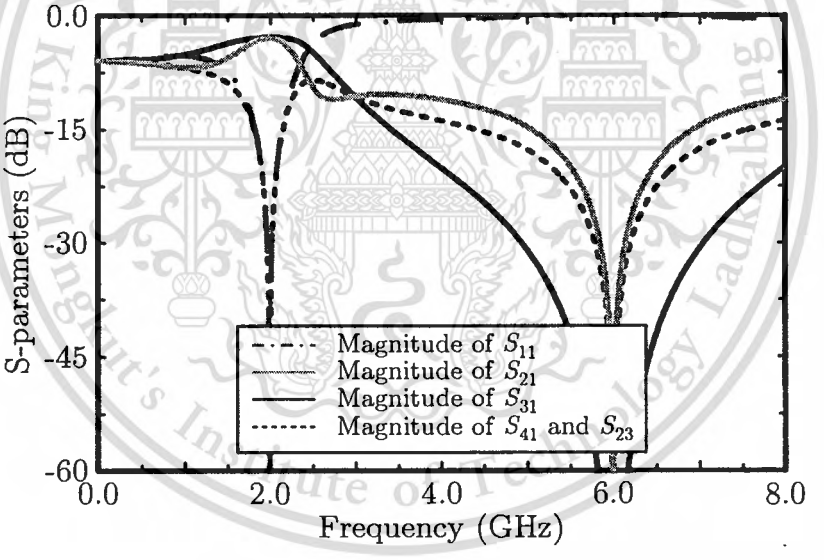

(b)

Figure 2.18 Simulated results based on the ideal transmission line of the (a) conventional Quadrature hybrid and (b) proposed Quadrature hybrid couplers.

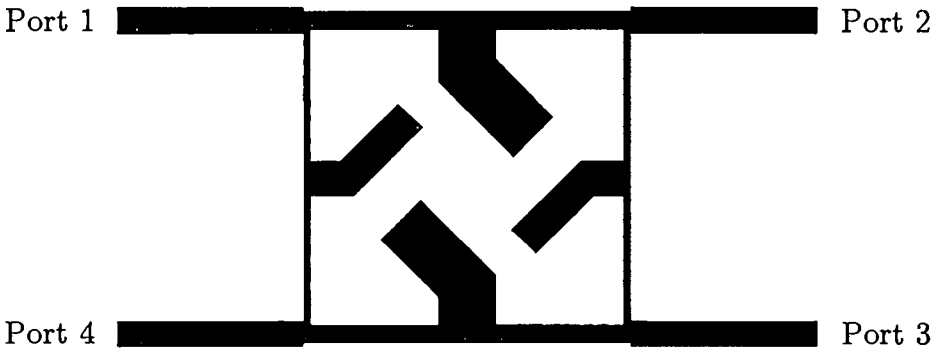

Figure 2.19 Layout of the proposed Quadrature hybrid coupler.

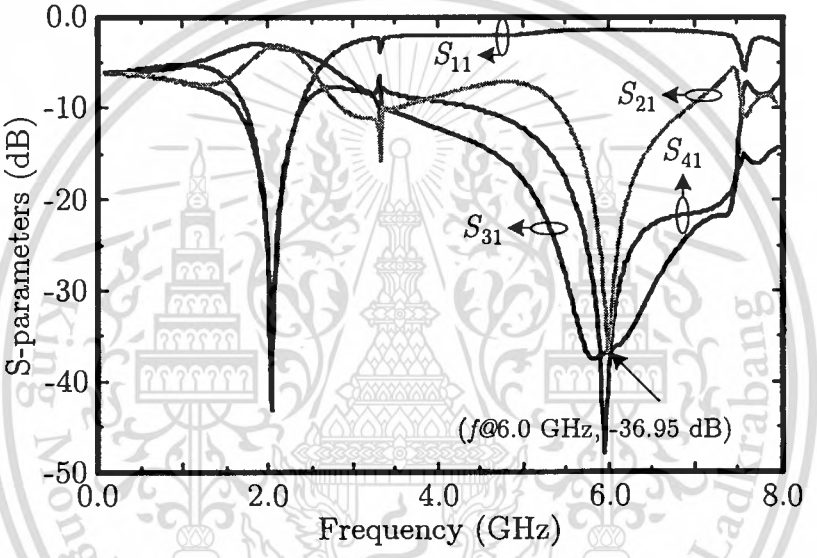

Figure 2.20 Simulated results based on the layout as shown in Figure 2.19.

An important characteristic between the transmission coefficients of Figure 2.18(a) and (b) is that the inclusion of open-stub in T-shaped transmission line can be rejected the spurious response at third harmonic frequency with no effect on the center passband response. This thus implies that the T-shaped line acts as bandstop characteristic located at the third harmonic if we select $\beta\ell_3^A = \beta\ell_3^B = \pi/6$ radian, while the T-shaped line has the same characteristics as the original line at the fundamental frequency.

To validate the design concept, the prototype of a compact Quadrature hybrid was designed and the physical parameters were synthesized on an FR-4

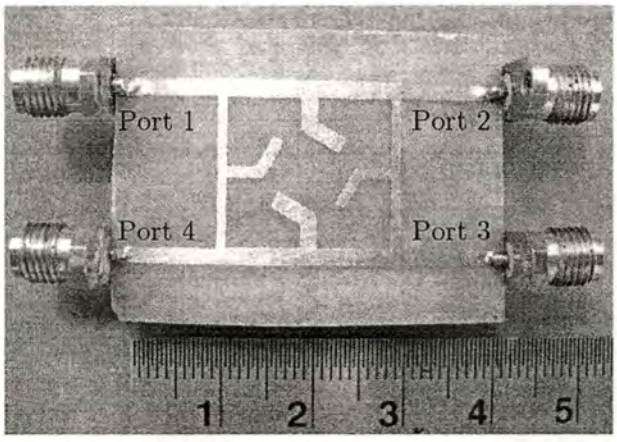

Figure 2.21 A photograph of the proposed Quadrature hybrid coupler.

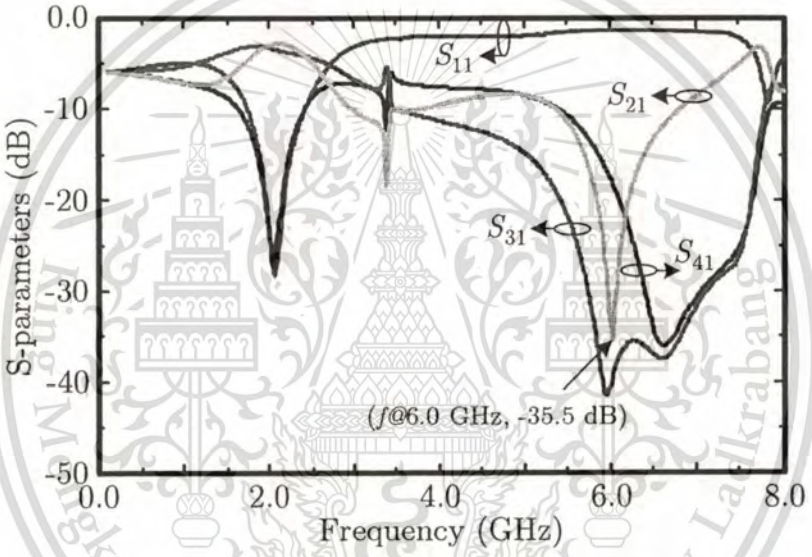

Figure 2.22 Measured results based on the fabrication as shown in Figure 2.21.

substrate. The layout of proposed Quadrature hybrid in the microstrip structure is shown in Figure 2.19. Figure 2.20 shows the EM-simulated results by using full-wave field solver for planar circuit, produced by *SONNET™ Lite* [55]. The center operating frequency and the third harmonic frequency are inspected. In the figure, the center frequency is located at 2 GHz with insertion losses (S_{21} and S_{31}) of -3.32 dB. Both input reflection coefficient at port 1 (S_{11}) and isolation between port 1 and port 4 (S_{14}) are kept below -40 dB. By inspecting at 6 GHz, it can be clearly observed that the prototype Quadrature hybrid exhibits transmission notch of the incident wave along the T-shaped transmission line at 6 GHz, thus introducing a total reflection at the

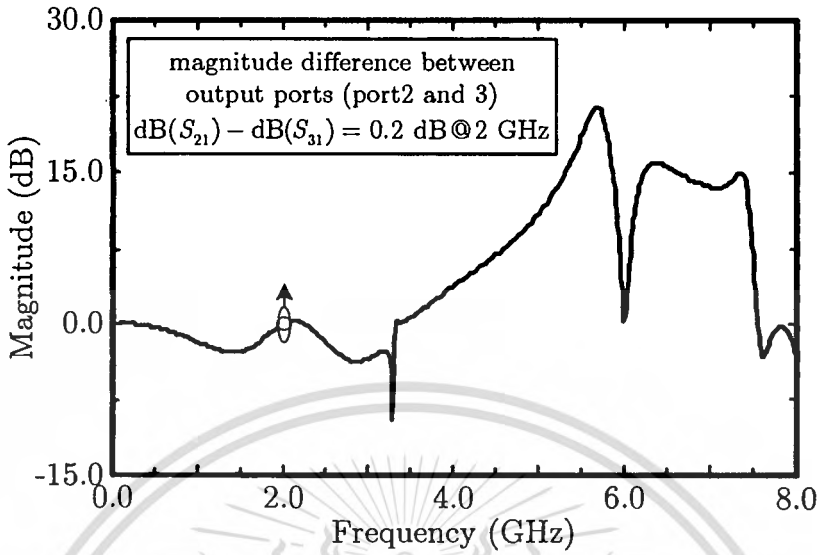

(a)

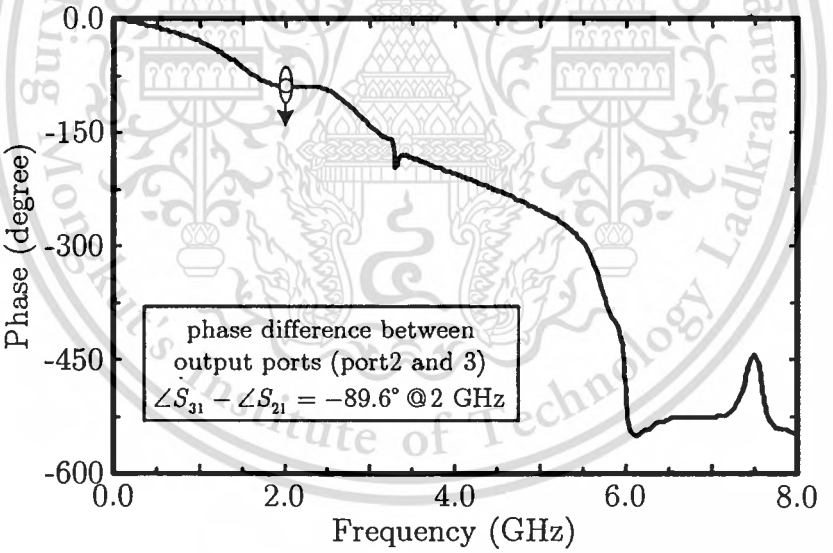

(b)

Figure 2.23 Measured results. (a) Magnitude imbalance. (b) Phase imbalance.

input port. The harmonic suppression is more than -36.95 dB at the third harmonic frequency. This is a remarkable advantage of the proposed size-reduction method.

2.5.3 Measurement Results

Figure 2.21 shows the fabricated Quadrature hybrid coupler, realized in the microstrip transmission line, which occupies 40 mm × 30 mm of PCB area excluding four-SMA connectors. The S-parameters are performed using an HP8510A vector network, which is calibrated using a SOLT calibration. As seen in Figure 2.22, the measured insertion losses (S_{21} and S_{31}) are about -3.6 and -3.8 dB, respectively, whereas both input and isolation losses (S_{11} and S_{14}) are kept below -28.5 dB at center frequency of 2.025 GHz. The measured third harmonic is lower than -35.5 dB. The prototype hybrid exhibits good isolation of -37 dB at 6.6 GHz, which is higher than the third harmonic due to our fabrication. The measured amplitude imbalance [see Figure 23(a)] and phase difference [see Figure 23(b)] between the two output ports are 0.2 dB and 89.6° over the operating frequency. Parts of these differences are due to the uncertainty of the fabrication process.

2.6 Chapter Summary

In this chapter, two microwave passive devices, namely the Wilkinson power divider and Quadrature hybrid coupler have been presented based on the T-shaped transmission line. Since the conventional passive devices employ the quarter-wavelength transmission line in the structure, they have relatively large size. The substitution of conventional transmission line with T-shaped line can be overcome this problem. This is because an open-ended stub is properly incorporated in the T-shaped line presenting slow-wave effect for size reduction and it acts as a series resonance at the unwanted harmonic frequency enhancing the spurious response in the conventional passive devices. The proposed microwave devices are very attractive to alleviate transmitter harmonic distortions in microwave systems. The measured results prove the validity and suitability of the technique for wireless communication applications.

CHAPTER 3
DUAL-MODE RING FILTER USING ARTIFICIAL LINE

The project motivations of dual-mode ring resonator and its application to bandpass filter are briefly introduced in Section 3.1. In section 3.2, we begin with the single-mode resonator and its perturbation schemes, i.e., series stub, shunt stub, series-capacitance, and shunt-capacitance perturbation, to achieve dual-mode response. However, some techniques cannot be realized in the conventional fabrication. The feeding structures are described in Section 3.3. The artificial transmission line with a symmetrical structure as detailed in Section 3.4 may be considered at the center frequency of operation. Section 3.5 conducts the analysis based on lossless lumped model of transmission line segment through the characteristic impedance and phase constant. Section 3.6 describes the design and demonstration of dual-mode ring bandpass filters in planar structure at 2.45 GHz for industrial, scientific, and medical (ISM) radio by using symmetrical artificial transmission line in the *right-* and *left-*handed forms. Section 3.7 summarizes the chapter with conclusion.

3.1 Introduction

Microwave filters play important role in many wireless communication systems, such as satellite and mobile communication systems [59]. In such kind of systems, many factors such as compact size, low cost, light weight, high performance, and low loss, are of primary importance for designing microwave filters [60-61]. The filters can be realized in different structures [47, 59-61]. By comparing the microstrip and waveguide filters, the microstrip filters are smaller in size and lighter weight than waveguide filters. In such applications mentioned before, they require microstrip filters.

Among various bandpass configurations, the dual-mode ring filters have been extensively used due to their attractive features [13, 35-42, 62-69] such as compact size, high selectivity, high-quality factor, and ease of design and

fabrication. A ring resonator filter can be seen as an asynchronously tuned resonant circuit [35], the two degenerated modes of which can be excited by a perpendicular feed-line structure with different forms of perturbations [35-42, 62-69]. Since a dual-mode ring resonator operates as a doubled-tuned resonant circuit, the filter order can be reduced to halved number of resonator achieving compact in size when it is use to implement a bandpass filter. These are main advantages of the dual-mode ring filter.

3.2 Dual-Mode Ring Resonator

The microstrip ring resonator was first introduced by P. Toughton in 1969 [70] for measuring the dispersive characteristic and phase velocity of a microstrip line. The dual-mode characteristic of the ring resonator was further intensively analyzed in 1971 by Wolff and Knoppik [71]. After the bandpass filters based on the dual-mode ring resonator has been investigated in 1972 [35], numerous researchers have extensively proposed various configurations for dual-mode filter [35-42, 62-69].

3.2.1 Principal Operation

Figure 3.1 shows a microstrip ring resonator weakly coupled to the feed lines. It consists of two feed-lines, two coupling-gaps, and a ring resonator. The ring resonator is merely a transmission line formed in a closed loop. Two reference planes at AA' and BB' are included in the figure for future reference. For a single ring resonator, the resonant frequency is established when the mean circumference of the ring resonator is equal to an integral multiple of the guided wavelength. This may be expressed as

$$\ell = 2\pi r = n\lambda_g, \qquad \text{for } n = 1, 2, 3,... \tag{3.1}$$

where ℓ represents the circumference of the ring, r is the mean radius of the ring that equals the average of the outer and inner radii, λ_g is the guided wavelength, and n is the mode number.

The λ_g is related to the effective dielectric constant as

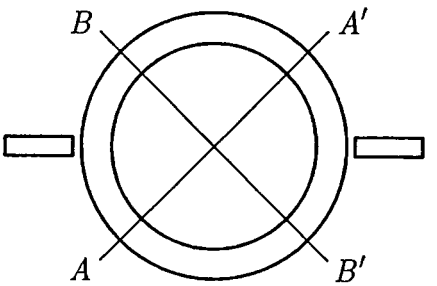

Figure 3.1 Weakly coupled microstrip ring resonator.

$$\lambda_g = \frac{\lambda_0}{\sqrt{\varepsilon_{eff}}}, \tag{3.2}$$

where λ_0 is the wavelength in free space and ε_{eff} is the effective dielectric constant of a microstrip line. Thus, the resonant frequency f_0 can be represented as

$$f_0 = \frac{nc}{2\pi r\sqrt{\varepsilon_{eff}}}, \qquad \text{for } n = 1, 2, 3,\ldots \tag{3.3}$$

where c is the speed of light.

To understand the basic phenomena underlying the operation of the ring resonator, it is imperative to first understand its field configuration for the different modes. The absolute values of maximum field points for the first four modes are depicted in Figure 3.2 [61], where the field is minimum midway between these points. In the absence of the slits or other discontinuities, a maximum field point occurs where the feed line excites the resonator. This point is independent of the azimuthal position of the feed line that extracts microwave power. This is important from the standpoint of mode suppression. For example, it can be seen from Figure 3.2 that when the azimuthal angle $\phi = 90°$, there is a field minimum for the first and third modes. These modes and other higher-order odd modes can be suppressed if the feed line that extracts power is located at $\phi = 90°$. In the presence of discontinuities such as slits, the fields in the resonator readjust themselves, so as to first satisfy the boundary conditions caused by the slits in the resonator.

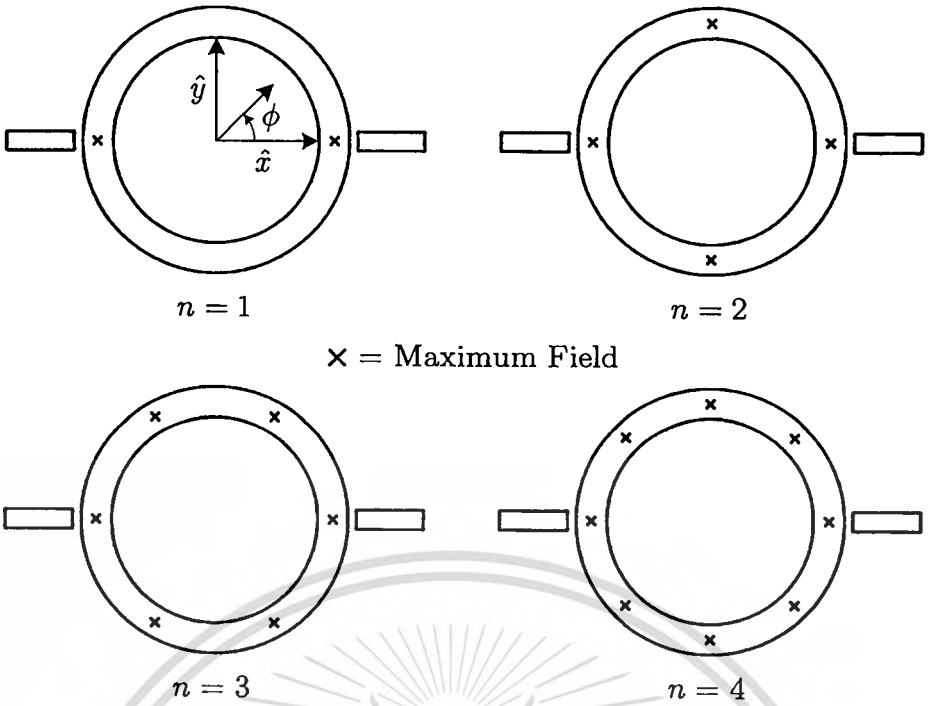

Figure 3.2 Maximum field points for the first four modes.

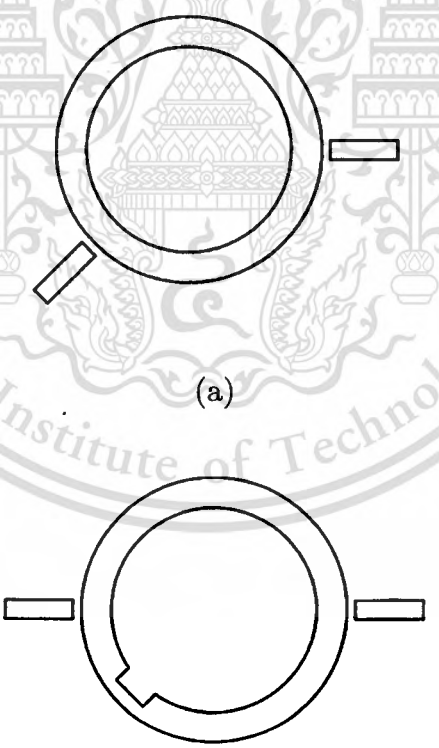

(a)

(b)

Figure 3.3 Arrangements of dual-mode ring resonator (a) asymmetrical feel-lines and (b) symmetrical feed-lines with notch perturbation.

In other words, if there are slits, then the maximum field point is not necessarily collinear with the feed line that excites the resonator.

A ring resonator circuit is an asymmetric structure. This is because when bisected one-half, it is not a mirror image of the other. Asymmetries are first introduced [35] either by skewing one of the feed lines with respect to the other [see Figure 3.3(a)], or by the introduction of a discontinuity (notch, slit, patch, etc.) [see Figure 3.3(b)]. This results in the generation of two split modes.

3.2.2 Dual-Mode Ring Resonator with Different Perturbation Topologies

The dual-mode ring resonators have been extensively investigated by using orthogonal feed-lines with various perturbations on the ring [42, 65-68]. When implementing a bandpass filter based on the ring resonator, it introduces two transmission zeros close to the passband. This implies that the ring filter can be used to enhance interference suppression of adjacent channels in communication systems.

General conditions to form dual-mode ring resonator are as follow:

i) The input and output ports should be spatially separated $\pi/2$ radians from each other.

ii) A discontinuity or some means of generating reflected waves against incident waves should exist within the resonator at a location that is offset $3\pi/4$ radians from the input and output ports.

iii) A plane of symmetry should exist in the circuit geometry.

3.2.2.1 Series Stub Perturbation [42]

Figure 3.4 shows a dual-mode resonator realized by changing the characteristic impedance of the ring transmission line in a step manner at certain position. The coupling strength between the orthogonal resonant modes can be controlled by both the impedance ratio of the stepped perturbation to the ring, and the length of the stepped transmission line. The introduction of lower stepped impedance than the characteristic impedance of the ring is displayed in Figure 3.4. Figure 3.5 shows the corresponding frequency responses simulated using Agilent-ADS [72]. Typical resonance

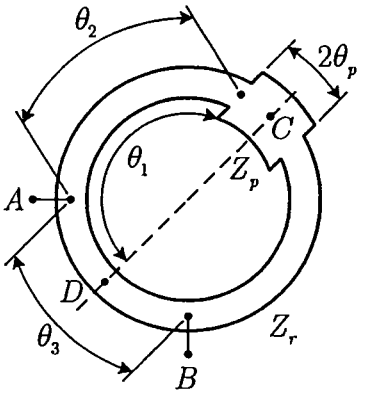

Figure 3.4 Structure of dual-mode filter applying an impedance step as perturbation.

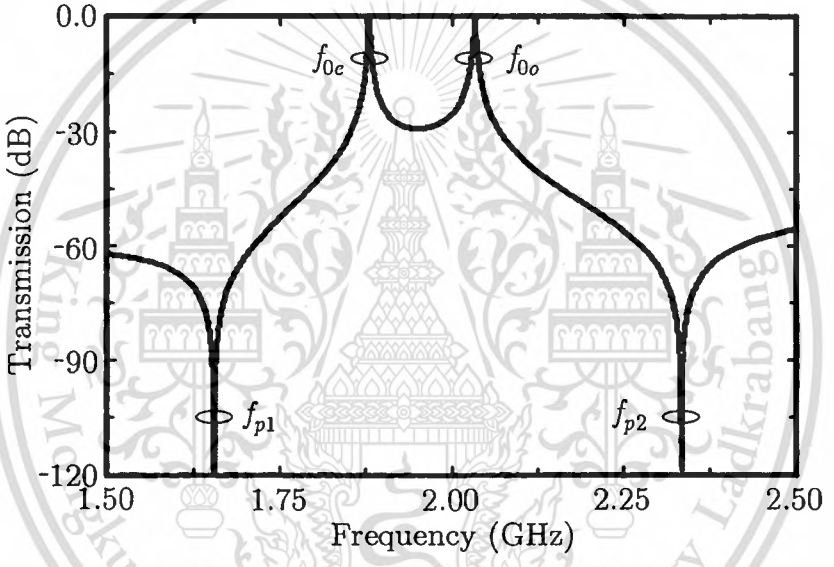

Figure 3.5 Example of resonance characteristic of stepped impedance type dual-mode resonator.

characteristic of the ring possess two resonance frequencies accompanied by attenuation poles on both sides. The center passband frequency shifted down to a lower passband frequency is observed in the figure. This is caused by the total *effective* length of the ring over than that of the original ring filter ($> 2\pi$ radian at f_0).

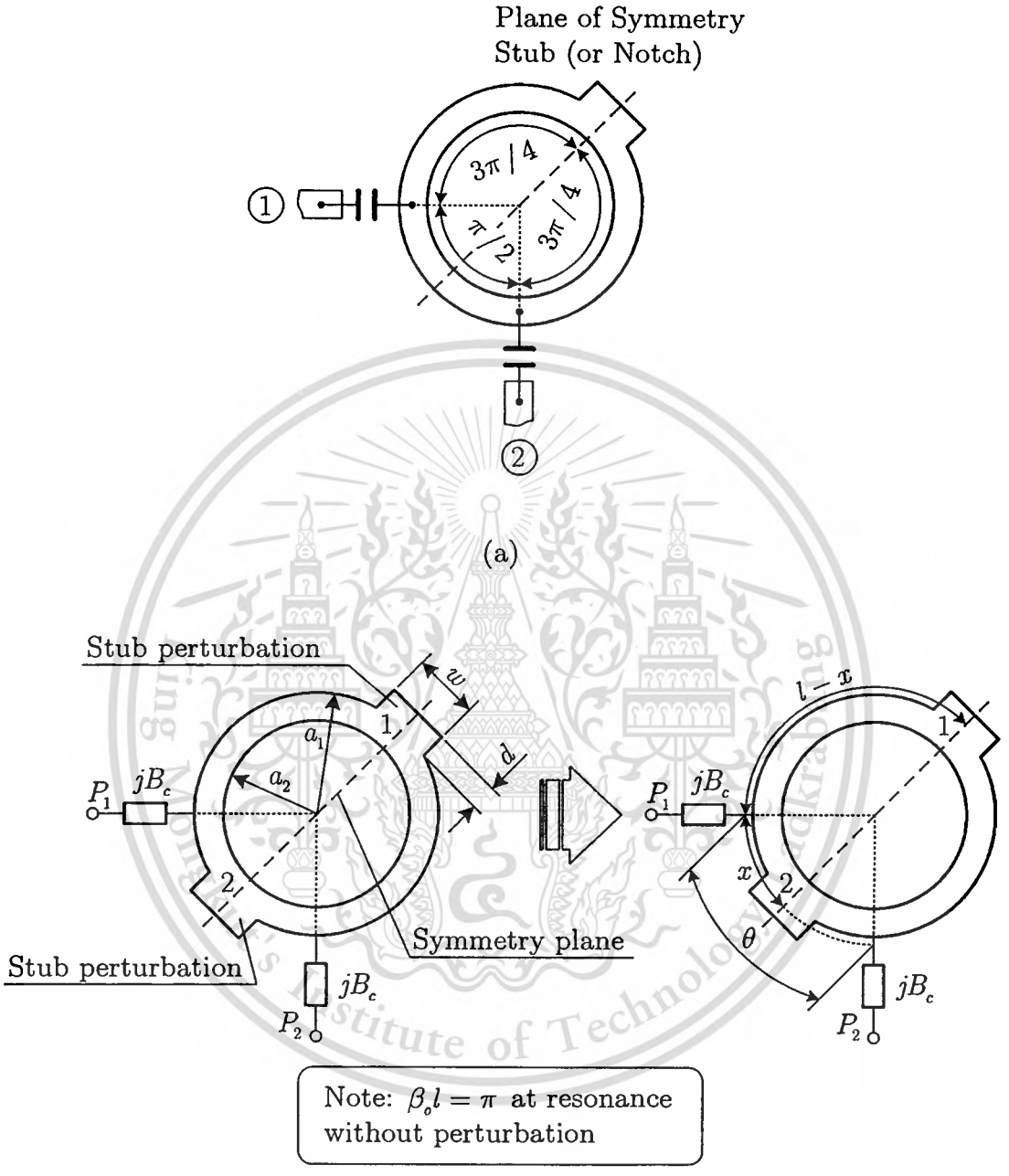

Figure 3.6 Structure of dual-mode filter applying shunt stub as perturbation at (a) $3\pi/4$ radians, and (b) $3\pi/4$ and $\pi/4$ radians from input and output ports.

3.2.2.2 Shunt Stub Perturbation [65-67]

The basic structure of a dual-mode resonator is shown in Figure 3.6. The coupling between two orthogonal modes can be accomplished by introducing the shunt stub perturbation within the resonator. Since the input and output ports are spatially separated $\pi/2$ radians from each other, two possible cases may be introduced within the resonator at two locations that are offset $3\pi/4$ radians and/or $\pi/4$ radians from input and output ports. The resonance and attenuation characteristics are also observed and determined by forcing the coupling between two feed lines and ring resonator under weak condition.

3.2.2.3 Series-Capacitance Perturbation [68]

By focusing the reference planes as previously shown in Figure 3.1 (Section 3.2.1), when a perturbation is introduced either along AA' or BB', reflections are generated in the two opposing traveling waves propagating along the ring [59]. This results in the generation of two split modes. Depending on the magnitude of the reflected waves, it will influence the level of coupling and bandpass response results. Perturbations in the form of a stepped impedance [42] and shunt stub [65-67] along one of the principal diagonals AA' or BB' have been reported. However, a single pair of perturbation with the use of shunt stub along AA', as described in [65-66], is able to influence only the even-mode frequency. This fact is later generalized in [62], whereby a single pair of perturbation is able to control the split modes. Although simultaneous control of the split modes is allowed in [42], a small impedance ratio might be difficult for a realization where a narrowband response is required.

Figure 3.7 indicates the structure of a dual-mode ring resonator, which is obtained from the introduction of series lumped-capacitors at both AA' and BB' planes. This technique relieves the burden which relies on high capacitance for narrowband filter design. However, for a practical implementation, the lumped-capacitor with high capacitance exhibits a relatively low self-resonant frequency since the extrinsic parameters associated

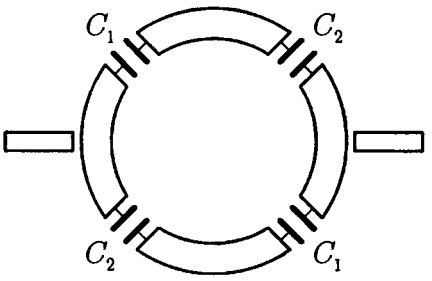

Figure 3.7 Structure of dual-mode ring filter using series-capacitance perturbation.

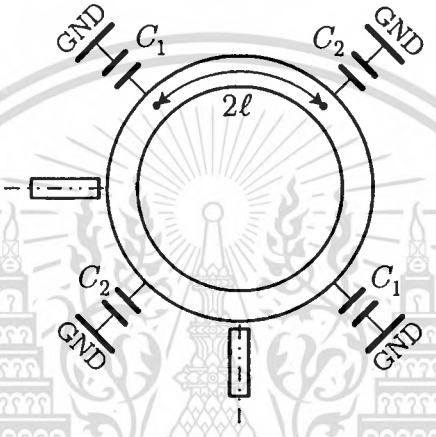

Figure 3.8 Structure of dual-mode ring resonator using shunt-capacitance perturbation.

with structure is relatively large. This technique is not suitable for high-frequency operation. This is a major drawback of this configuration. Another disadvantage is that the total circumference of the ring for the series capacitance perturbation must be greater than one wavelength to satisfy the resonant conditions.

3.2.2.4 Shunt-Capacitance Perturbation [69]

Figure 3.8 describes a dual-mode ring resonator using shunt capacitance perturbations at the symmetry and anti-symmetry plane. The even- and odd-mode resonances of the ring resonator, based on the even- and odd-mode analysis, are governed independently by C_2 and C_1, respectively. The ring resonator can be reduced significantly in size by increasing C_1 and C_2 which depends on self-resonant frequency of their lumped-capacitors.

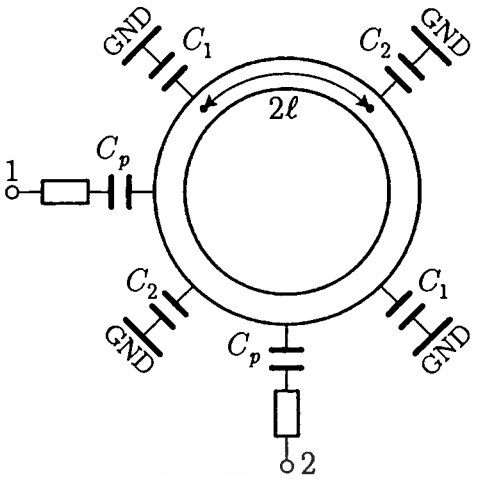

Figure 3.9 Structure of the coupling feed ring bandpass filter.

Furthermore, the shunt configuration allows easier bias, making varactor-tuned filters realizable for this type of resonator. The possibility of tunable frequency response of this structure makes it attractive for monolithic microwave integrated circuits (MMICs) and system-on-chip (SOC) applications.

3.3 Dual-Mode Ring Based Bandpass Filter

When the resonator is weakly coupled, the resonator characteristics are basically the same as the analysis based on the even- and odd-mode excitations since the coupling capacitance affects the resonator characteristics very little. In filter applications, a minimum insertion loss is required at the passband characteristic, which means that the resonator is connected to the signal path via relatively large capacitors.

3.3.1 Coupling Feed Structure

Figure 3.9 illustrates the schematic of the ring resonator used as filter, which is similar to Figure 3.8 with the inclusion capacitance C_p between two feed-lines and ring resonator. The value of C_p depends on the minimization of the insertion loss (S_{21}) of the entire filter with flat response at the passband. However, the relatively large capacitance will affect the resonance characteristic, possibly affecting the coupling coefficient (k). The effects of the

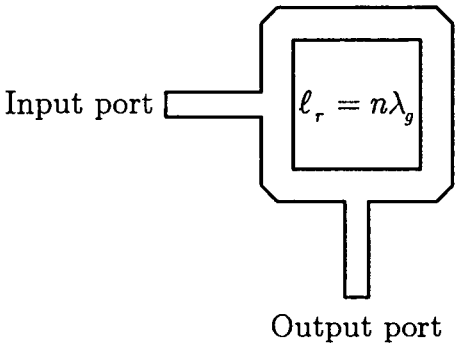

Figure 3.10 Structure of the direct-connected orthogonal feed ring bandpass filter.

added capacitors C_p must be taken into account for a more accurate filter design.

3.3.2 Direct Feed Structure

A ring resonator directly connected to a pair of orthogonal feed–lines is demonstrated in Figure 3.10 [43]. In this case, no coupling gaps are used between the resonator and the feed lines for low insertion loss. There are no mismatch and radiation loss between feed-lines and ring resonator. The ring filter can thus obtain a low insertion loss. This implies that the major losses of the filter are contributed only by dielectric and conductor losses.

3.4 Artificial Transmission Lines

A transmission line can be modeled as a distributed network circuit consisting of a periodic structure of inductors, capacitors, and resistors. In a lossless line, we will have only capacitors and inductors as shown in Figure 3.11. Each infinitesimal element of length Δz along the line is a circuit with a total inductance of $L\Delta z$ and a total capacitance of $C\Delta z$. L and C are in units of inductance and of capacitance per unit lengths, respectively. A physical approximation to the distributed model circuit is therefore a circuit consisting of lumped inductances and capacitances.

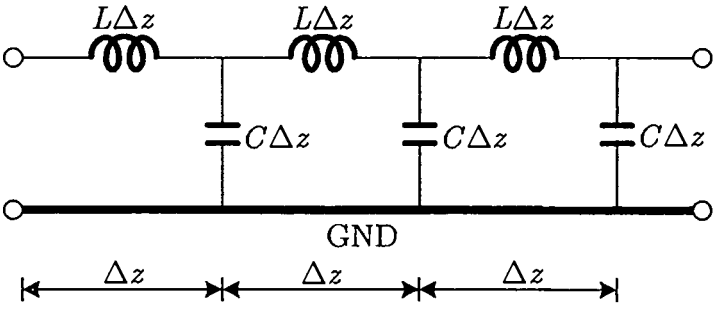

Figure 3.11 Schematic of the lossless transmission line.

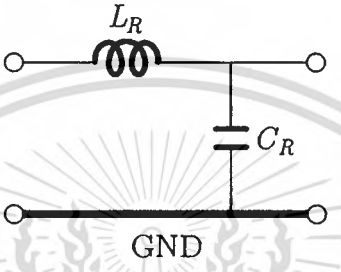

Figure 3.12 Unit-cell equivalent circuit model of the right-handed transmission line.

In exploring the properties of wave propagation in a lumped-element transmission line, a single section of the periodic structure will be examined.

3.4.1 Right-Handed Transmission Line: RH-TL

The unit-cell equivalent circuit model for a right-handed transmission line under lossless condition is described in Figure 3.12 [73]. Its configuration contains a series inductor and a shunt capacitor. The transmission approach of right-handed materials is obviously of a lowpass characteristic.

The propagation constant of the right-handed transmission line can be determined as

$$\beta_R = \omega\sqrt{L_R C_R} > 0\,, \tag{3.4}$$

where the subscript R designates the *right*-handed transmission line. The phase response of the unit cell can be expresses as

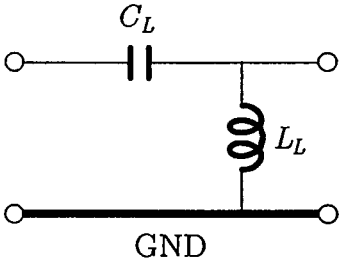

Figure 3.13 Unit-cell equivalent circuit model of the left-handed transmission line.

$$\varphi_R = -\arctan\left[\frac{\omega(L_R / Z_{0R} + C_R Z_{0R})}{2 - \omega^2 L_R C_R}\right] < 0\,, \tag{3.5}$$

where the characteristic impedance of the right-handed transmission line Z_{0R} is given as

$$Z_{0R} = \sqrt{\frac{L_R}{C_R}}\,. \tag{3.6}$$

3.4.2 Left-Handed Transmission Line: LH-TL

The transmission line approach of left-handed materials is based on the *electrical dual* of the conventional transmission line, where the equivalent circuit is shown in Figure 3.13 [73]. This circuit, obtained by interchanging the inductance/capacitance and inverting the series/parallel arrangements in the equivalent circuit of the conventional right-handed transmission line, is obviously of a highpass characteristic.

Using a similar analysis, the propagation constant of the left-handed transmission line can be calculated from

$$\beta_L = -\frac{1}{\omega\sqrt{L_R C_R}} < 0\,, \tag{3.7}$$

where the subscript L designates the *left*-handed transmission line. The phase-rotation of the unit cell is given by

$$\varphi_L = -\arctan\left[\frac{\omega(L_L / Z_{0L} + C_L Z_{0L})}{1 - 2\omega^2 L_L C_L}\right] > 0\,. \tag{3.8}$$

The characteristic impedance of the left-handed transmission line Z_{0L} is given as follows

$$Z_{0L} = \sqrt{\frac{L_L}{C_L}}\,. \tag{3.9}$$

Equation (3.9) shows that this left-handed transmission line can reduce the limitation of practical concern when implementing a microstrip. The left-handed transmission line is characterized by a negative propagation constant and positive phase response or phase advance. These unique features may be exploited in the design of new types of microwave circuits.

3.5 Characteristic of Stepped Impedance Ring Resonator

The structure in Figure 3.4 can be analyzed using even-odd-mode analysis [50]. For the sake of simplicity, the discontinuity between the ring resonator and the perturbation is neglected and the lossless transmission line is also assumed. By dividing the ring resonator along the plane of symmetry, the resonance frequency in even-mode and odd-mode can be obtained. In addition, the principle of a two port network must be used to calculate the attenuation pole frequencies occurring in the ring resonator.

3.5.1 Even-Mode Analysis

Let us consider the stepped ring resonator as also shown in Figure 3.4 [42]. Z_r is the characteristic impedance of the ring and Z_p is the characteristic impedance of the perturbation. For the case of $Z_r = Z_p$, the structure is a simple ring resonator. It is implied that the perturbation does not exist in the ring structure (without perturbation). At reference plane of symmetry, the electrical length from Point C to D is π at the fundamental frequency of the ring f_r.

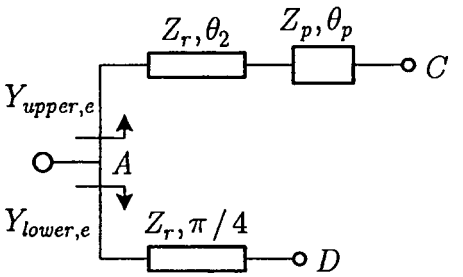

Figure 3.14 Equivalent circuits of the stepped impedance dual-mode ring resonator under even-mode excitation.

Using ideal transmission-line model, Figure 3.14 illustrates the equivalent circuits for even-mode excitation, where a magnetic wall is applied along the symmetry plane of $C - D$, which is an open circuit at this plane. The circuits are a cascaded connection of transmission lines. When the electrical length of the perturbation is $2\theta_p$ at the fundamental frequency of the transmission line, the electrical length θ_2 from Point A to the step is thus equal to $\theta_2 = \theta_1 - \pi/4$ since the electrical length from Point A (or B) to D is $\pi/4$ radian. The electrical length θ_1 from Point D to the step is $\pi - \theta_p$. This means that the electrical length θ_3 from Point A to C with counterclockwise is $3\pi/4$ radian.

Also indicated in Figure 3.14 is an equivalent circuit of even-mode excitation acting as a shunt circuit configuration. It consists of upper and lower sections. The *input* admittance of upper section $Y_{upper,e}$ is expressed as

$$Y_{upper,e} = \frac{Z_r + jZ_{in1,e}\tan\theta_2}{Z_r(Z_{in1,e} + jZ_r\tan\theta_2)}, \tag{3.10}$$

where $Z_{in1,e} = -jZ_p\cot\theta_p$ is the *input* impedance of perturbation with θ_p for open-ended transmission line.

The lower-half *input* admittance $Y_{lower,e}$ is given as

$$Y_{lower,e} = \frac{j\tan(\pi/4)}{Z_r}. \tag{3.11}$$

Therefore, the *input* admittance of the even-mode Y_e can be determined by

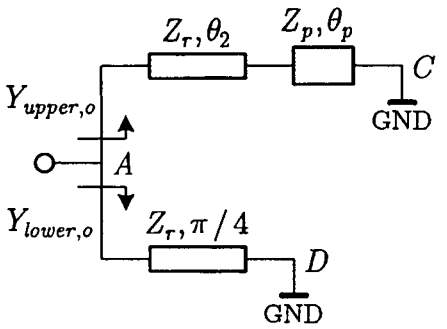

Figure 3.15 Equivalent circuits of the stepped impedance dual-mode ring resonator under odd-mode excitation.

$$Y_e = Y_{upper,e} + Y_{lower,e} . \tag{3.12}$$

By letting $Y_e = 0$, the even-mode resonance frequency f_{0e} can be obtained under the condition as follows

$$K \tan\left(\theta_1 \frac{f_{0e}}{f_r}\right) + \tan\left(\theta_p \frac{f_{0e}}{f_r}\right) = 0 , \tag{3.13}$$

where $K = Z_p / Z_r$ is the impedance ratio of the characteristic impedance of the perturbation to the characteristic impedance of ring resonator.

3.5.2 Odd-Mode Analysis

Figure 3.15 depicts the equivalent circuit representation of half the ring resonator for odd-mode excitation, where an electric wall is applied along the symmetry plane of $C - D$, which is thus a short circuit at this plane. Similar to the even-mode case, by inspecting the equivalent circuit as shown in the figure, the *input* admittance of odd-mode is equal to zero at the resonance frequency, which yields

$$Y_o = Y_{upper,o} + Y_{lower,o} = 0 . \tag{3.14}$$

For the upper section of the odd-mode circuit, the *input* admittance in terms of the characteristic impedance of the line and their electrical lengths can be determined analytically as follows

$$Y_{upper,o} = \frac{(Z_r + jZ_{in1,o}\tan\theta_r)}{Z_r(Z_{in1,o} + jZ_r\tan\theta_r)}, \tag{3.15}$$

where $Z_{in1,o} = jZ_p\tan\theta_p$ is the *input* impedance of perturbation with θ_p for short-ended transmission line.

In addition, the lower-half *input* admittance $Y_{lower,o}$ is further given as

$$Y_{lower,o} = -\frac{j\cot(\pi/4)}{Z_r}. \tag{3.16}$$

By substituting equations (3.15) and (3.16) into (3.14), the odd-mode resonance frequency f_{0o} can be obtained by the following relation

$$\tan\left(\theta_1\frac{f_{0o}}{f_r}\right) + K\tan\left(\theta_p\frac{f_{0o}}{f_r}\right) = 0. \tag{3.17}$$

Furthermore, the coupling constant can be expressed in terms of f_{0e} and f_{0o} by the following relation

$$k = 2\frac{|f_{0e} - f_{0o}|}{f_{0e} + f_{0o}}. \tag{3.18}$$

3.5.3 Attenuation Pole Analysis

The attenuation pole frequency can be analyzed in the following manner. Consider the stepped impedance ring resonator using a simplified transmission line model as depicted in Figure 3.16(a). It is found that the two sections form a parallel connection. For this parallel circuit, a transmission line *ABCD* matrix is utilized to find each section parameters. The *ABCD* matrix of the upper section can be computed by multiplying the matrices of subsections mathematically given as

$$[M_{upper}] = [M_r][M_p][M_p], \tag{3.19}$$

where $[M_r] = \begin{bmatrix} \cos\theta_2 & jZ_r\sin\theta_2 \\ jY_r\sin\theta_2 & \cos\theta_2 \end{bmatrix}$, $[M_p] = \begin{bmatrix} \cos 2\theta_p & jZ_p\sin 2\theta_p \\ jY_p\sin 2\theta_2 & \cos 2\theta_p \end{bmatrix}$, $Y_r = 1/Z_r$,

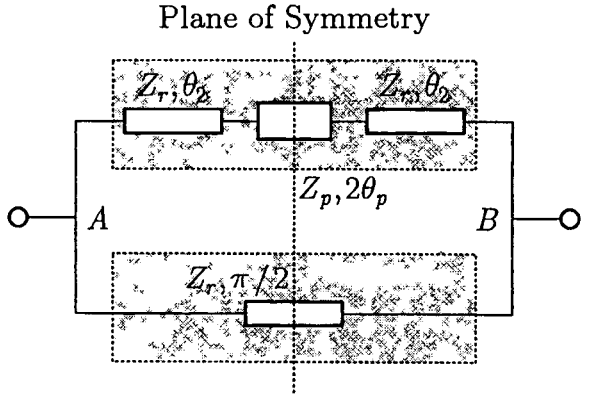

(a)

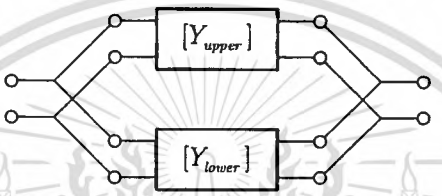

(b)

Figure 3.16 The stepped impedance ring resonator with (a) simplified transmission line model and (b) simplified two-port network.

and $Y_p = 1/Z_p$ are the characteristic admittance of the ring line and of the perturbation line. The upper-half admittance matrix $[Y_{upper}]$ can then be calculated from $[M_{upper}]$ by using the conversion formulas as displayed in [47].

Consider the lower-half of the ring resonator. The admittance matrix $[Y_{lower}]$ of the two-port network in Figure 3.16(b) can be given as follows:

$$[Y_{lower}] = \begin{bmatrix} -jY_r \cot(\pi/2) & jY_r \csc(\pi/2) \\ jY_r \csc(\pi/2) & -jY_r \cot(\pi/2) \end{bmatrix}. \tag{3.20}$$

The whole admittance matrix $[Y_T]$ can be easily obtained by adding the upper- and lower-half admittance matrices, i.e., $[Y_T] = [Y_{upper}] + [Y_{lower}]$, which follows from equations (3.19) and (3.20), respectively. The forward transmission coefficient (S_{21}) can then be calculated from $[Y_T]$. By letting $|S_{21}| = 0$, the attenuation pole frequencies can be solved under the following condition.

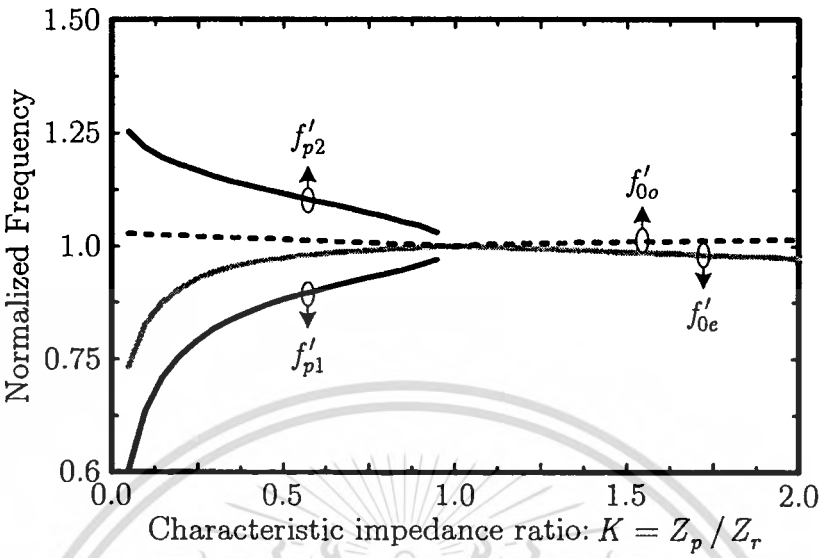

(a)

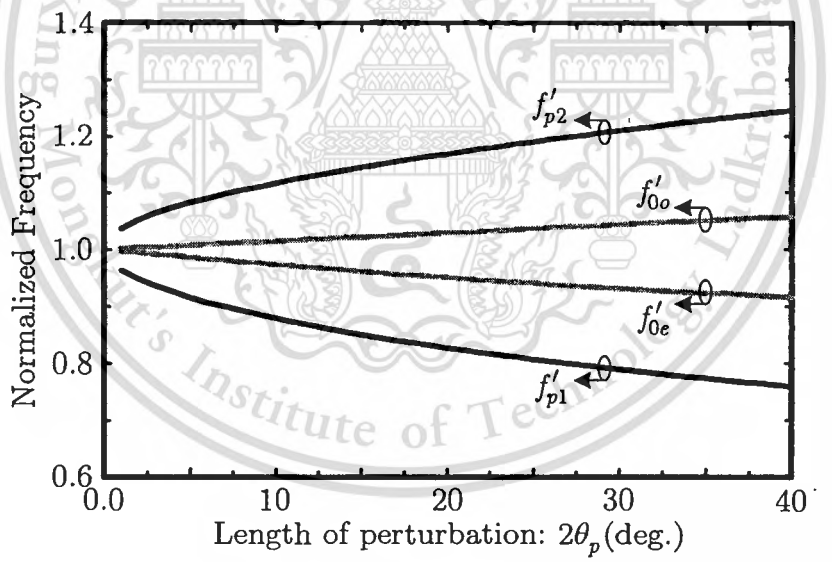

(b)

Figure 3.17 Normalized Characteristic frequency of the stepped impedance ring resonator at (a) $2\theta_p = 10^\circ$ and (b) $K = 0.5$.

$$\left\{K\cos^2\left(\theta_2\frac{f_p}{f_r}\right)+\frac{1}{K}\sin^2\left(\theta_2\frac{f_p}{f_r}\right)\right\}\sin\left(2\theta_p\frac{f_p}{f_r}\right)$$
$$+\sin\left(2\theta_2\frac{f_p}{f_r}\right)\cos\left(2\theta_p\frac{f_p}{f_r}\right)+\sin\left(\frac{\pi}{2}\frac{f_p}{f_r}\right)=0. \quad (3.21)$$

Also, by considering the admittance parameter at the upper- and lower-half of the ring, the attenuation poles will be appeared when total forward transfer admittance parameter is satisfied under the condition.

$$Y_{21,upper}+Y_{21,lower}=0. \quad (3.22)$$

Note that such an equation is equivalent to $|S_{21}|=0$ for the two ports terminated with the characteristic impedance of the system, i.e., $Z_0=50\ \Omega$.

With the use of equation (3.21), the dependence between normalized pole frequencies (f_p/f_r) and impedance ratio (K) can be plotted and this is shown in Figure 3.17(a). In this case, we assume that the electrical perturbation $2\theta_p$ is set as 10° at the resonance frequency. Since the perturbation is partially short length, the large coupling coefficient cannot be accomplished by simply changing the impedance ratio K. Note that when $K=1$ (or $Z_p=Z_r$) is the case of a uniform ring resonator and there is no coupling between the two orthogonal mode, yielding $f'_{0e}=f'_{0o}$ (or $f_{0e}/f_r=f_{0o}/f_r$). Under the condition of $K>1$ (or $Z_p>Z_r$), it should be pointed out that the attenuation pole frequencies will not be generated, due to the fact that the perturbation in the ring doest not satisfy the condition in equation (3.21). Therefore, we understand that the attenuation poles are dependent on the perturbation structure, and the cases where they do not exist can be identified. The normalized even- and odd-mode resonance frequencies based on the equations (3.13) and (3.17) are also plotted in the figure. This can be accomplished by setting the impedance ratio at less than unity, i.e., $K=0.5$.

Figure 3.17(b) plots the relationship between the length of perturbation $2\theta_p$ and normalized resonance and pole frequencies based on equations (3.13), (3.17), and (3.21). As noticed from the figure, when the perturbation length is increased, the normalized frequency location between even- and odd-mode frequencies will be shifted away from the normalized resonance ring frequency.

3.6 Practical Considerations in Microstrip Ring Resonator Based Bandpass Filter Design

In the microstrip bandpass filter based on dual-mode ring resonator with stepped impedance perturbation, the wideband response can be accomplished by selecting a high coupling coefficient k of the ring resonator. This requires a small impedance ratio K (or $Z_p < Z_r$). When the perturbation exists in the ring structure, the center frequency is *shifted* down to a lower frequency. For practical implementation, the discontinuity at the ring and the stepped transmission lines yielding from the layout affects the resonance frequency since it introduces an extra-capacitance at the step transition. The center frequency is thus additionally shifted toward a lower frequency. This implies that the *effective* length of the ring resonator has more than one guided wavelength at the fundamental frequency of the ring. Another important issue to be considered is the *large* impedance ratio K (or $Z_p > Z_r$). The attenuation pole frequency, however, does not exist as mentioned earlier in section 3.5.3.

Therefore, to achieve the requirement of bandpass characteristic with two attenuation poles on both sides of the passband under the impedance ratio K at higher or lower than unity, two possible configurations of perturbation can be applied: the lumped *right-* and *left-*handed transmission lines in the forms of symmetrical networks.

3.6.1 Capacitive Coupling Using Lumpled Components

To couple energy from the input port to the ring resonator and from the ring to the output port, the input and output coupling capacitors C_S may be introduced where the equation derived for capacitor coupled bandpass filter is given by [59]

$$C_S = \frac{G_S}{\omega_0}\sqrt{\frac{b_r\Delta}{g_0 g_1 G_S - b_r\Delta}}. \tag{3.23}$$

$G_S = 1/Z_S$ is the source conductance and Z_S is the source impedance of the filter. $\Delta = BW/\omega_0$ is the fractional bandwidth. The g_0 and g_1 are the low-

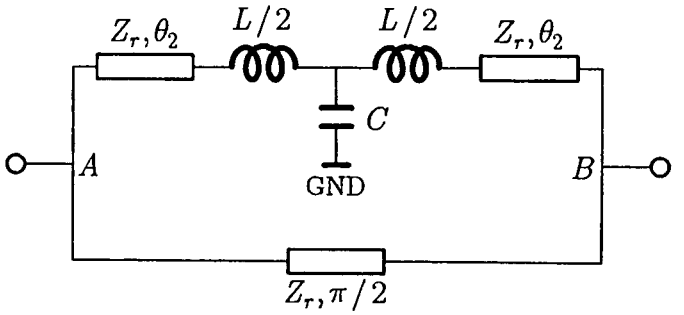

Figure 3.18 Dual-mode ring filter using a SRH-TL as a stepped impedance perturbation.

pass element values, which can be obtained from the the formulas given in [74]. In addition, the slope parameter b_r can be calculated under the assumption of a one-wavelength resonator, i.e., $b_r \cong \pi / Z_r$.

3.6.2 Dual-Mode Ring Filter's Implementation

3.6.2.1 SRH-TL Perturbation

Here, the implementation of the dual-mode ring resonator based bandpass filter is presented. The proposed technique trades the implementation complexity with the insertion loss by substituting the conventional perturbation with symmetrical *right-* and *left-*handed transmission lines.

Figure 3.18 shows the proposed circuit with symmetrical right-haned transmission line, which improves the step discontinuity at the ring and the perturbation. Based on the above design equations, three bandpass filters using ring-type stepped impedance perturbation with discrete component devices were proved and verified with simulation at the center frequency of 2.45 GHz.

In this design, the impedance ratio K was selected as 0.2 ($Z_r = 50\ \Omega$ and $Z_p = 10\ \Omega$) and the coupling length was controlled by adjusting the length of perturbation. Let us consider the dual-mode ring filter as a design case example. The increase of θ_p pushes the even-resonance frequency away from the odd-resonance frequency. The center frequency of the filter is thus decreased since the center of the resonance frequencies of the

Table 3.1 Parameters for dual-mode ring filter using SRH-TL perturbation at $f_0 = 2.45$ GHz and $K = 0.2$ ($Z_r = Z_0 = 50\ \Omega$ and $Z_p = 10\ \Omega$).

(a) Case A at $2\theta_p = 5°$

SRH-TL	$L/2 = 0.028$ nH $C = 0.566$ pF	
Ring Parameters	Initial	Final
	$\theta_2 = 132.5°$ $\theta_3 = 90°$ $C_s = 0.6$ pF	$\theta_2 = 121.792°$ $\theta_3 = 82.727°$ $C_s = 0.58$ pF
Simulation	Initial	Final
	$f_0 = 2.252$ GHz FBW = 7.6 %	$f_0 = 2.437$ GHz FBW = 8.3 %

(b) Case B at $2\theta_p = 10°$

SRH-TL	$L/2 = 0.056$ nH $C = 1.128$ pF	
Ring Parameters	Initial	Final
	$\theta_2 = 130°$ $\theta_3 = 90°$ $C_s = 0.92$ pF	$\theta_2 = 114.771°$ $\theta_3 = 79.457°$ $C_s = 0.89$ pF
Simulation	Initial	Final
	$f_0 = 2.163$ GHz FBW = 13.4 %	$f_0 = 2.421$ GHz FBW = 17 %

(c) Case C at $2\theta_p = 20°$

SRH-TL	$L/2 = 0.111$ nH $C = 2.225$ pF	
Ring Parameters	Initial	Final
	$\theta_2 = 125°$ $\theta_3 = 90°$ $C_s = 1.45$ pF	$\theta_2 = 105.15°$ $\theta_3 = 75.71°$ $C_s = 1.40$ pF
Simulation	Initial	Final
	$f_0 = 2.061$ GHz FBW = 28.6 %	$f_0 = 2.401$ GHz FBW = 33 %

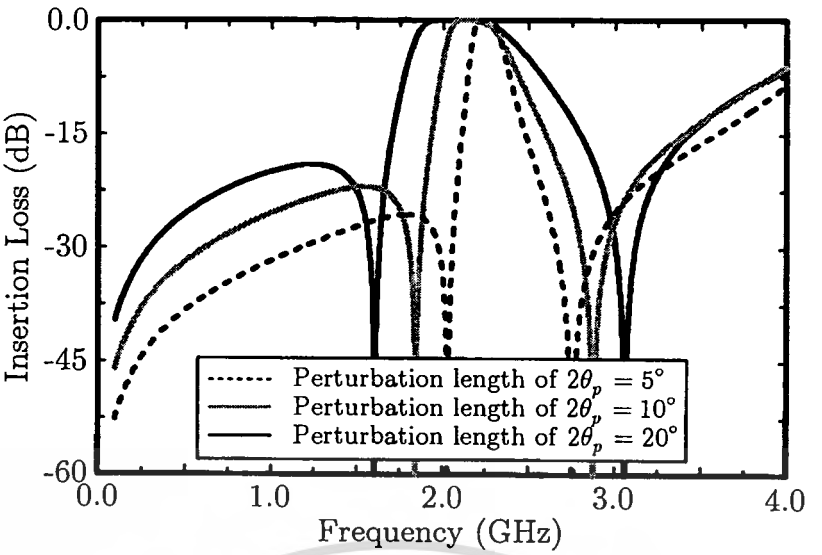

Figure 3.19 Simulated frequency responses for dual-mode ring filter under $K = 0.2$ using SRH-TL as a stepped impedance perturbation.

even- and odd-modes is due to the inter-stage coupling at the input and output. The adjustment of the resonator length is possible to obtain the desired center frequency. The electrical parameters before and after fine tuning with the help of ADS circuit simulator [72] are summarized in Table 3.1. The detailed physical dimensions w and ℓ are then synthesized using LineCalc tool in ADS software. For a small impedance ratio, it was found that the change of the width becomes significant and the effects of the parasitic capacitance at the step transition can no longer be neglected. The right-handed transmission line is thus required. Nevertheless, this artificial transmission line has a limitation at a particular frequency range of 1-2 GHz. Since the lumped inductors and capacitor which form a perturbation line at higher frequencies are very small and hence this line is impractical for implementation. In this SRH-TL perturbation case, only simulation will be presented for the sake of understanding the bandpass filter based on the dual-mode ring resonator. Figure 3.19 plots the filter performance over the frequency range of 4 GHz. As noticed from the figure, when θ_p is increased, the bandwidth is also increased. For a fixed specification at the desired bandwidth, the passband characteristic can be controlled while the attenuation response will change in accordance with the discontinuity structure.

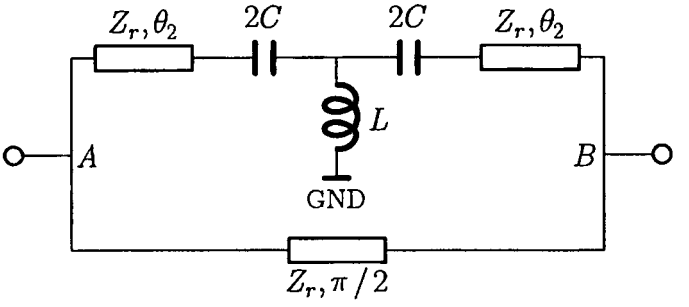

Figure 3.20 Dual-mode ring filter using a SLH-TL as a stepped impedance perturbation.

3.6.2.2 SLH-TL Perturbation

Figure 3.20 illustrates a new symmetrical left-handed transmission line (SLH-TL) [75] to serve as a perturbed line. With reference to Table 3.1, the calculated of SLH-TL using equations (3.7) to (3.9) are listed in Table 3.2. Figure 3.21 shows the simulated frequency response of the SLH-TL based dual-mode bandpass filter. Unlike the response in Figure 3.19, the attenuation poles do not exist in the Figure 3.21. This is because the equation (3.22) is not valid due to the difference in the perturbation scheme. However, the equation (3.22) is valid only when the impedance ratio is greater than unity, i.e., $K > 1$.

Let us consider the dual-mode ring filter with SLH-TL as the design case at $K > 1$. Listed in Table 3.3 are the electrical parameters of the ring filter operating at $f_0 = 2.45$ GHz with an impedance ratio $K = 4.4$ and the perturbation length $2\theta_p$ of 5°, 10°, and 20°. After adjusting the length, the detailed electrical parameters are also included in Table 3.3. Figure 3.22 shows the simulated performances of the dual-mode ring bandpass filter based on an ideal transmission line model. With the use of the SLH-TL, the equation (3.22) is valid when the impedance ratio is greater than unity. This enables two attenuation poles at the lower and higher the passband frequency as depicted in Figure 3.22(a) and hence an improved rejection performance in the bandpass filter. As observed in the figure, two resonant peaks emerge at the very low frequency beyond the center frequency of the filter. However, this is not a practical concern since the filter is implemented in lossy material. Another important characteristic for the filter is the reflection coefficient. This dual-mode filters with the difference of perturbation lengths in SLH-TL exhibit perfect match in all cases as illustrated in Figure 3.22(b).

Table 3.2 Parameters for dual-mode ring filter using SLH-TL perturbation at $f_0 = 2.45$ GHz and $K = 0.2$ ($Z_r = Z_0 = 50\ \Omega$ and $Z_p = 10\ \Omega$).

$2\theta_p = 5°$	
SLH-TL	$L = 7.453$ nH
	$2C = 149.068$ pF
Ring Parameters	$\theta_2 = 137.5°$
	$\theta_3 = 90°$
	$C_s = 0.6$ pF
$2\theta_p = 10°$	
SLH-TL	$L = 3.740$ nH
	$2C = 74.810$ pF
Ring Parameters	$\theta_2 = 140°$
	$\theta_3 = 90°$
	$C_s = 0.92$ pF
$2\theta_p = 20°$	
SLH-TL	$L = 1.896$ nH
	$2C = 37.921$ pF
Ring Parameters	$\theta_2 = 145°$
	$\theta_3 = 90°$
	$C_s = 1.45$ pF

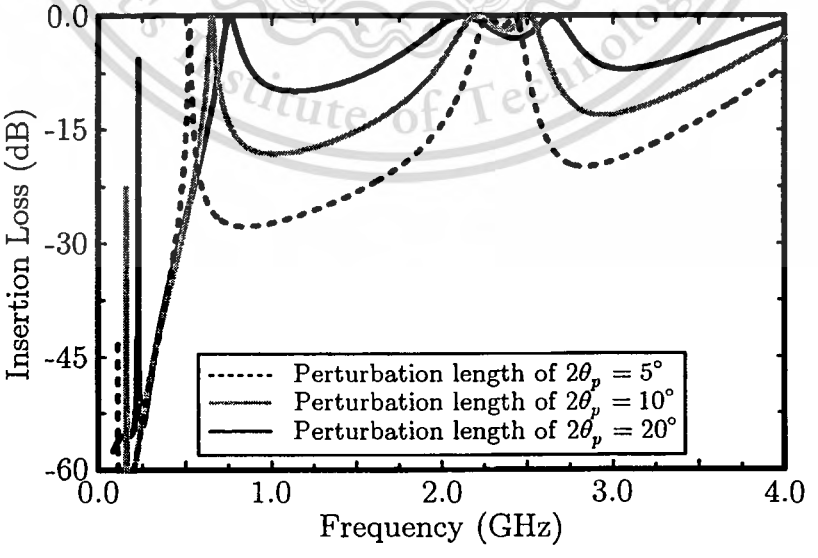

Figure 3.21 Simulated frequency responses for dual-mode ring filter under $K = 0.2$ using SLH-TL as a stepped impedance perturbation.

Table 3.3 Parameters for dual-mode ring filter using SLH-TL perturbation at $f_0 = 2.45$ GHz and $K = 4.4$ ($Z_r = Z_0 = 50\,\Omega$ and $Z_p = 220\,\Omega$).

(a) Case A at $2\theta_p = 5°$

SLH-TL	$L = 163.975$ nH $2C = 6.775$ pF	
Ring Parameters	Initial	Final
	$\theta_2 = 137.5°$ $\theta_3 = 90°$ $C_s = 0.53$ pF	$\theta_2 = 132.168°$ $\theta_3 = 86.51°$ $C_s = 0.5$ pF
Simulation	Initial	Final
	$f_0 = 2.355$ GHz FBW = 6.2 %	$f_0 = 2.45$ GHz FBW = 6 %

(b) Case B at $2\theta_p = 10°$

SLH-TL	$L = 82.292$ nH $2C = 3.4$ pF	
Ring Parameters	Initial	Final
	$\theta_2 = 140°$ $\theta_3 = 90°$ $C_s = 0.77$ pF	$\theta_2 = 133.886°$ $\theta_3 = 86.069°$ $C_s = 0.73$ pF
Simulation	Initial	Final
	$f_0 = 2.343$ GHz FBW = 11.7 %	$f_0 = 2.447$ GHz FBW = 11.3 %

(c) Case A at $2\theta_p = 20°$

SLH-TL	$L = 41.713$ nH $2C = 1.723$ pF	
Ring Parameters	Initial	Final
	$\theta_2 = 145°$ $\theta_3 = 90°$ $C_s = 1.12$ pF	$\theta_2 = 138.253°$ $\theta_3 = 85.812°$ $C_s = 1.07$ pF
Simulation	Initial	Final
	$f_0 = 2.336$ GHz FBW = 20.7 %	$f_0 = 2.445$ GHz FBW = 19.7 %

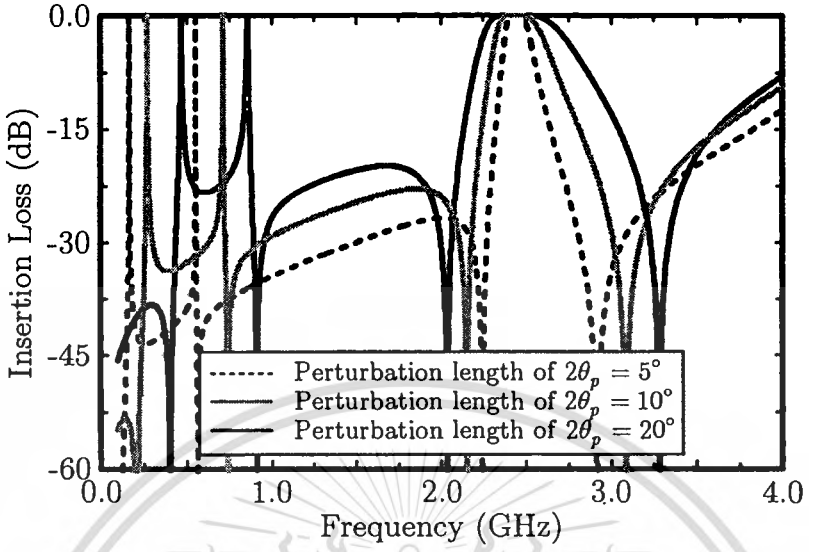

(a)

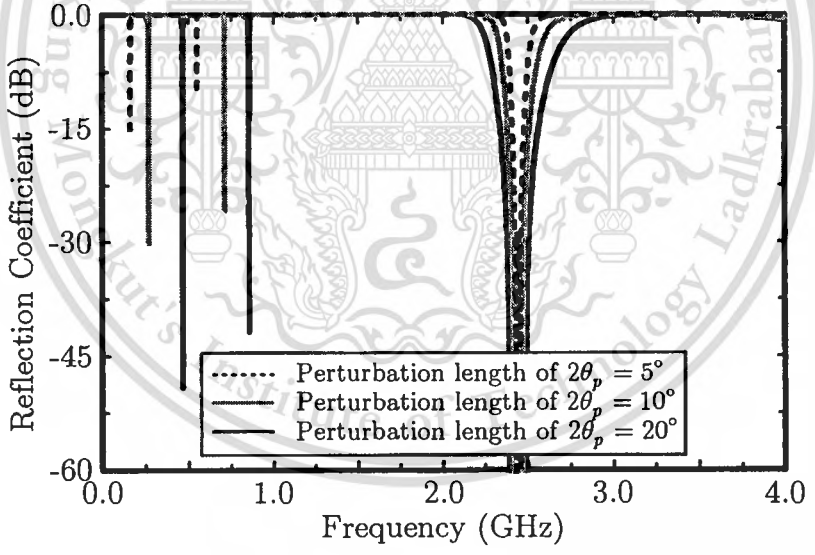

(b)

Figure 3.22 Simulated frequency responses for dual-mode ring filter under $K = 4.4$ at different perturbation length of SLH-TL. (a) Insertion loss. (b) Reflection coefficient.

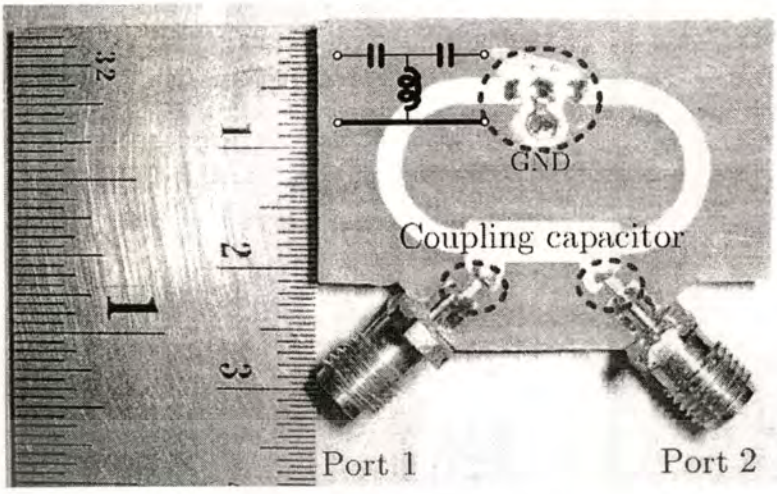

Figure 3.23 Photograph of dual-mode ring filter employing SLH-TL.

3.6.3 Measurement Results

Based on the previous discussion, a dual-mode ring bandpass filter employed a SLH-TL as stepped perturbation is designed at the center frequency of 2.45 GHz and implemented on an FR-4 printed circuit board. Under the constraint of commercial values for lumped inductor and capacitor and their self-resonance frequencies, the characteristic impedance and the length of stepped perturbation are selected at 71Ω and 15 degree, respectively. The lumped components of SLH-TL can be obtained, which are $2C = 7.066$ pF and $L = 17.81$ nH. Subsequently, the physical dimensions can be synthesized on an FR-4 PCB (PCB: a relative dielectric constant $\varepsilon_r = 4.55$, a thickness $h = 0.8$ mm, a loss tangent of $\tan\delta = 0.02$, and a metal thickness $t = 18$ μm) by using LineCalc tool in ADS. The SLH-TL was implemented using chip components ($2C \approx 6.8$ pF of 0403 SMT model and $L = 17.15$ nH of 0603 SMT model inductor). Since there are some parasitic elements in the lumped package and certain deviation from the calculated values, the characteristic impedance of each transmission line may be adjusted to obtain a good filter's performance. The actual board layout is shown in Figure 3.23. The dimensions excluding two SMA connectors are approximately 40 mm × 30 mm. All the measurements were performed on a network analyzer test system, the HP8510A system, with the Short-Open-Load-Through (SOLT) calibration.

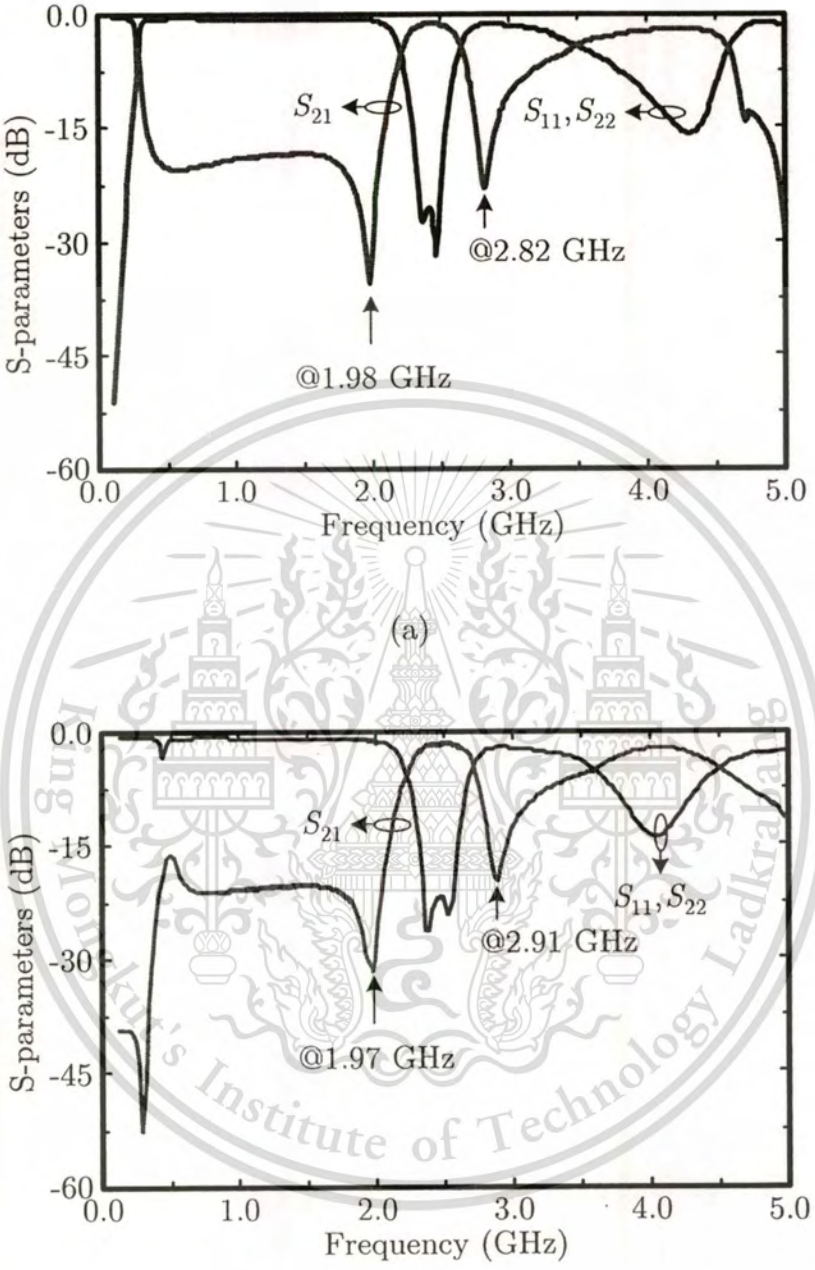

Figure 3.24 Performances of dual-mode ring filter using SLH-TL as a stepped impedance perturbation at $K = 1.42$. (a) Simulation. (b) Measurement.

The simulated performances of the proposed bandpass filter are shown in Figure. 3.24(a). As shown in the figure, the simulated insertion loss is less than -1.1 dB at a center frequency of 2.43 GHz, while both input and output reflection coefficients are better than -20 dB. Moreover, the prototype bandpass filter enables two attenuation pole frequencies at 1.98 GHz and 2.82 GHz on either side of the center frequency.

Figure 3.24(b) shows the measured results. The center frequency of the filter is at 2.48 GHz with a 3-dB fractional bandwidth of 16.2 %. The filter exhibits an insertion loss better than -1.5 dB at 2.48 GHz, which is mainly due to the conductor loss of copper and two SMA connectors. In addition, the input/output reflection coefficients are lower than -20 dB within 2.37–2.59 GHz. The attenuation poles are at 1.97 and 2.91 GHz. Furthermore, the insertion loss from 0.1 GHz to 1.97 GHz is suppressed by more than -16.2 dB. Good agreement between simulated and measured results is observed.

3.7 Chapter Summary

It has been clearly demonstrated through simulations that symmetrical right- and left-handed transmission lines can be employed in the implementation of the dual-mode stepped impedance ring resonator for microstrip bandpass filter applications with small and high impedance ratios. At the same length of perturbation, the dual-mode ring filter based on a symmetrical left-handed transmission line perturbation exhibits attenuation slope better than a right-handed line perturbation. The existence of attenuation poles, at lower and higher the passband frequencies, depends on the structure of perturbation, i.e., SRH-TL and SLH-TL. The SRH-TL perturbation structure may be applied for $K < 1$. On the other hand, the SLH-TL may be employed for $K > 1$. Note that when employed in the dual-mode filter, they are attractive because of their simplicity and practicality.

CHAPTER 4

TRIPLE-MODE RING RESONATOR FOR WIDEBAND BANDPASS FILTER

In the past, the bandpass filters based on triple-mode resonator have been reported using dielectric filled waveguide resonators of rectangular [76] and cylindrical shape [77]. Most of all, triple-mode operation is achieved by a dielectric filled structure inside a resonant metal cavity [78-79]. Mode degeneracy occurs when different cavity modes resonate at the same frequency. In this circumstance, it is essential for each mode to produce a distinct field pattern. This allows the coupling elements to interfere with the field paths differently from mode to mode and produce a split in the resonant frequencies.

A triple-mode resonator is difficult to realize in planar form. This is due to all of the inherent 3-D requirements. For the most part, the tuning and coupling elements such as screws or metal rods [76] are thus required to exist at angles for modal coupling, which perturb the modes in all three dimensions. For this reason, triple-mode filters have only been accomplished in the waveguide structure. A multilayer approach reported in [80-81] is the first effort to implement in the planar configuration for making a triple-mode resonator where the performance of waveguide filter in terms of loss is concerned. It also has a rather large amount of weights comparable to the standard planar filters.

In this chapter, the project motivations and goals of implementing triple-mode planar filters are briefly introduced in Section 4.1. Section 4.2 describes the proposed configuration of a triple-mode ring resonator and its characteristic response. In Section 4.3, the method to obtain the attenuation pole associated in the ring is presented. Section 4.4 illustrates the method to find the resonance frequencies. The graphical representations of the attenuation poles and resonance frequencies, as a function of the characteristic impedance that employed in the triple-mode ring structure, are explained in Section 4.5. To understand the operation mechanism of triple-mode ring

resonator, the physical interpretation is then described in Section 4.6. In Section 4.7, the design example of the triple-mode ring for wideband bandpass filter is presented as a proof of concept to the ring structure presented in Section 4.2. To achieve a higher out-of-band rejection and wide stopband attenuation, the multi-frequency suppression is also presented in a cascaded single-ring version. Section 4.8 summarizes the chapter with conclusion.

4.1 Introduction

Microwave bandpass filters commonly utilize a ring resonator with the benefit of small circuit size and sharp rejection response [60-61]. The ring resonator originally proposed by I. Woff and N. Knoppik was introduced for microwave substrate measurement [71]. Subsequently, with the use of asymmetrical coupling or asymmetrical perturbation, the dual-mode ring bandpass filter was initially reported in [35]. Soon afterward, the ring resonator was established as one of the main structures for planar microwave bandpass filter implementations [36-37, 40-42, 64, 67, 82-83]. Many research works on the miniaturization were conducted with different perturbation schemes [36-37, 41-42, 64, 67] in the symmetrical plane. In addition, the insertion loss associated with the ring is another improvement by putting the lumped capacitor [42], the edged coupling [13, 40] or the inter-digital side-coupling [41, 83] between two feed lines and the ring resonator. These structures do not, however, lend themselves to closed-form analysis and straightforward filter design. They thus require the design iterations with the help of electromagnetic simulation.

The dual-mode ring resonators, which enable closed-form analysis and systematic design methodology, were reported in [65-66, 68-69]. Various parameters useful for filter design were investigated and derived, including the resonance frequencies, attenuation poles, and coupling constant, etc. The dual-mode bandpass filter in [42] made use of the series-stub and that in [66] made use of the shunt-stub perturbations. To achieve better control of the coupling constant and, hence, the odd/even resonance frequency locations, the dual-mode bandpass filter in [68] utilized lumped capacitors for series perturbation. The same benefit was obtained for the shunt perturbation using lumped

capacitors in [69], with the additional advantage of electronic tunability due to the use of grounded elements.

With the emerging broadband communication systems [84], the demand on the bandwidth in microwave bandpass filters has been unprecedentedly increasing. To accomplish such a wideband characteristic in the ring-based bandpass filters, the dual-mode square-ring bandpass filters and its performance enhancement were investigated [43, 85-86]. In [43, 85], the filter employed two tuning open stubs for conversion from a bandstop to a bandpass characteristic with direct-orthogonal feed lines for low insertion loss. With the addition of the four open-loop arms [85], or the patterned ground plane sometimes referred to as a defected ground structures [86], the spurious responses, particularly in the stopband, in the ring filter can be alleviated. Another wideband ring bandpass filter in [87] was obtained by applying two short outer-tuning stubs and a resistor at the symmetrical plane of the ring. However, the need for outer-tuning stubs entails a major drawback in terms of compactness, particularly when connected in cascade to form a higher-order bandpass filter.

To achieve further improvement in the passband flatness and sharp rejection in the bandpass filter characteristic, the quadruple-mode [88] and quintuple-mode [89-90] ring bandpass filters were developed in microstrip forms. In fact, the quintuple-mode bandpass filter in [89-90] essentially relies upon the triple-mode resonator core using two equal [89] and unequal [90] stub perturbation lengths, with lumped capacitors feed lines. Though the triple-mode resonator resulted in lower insertion loss and better flatness in the passband response than the dual-mode counterparts, the improvements concerning sharp rejection and out-of-band attenuation were rather modest. As presented in [89-90], by replacing the lumped feed lines with the inter-digital coupled lines, two additional resonances were created *close* to the original attenuation poles on both sides of the edges of the passband, thus yielding sharper rejection and high stopband attenuation quintuple-mode bandpass filter. It is the use of the inter-digital coupling, however, that makes it difficult for a systematic filter design. As evident in [89-90], whereas the analytical treatment could be developed for the triple-mode resonator core, design iterations based on extensive electromagnetic simulations must be

carried out to find appropriate parameters of the inter-digital feed lines in the quintuple-mode filter.

In this chapter, we present the design and analysis of a triple-mode ring resonator core [91] that enables inherent sharp rejection with excellent gain flatness and good insertion loss in the passband, while offering a systematic analytical design.

4.2 Triple-Mode Ring Resonator

This section provides a brief introduction to a triple-mode ring resonator followed by a description of the configuration and its characteristic, and the physical interpretation is also described this last section.

4.2.1 Triple-Mode Configuration

Figure 4.1(a) shows the primitive single-mode ring resonator in the form of a square ring transmission line at one wavelength λ_g. It provides the resonance frequencies at nf_{r0}, where n is an integer number; $f_{r0} = c/\lambda_g\sqrt{\varepsilon_{eff}}$ is the center frequency of the resonator; c and ε_{eff} are the velocity of light in free space and the effective dielectric constant, respectively. Note that the term $c/\sqrt{\varepsilon_{eff}}$ is the guided-wave's velocity along the medium that forms the transmission lines. Based on the primitive structure, Figure 4.1(b) shows the proposed ring resonator [91] where one-half of the transmission line's square ring (*lower half in the figure*) is replaced by a pair of $\lambda_g/4$ open-ended coupled lines connected in cascade with a $\lambda_g/4$ shunt open stub inserted in between. The length of the transmission line in the other half of the ring is at a half wavelength $\lambda_g/2$.

4.2.2 Triple-Mode Characteristic

Using ideal transmission line models, Figure 4.2 depicts typical *resonance* characteristics of the proposed resonator structure under weak coupling condition. Let us first consider the case without the shunt stub (dashed response). As shown in the dashed response of Figure 4.2, the resonator without the shunt stub exhibits one resonance at the center frequency $f_{r,o}$; the other two resonances are at $f_{tr,o}$ and $f_{rr,o}$, located away

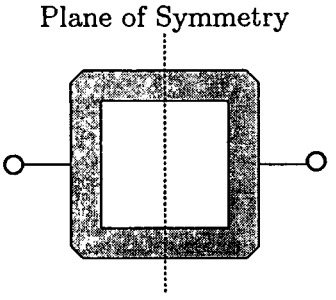

(a)

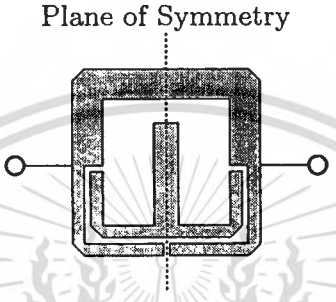

(b)

Figure 4.1 Configuration of (a) the preliminary single-mode ring and (b) the proposed triple-mode ring resonator.

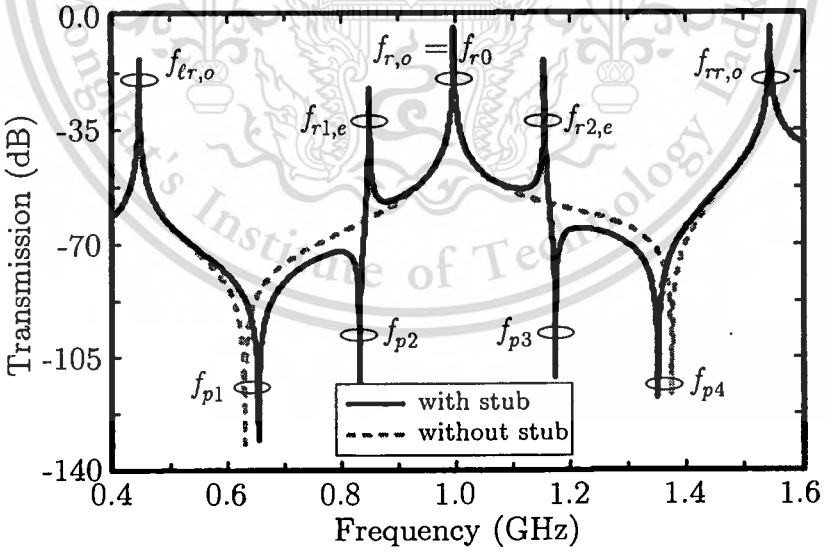

Figure 4.2 Characteristic of the proposed triple-mode ring resonator in Figure 4.1(b) with shunt stub (solid response) and without stub (dash response).

from $f_{r,o}$ at the far left and right regions of the response. On both sides of the center frequency $f_{r,o}$, there are two attenuation poles at f_{p1} and f_{p4}. Consider now the case with the inclusion of the shunt stub. It is seen from the solid response in Figure 4.2 that the resonance characteristic, particularly around $f_{r,o}$, is degenerated. In particular, there are two more resonance frequencies at $f_{r1,e}$ and $f_{r2,e}$, near the original resonance at $f_{r,o}$. Also shown in the solid response is that each side of $f_{r1,e}$ and $f_{r2,e}$ is accompanied by an additional attenuation pole, which appears very close to the resonance frequency (f_{p2} close to $f_{r1,e}$, and f_{p3} close to $f_{r2,e}$). It should be noted that, as will be shown in the analysis of Section 4.3 and 4.4, the resonance frequencies $f_{r,o}$, $f_{\ell r,o}$, and $f_{rr,o}$ correspond to odd-mode excitation, where $f_{r1,e}$ and $f_{r2,e}$ correspond to even-mode excitation.

It is the locations of the resonance and attenuation pole frequencies at the central frequency region in Figure 4.2 that underlies the major advantages of the proposed resonator of Figure 4.1(b). Since there are as many as three passband resonance frequencies ($f_{r,o}$, $f_{r1,e}$, and $f_{r2,e}$), the bandpass filter based on the resonator exhibits a triple-mode response with a broad bandwidth while still maintaining a good flatness within the passband. In addition, the presence of the attenuation poles f_{p2} and f_{p3}, adjacent to $f_{r1,e}$ and $f_{r2,e}$, respectively, provides a highly steep transition characteristic. This practically yields the edges of the passband of the filter at $f_{r1,e}$ and $f_{r2,e}$. Thus, the bandwidth of the bandpass filter can be approximated from $f_{r1,e}$ to $f_{r2,e}$, whereas the center frequency is located at about $f_{r,o}$.

It is important to note that the typically high loss associated with the coupled lines in most practical realizations has practically no impact on the passband insertion loss of the filter based on the proposed resonator. This is because the shunt open stub inserted between the cascaded coupled lines acts as a series resonance to ground at the center frequency $f_{r,o}$ of the passband; this introduces a total reflection and, hence, a transmission notch of the incident wave along the coupled lines' path. As a consequence, the wave applied at the input port is effectively forced to travel mainly through the transmission line over the passband frequency; the loss incurred by the wave traveling via the coupled lines is, therefore, minimized. This, combined with

the direct feed structure of the proposed resonator, results in a low insertion loss filter.

4.3 Two-Port Network Method

In this section, we present the analysis method of the proposed resonator in Figure 4.1(b) by using the two-port network theorem for computing the attenuation pole frequencies. Subsequently, the even- and odd-mode analysis will be performed to determine the resonance frequencies. For simplicity, the quasi-static TEM-mode of operation is assumed [51]. Also, the losses and discontinuity effects of the transmission lines and coupled lines are not taken into account.

The circuit model corresponding to the proposed triple- mode ring resonator in Figure 4.1(b) is shown in Figure 4.3(a). A simplified two-port network, depicted in Figure 4.3(b), comprises the upper and lower halves of the model. The upper half is formed by the transmission line with the characteristic impedance of Z_{T1}, and the electrical length of θ_1. For the lower half, there are two identical open-ended coupled lines in cascade and a shunt open stub connected in between. The even- and odd-mode impedances of the coupled lines are represented by Z_{0e} and Z_{0o}, respectively. Also, the even- and -odd mode electrical lengths are given by θ_e and θ_o, respectively. The shunt stub has the characteristic impedance of Z_{T2} and the electrical length of θ_2.

4.3.1 Attenuation Pole Location

From the transmission line in the upper half of the circuit model in Figure 4.3(a), the admittance matrix $[Y_{\text{upper}}]$ of the two-port network in Figure 4.3(b) can be written as follows

$$[Y_{\text{upper}}] = \begin{bmatrix} -jY_{T1}\cot(\theta_1) & jY_{T1}\csc(\theta_1) \\ jY_{T1}\csc(\theta_1) & -jY_{T1}\cot(\theta_1) \end{bmatrix}, \tag{4.1}$$

where $Y_{T1} = 1/Z_{T1}$ is the characteristic admittance of the transmission line.

Considering the lower half in Figure 4.3(a), the ABCD matrix of the open-ended coupled line is given as follows [92]

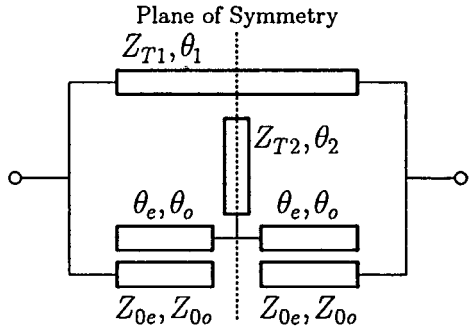

(a)

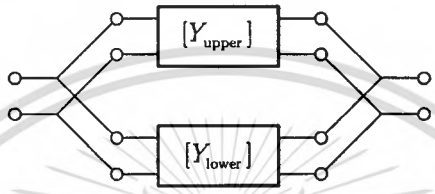

(b)

Figure 4.3 Model of Figure 4.1(b) for analyzing attenuation poles. (a) Circuit detail. (b) Simplified two-port network.

$$[M_{C1}] = \begin{bmatrix} A_{C1} & B_{C1} \\ C_{C1} & D_{C1} \end{bmatrix}, \tag{4.2}$$

where

$$A_{C1} = \frac{Z_{0e}\cot\theta_e + Z_{0o}\cot\theta_o}{Z_{0e}\csc\theta_e - Z_{0o}\csc\theta_o} = D_{C1}, \tag{4.3a}$$

$$B_{C1} = \frac{j}{2}\left(\frac{Z_{0e}^2 + Z_{0o}^2 - 2Z_{0e}Z_{0o}(\cot\theta_e\cot\theta_o + \csc\theta_e\csc\theta_o)}{Z_{0e}\csc\theta_e - Z_{0o}\csc\theta_o}\right), \tag{4.3b}$$

and

$$C_{C1} = \frac{2j}{Z_{0e}\csc\theta_e - Z_{0o}\csc\theta_o}. \tag{4.3c}$$

For the shunt open stub, the ABCD matrix is given by

$$[M_2] = \begin{bmatrix} 1 & 0 \\ jY_{T2}\tan\theta_2 & 1 \end{bmatrix}, \tag{4.4}$$

where $Y_{T2} = 1/Z_{T2}$ is the characteristic admittance of the shunt stub. With reference to Figure 4.3(a), the overall ABCD matrix of the lower half can be calculated by multiplying $[M_{C1}]$,$[M_2]$, and $[M_{C1}]$, respectively, as follows

$$[M_{\text{lower}}] = [M_{C1}][M_2][M_{C1}]. \tag{4.5}$$

The admittance matrix of the lower half $[Y_{\text{lower}}]$ can then be calculated by performing a conversion of the ABCD matrix $[M_{\text{lower}}]$ in equation (4.5) to $[Y_{\text{lower}}]$.

Based on the reciprocal property of the passive network, the attenuation pole is located at the frequency where the eigenimpedances of both the even- and odd-mode are equal [65]. Thus, the attenuation pole frequencies can be obtained under the condition

$$Y_{21,\text{upper}} + Y_{21,\text{lower}} = 0. \tag{4.6}$$

It should be noted that such a condition is equivalent to $|S_{21}| = 0$ for the two ports terminated with 50 ohm. Under the assigned characteristic impedances and electrical lengths in Figure 4.3(a), and based on the condition in equation (4.6), we then obtain four attenuation pole frequencies at f_{p1}, f_{p2}, f_{p3} and f_{p4}. With reference to the response in Figure 4.2 where $f_{p1} < f_{p2} < f_{p3} < f_{p4}$, these attenuation poles are given in the following

$$f_{p1} = \frac{2f_{r0}\tan^{-1}\left\{\dfrac{\sqrt{2}}{(Z_{0e}-Z_{0o})}\sqrt{\dfrac{G_n - F_n(Z_{0e}-Z_{0o})^2}{E_d + 2F_d}}\right\}}{\pi}, \tag{4.7}$$

$$f_{p2} = \frac{2f_{r0}\tan^{-1}\left\{\dfrac{\sqrt{2}}{(Z_{0e}-Z_{0o})}\sqrt{\dfrac{G_n + F_n(Z_{0e}-Z_{0o})^2}{E_d - 2F_d}}\right\}}{\pi}, \tag{4.8}$$

$$f_{p3} = 2f_{r0} - f_{p2}$$
$$= \frac{2\pi f_{r0} - 2f_{r0}\tan^{-1}\left\{\dfrac{\sqrt{2}}{(Z_{0e}-Z_{0o})}\sqrt{\dfrac{G_n + F_n(Z_{0e}-Z_{0o})^2}{E_d - 2F_d}}\right\}}{\pi}, \tag{4.9}$$

$$f_{p4} = 2f_{r0} - f_{p1}$$
$$= \frac{2\pi f_{r0} - 2f_{r0}\tan^{-1}\left\{\dfrac{\sqrt{2}}{(Z_{0e}-Z_{0o})}\sqrt{\dfrac{G_n - F_n(Z_{0e}-Z_{0o})^2}{E_d + 2F_d}}\right\}}{\pi}, \tag{4.10}$$

where

$$E_d = Y_{T1}(Z_{0e}+Z_{0o})\{Y_{T2}(Z_{0e}+Z_{0o})+2\}+4\,, \tag{4.11a}$$

$$F_d = F_n$$
$$= \sqrt{\{Y_{T1}(Z_{0e}+Z_{0o})\}^2 + 4Y_{T1}\{Z_{0e}(2Y_{T2}Z_{0o}+1)+Z_{0o}\}+4}\,, \tag{4.11b}$$

and

$$G_n = Y_{T1}(Z_{0e}^3 + Z_{0o}^3) + 2(Y_{T1}Y_{T2}Z_{0e}Z_{0o}+1)(Z_{0e}^2+Z_{0o}^2)$$
$$+\{7Y_{T1}(Z_{0e}+Z_{0o}) + 4(Y_{T1}Y_{T2}Z_{0e}Z_{0o}-1)\}Z_{0e}Z_{0o}. \tag{4.11c}$$

Note that the subscripts n and d represent the nominator and denominator in equations (4.7)-(4.11), respectively.

4.4 Even- and odd-mode Methods

To determine the resonance frequencies of the ring resonator, we use the circuit model in Figure 4.3(a) and apply the even- and odd-mode analysis methods along the symmetry plane. At the resonance frequencies, the *input* admittance of each mode will be equal to zero when the resonator is assumed lossless. Hence, the *input* admittance of the even-mode Y_e is given by

$$Y_e = Y_{upper,e} + Y_{lower,e} = 0. \tag{4.12}$$

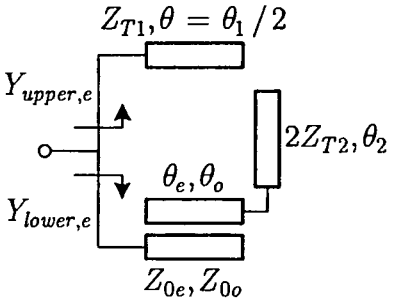

Figure 4.4 Even-mode equivalent circuit of the proposed ring resonator in Figure 4.3(a).

4.4.1 Even-Mode

By exciting the equivalent circuit in the even-mode, it appears that the symmetry plane acts as a perfect magnetic-wall so that this plane represents the open circuit as shown in Figure 4.4. This divides the length of the upper transmission line with Z_{T1} into one-half, i.e., $\theta = \theta_1 / 2$. The width of the shunt stub Z_{T2} in the lower half is also separated into one-half, yielding twice in the equivalent characteristic impedance, i.e., $2Z_{T2}$. The upper-half *input* admittance $Y_{upper,e}$, calculated from $[Y_{\text{upper}}]$, is then given by

$$Y_{upper,e} = jY_{T1} \tan\theta = jY_{T1} \tan(\theta_1 / 2). \tag{4.13}$$

A convenient method to determine the lower *input* admittance $Y_{lower,e}$ is to consider the cascading ABCD matrices of the coupler in equations (4.2) and (4.3), and the shunt stub $2Z_{T2}$. The ABCD matrix of this stub is

$$[M_{T2}] = \begin{bmatrix} \cos\theta_2 & j2Z_{T2}\sin\theta_2 \\ j\dfrac{Y_{T2}\sin\theta_2}{2} & \cos\theta_2 \end{bmatrix}. \tag{4.14}$$

The resulting ABCD matrix in the lower half can be obtained from

$$\begin{aligned} [M_{lower,e}] &= [M_{C1}][M_{T2}] \\ &= \begin{bmatrix} A_{lower,e} & B_{lower,e} \\ C_{lower,e} & D_{lower,e} \end{bmatrix}. \end{aligned} \tag{4.15}$$

Subsequently, the lower-half *input* admittance $Y_{lower,e}$ is calculated from $[M_{lower,e}]$ as

$$Y_{lower,e} = \frac{P}{Q}, \tag{4.16}$$

where

$$P = 2j\begin{bmatrix} 4Z_{T2}\cos\theta_2 \sin\theta_e \sin\theta_o + Z_{0e}\sin\theta_2 \cos\theta_e \sin\theta_o \\ +Z_{0o}\sin\theta_2 \cos\theta_o \sin\theta_o \end{bmatrix}, \tag{4.17a}$$

and

$$Q = \begin{bmatrix} 2Z_{0e}Z_{0o}\sin\theta_2(\cos\theta_e \cos\theta_o + 1) \\ +4Z_{T2}\cos\theta_2(Z_{0e}\cos\theta_e \sin\theta_o + Z_{0o}\cos\theta_o \sin\theta_e) \\ -\sin\theta_2 \sin\theta_e \sin\theta_o(Z_{0e}^2 + Z_{0o}^2) \end{bmatrix}. \tag{4.17b}$$

Therefore, the resonance frequencies [see Figure 4.2] can be solved by substituting equations (4.13), (4.16), and (4.17) into (4.12). After rearrangement, the first even-mode frequency $f_{r1,e}$ can be given by the relationship

$$f_{r1,e} = \frac{2f_{r0}}{\pi}\tan^{-1}\frac{\sqrt{8Z_{T1}Z_{T2} + 4Z_{0e}Z_{0o} + 2(Z_{T1} + 2Z_{T2})(Z_{0e} + Z_{0o})}}{(Z_{0e} - Z_{0o})}, \tag{4.18}$$

and the second even-mode frequency $f_{r2,e}$ can be given by

$$f_{r2,e} = 2f_{r0} - f_{r1,e}. \tag{4.19}$$

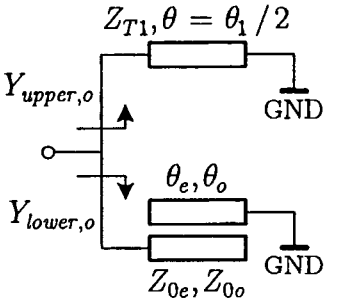

Figure 4.5 Odd-mode equivalent circuit of the proposed ring resonator in Figure 4.3(a).

4.4.2 Odd-Mode

The odd-mode analysis is considered to have a perfect electric-wall along the plane of symmetry, so that the electrical equivalent circuit at this plane behaves as a short circuit as shown in Figure 4.5. Hence, the *input* admittance in this mode at resonance frequency can be expressed as

$$Y_o = Y_{upper,o} + Y_{lower,o} = 0. \tag{4.20}$$

With reference to Figure 4.5, the *input* admittances of the short-circuited transmission line in the upper-half $Y_{upper,o}$, also calculated from $[Y_{\text{upper}}]$, and that of the coupled line in the lower-half $Y_{lower,o}$, based on the calculation similar to $Y_{lower,e}$, are given by

$$Y_{upper,o} = -jY_{T1}\cot\theta = -jY_{T1}\cot(\theta_1/2), \tag{4.21}$$

and

$$Y_{lower,o} = \frac{j(Z_{0e}\cot\theta_e + Z_{0o}\cot\theta_o)}{\frac{1}{2}(Z_{0e}\csc\theta_e + Z_{0o}\csc\theta_o)^2 - \frac{1}{2}(Z_{0e}\cot\theta_e + Z_{0o}\cot\theta_o)^2}. \tag{4.22}$$

By using equations (4.20)-(4.22), the odd-mode resonance frequencies can be derived in a similar fashion. There are three odd-mode resonance frequencies as indicated in Figure 4.2. The first two resonances are addressed in the far left and right regions at $f_{tr,o}$ and $f_{rr,o}$, respectively. These are given by

$$f_{\ell r,o} = \frac{2f_{r0}\tan^{-1}\left\{2\sqrt{\dfrac{Z_{0e}Z_{0o}}{(Z_{0e}-Z_{0o})^2+2Z_{T1}(Z_{0e}-Z_{0o})}}\right\}}{\pi}, \tag{4.23}$$

and

$$\begin{aligned} f_{rr,o} &= 2f_{r0} - f_{\ell r,o} \\ &= \frac{2\pi f_{r0} - 2f_{r0}\tan^{-1}\left\{2\sqrt{\dfrac{Z_{0e}Z_{0o}}{(Z_{0e}-Z_{0o})^2+2Z_{T1}(Z_{0e}-Z_{0o})}}\right\}}{\pi}. \end{aligned} \tag{4.24}$$

Another resonance is located at $f_{r,o}$ which is the resonance of the basic ring resonator f_{r0}, i.e., $f_{r,o} = f_{r0}$. As indicated by the attenuation poles in equations (4.7)-(4.11) and resonances in equations (4.18) and (4.19), we have four unknown parameters. These are Z_{T1}, Z_{T2}, Z_{0e}, and Z_{0o}. The equations require the pre-assigned locations of the attenuation poles and resonances to solve these parameters, which can be obtained from the specified stopband characteristics and the edges of the passband.

4.5 Graphical Considerations

The effects of the shunt stub impedance and even- and odd-mode impedances on the resonance and attenuation pole frequencies are investigated as follows. In this study, the transmission line in the upper half ring is considered as a constant parameter where $Z_{T1} = 50\ \Omega$.

Figure 4.6(a) shows the calculated location of the poles and resonance frequencies *normalized* with $f_{r,o}$ versus the *normalized* impedance of the shunt stub Z_{T2} with Z_0 under the condition $Z_{0e} = 150\ \Omega$ and $Z_{0o} = 50\ \Omega$. As shown in Figure 4.6(a), the normalized odd-mode frequencies $f'_{\ell r,o}$, $f'_{r,o}$, and $f'_{rr,o}$ are independent on Z'_{T2}, as the shunt stub does not exist in the equivalent circuit due to odd-mode excitation [cf. Figure 4.5]. Similarly, the other two attenuation poles at f'_{p1} and f'_{p4}, only slightly varies with Z'_{T2}. On the other hand, the shunt stub impedance affects the normalized even-mode frequencies $f'_{r1,e}$ and $f'_{r2,e}$. In particular, when Z'_{T2} is increased, the two attenuation poles at f'_{p2} and f'_{p3} move closer to the low and the high edges of the resonances at

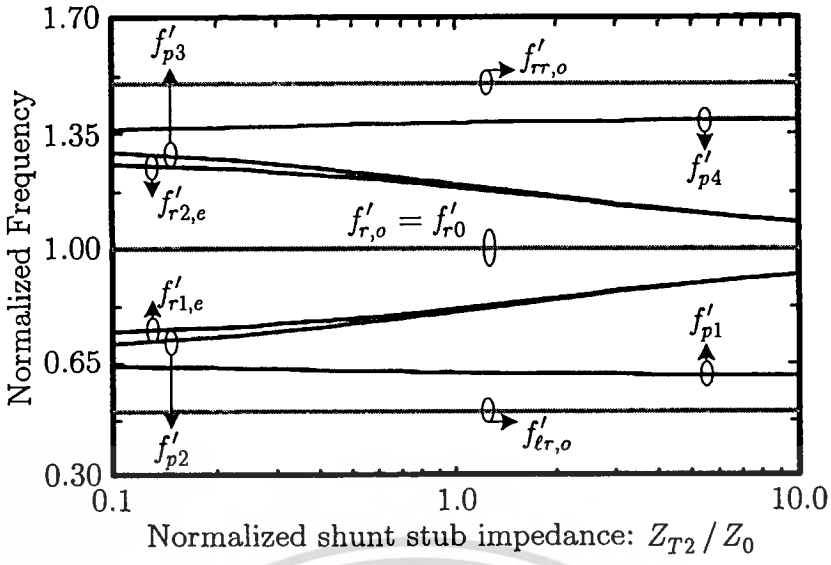

(a)

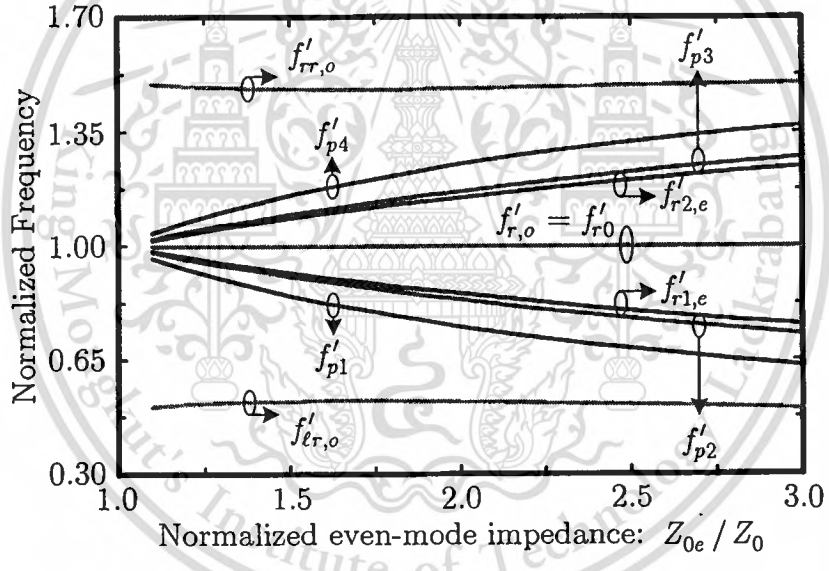

(b)

Figure 4.6 Normalized attenuation pole and resonance frequencies of the triple-mode ring resonator as a function of the normalized (a) shunt stub impedance $Z'_{T2} = Z_{T2} / Z_0$, (b) even-mode impedance $Z'_{0e} = Z_{0e} / Z_0$, and (c) odd-mode impedance $Z'_{0o} = Z_{0o} / Z_0$.

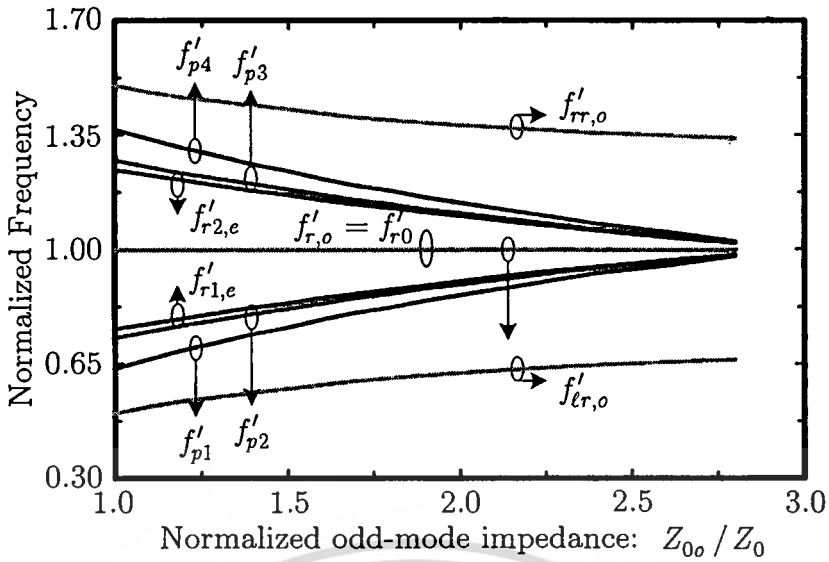

(c)

Figure 4.6 (Con't)

$f'_{r1,e}$ and $f'_{r2,e}$, respectively. A sharp transition band can be thus achieved. Eventually, these poles and resonances converge to $f'_{r,o} = f'_{r0} = 1$ for a very large Z'_{T2}. It is thus evident that these attenuation poles and resonances of the proposed resonator have symmetrical properties around $f'_{r,o}$.

Figure 4.6(b) and (c) show the normalized attenuation pole and resonance characteristics in relation to the even- and odd-mode impedances, respectively. As illustrated in Figure 4.6(b) under the condition of $Z_{0o} = 50\ \Omega$ and $Z_{T2} = 10\ \Omega$, the normalized resonance frequencies $f'_{\ell r,o}$ and $f'_{rr,o}$ are practically constant against Z'_{0e}. On the other hand, the other resonances ($f'_{r1,e}$ and $f'_{r2,e}$) and the attenuation poles frequencies (f'_{p1}, f'_{p2}, f'_{p3}, and f'_{p4}) move apart from the center frequency $f'_{r,o}$ when Z'_{0e} increases. For Figure 4.6(c) under the condition of $Z_{0e} = 150\ \Omega$ and $Z_{T2} = 10\ \Omega$, the resonance and attenuation pole frequencies move closer to $f'_{r,o}$ when Z'_{0o} increases. It is noticed that the frequencies $f'_{r1,e}$ and f'_{p2}, as well as $f'_{r2,e}$ and f'_{p3} are always in close proximity in all the plots. Therefore, the sharp transition band should be maintained against the impedance parameter selections.

4.6 Physical Interpretation

The resonances can be physically explained by virtue of the equivalent models for the even- and odd-mode in Figure 4.4 and 4.5. Consider first the odd-mode model in Figure 4.5. It is essentially a parallel of the shorted transmission line and open-ended coupled line, both at the length of $\lambda_g/4$ (with reference to the center frequency $f_{r,o}$). At frequencies around $f_{\ell r,o}$, the transmission line behaves like a lumped inductor (L), whereas the coupled line behaves like a lumped capacitor (C). This as a consequence forms a parallel LC resonator that gives rise to the resonance at $f_{\ell r,o}$ in the proposed ring structure. At frequencies around $f_{rr,o}$, the behaviors of the $\lambda_g/4$ shorted transmission line and coupled line are in dual fashion. Whereas the transmission line behaves like a capacitor, the coupled line behaves like an inductor. This thus forms a parallel LC resonator that gives rise to the resonance at $f_{rr,o}$. At around the center frequencies $f_{r,o}$, however, both the transmission line and the coupled line exhibit *self*-resonance where the electric and magnetic energies are equal within their own structures. This thereby gives rise to the resonance frequency of the ring at $f_{r,o}$.

Now consider the even-mode model in Figure 4.4. It is essentially a parallel of the open transmission line and open-ended coupled line at $\lambda_g/4$. At frequencies around $f_{r1,e}$, the transmission line behaves like a capacitor whereas the coupled line behaves like an inductor, giving rise to the resonance at $f_{r1,e}$. At frequencies around $f_{r2,e}$, the transmission line and coupled line behaves in dual fashion, yielding the resonance at $f_{r2,e}$.

The physical mechanism that is attributed to the attenuation poles at f_{p1} and f_{p4} is based upon the output cancellation of the signals propagating along the upper transmission line path and the lower open-ended coupled line path. For the attenuation poles at f_{p2} and f_{p3}, they are attributed to the input/output characteristics of the cascaded coupled lines with $\lambda_g/4$ shunt open stub which is effectively shorted to ground at f_{p2} and f_{p3}.

4.7 Design Examples: Wideband Bandpass Filter

This section describes the design evolution of the triple ring resonator based bandpass filter. First, triple-mode ring bandpass filter has been designed at 1 GHz center frequency and a 30 % fractional bandwidth and fabricated on a low cost FR-4 PCB. Next, the cascade of single ring filter is further illustrated to improve the stopband attenuation level. Finally, the techniques used to minimize the effect of coupled microstip line in the structure that produces the spurious response will be described.

4.7.1 Single Ring Resonator Filter

To validate the feasibility of the proposed ring resonator, a single ring bandpass filter with a system impedance of $Z_0 = 50\ \Omega$ was designed and fabricated on an FR-4 substrate ($\varepsilon_r = 4.55$, $h = 0.8$ mm, and $\tan\delta = 0.02$) at $f_0 = 1$ GHz center frequency, with a 30 % fractional bandwidth.

Based on the theoretical analysis in Section 4.3 and 4.4, and the required specification, we may first assume that the low edge of the resonances is at $f_{r1,e} = 0.85$ GHz, and the high edge of the resonances is at $f_{r2,e} = 2f_0 - f_{r1,e} = 1.15$ GHz. The attenuation pole f_{p2} is selected at 0.82 GHz to obtain a sharp rejection response, whereas the lower pole f_{p1} is at 0.7 GHz. This subsequently yields $f_{p3} = 1.18$ GHz and $f_{p4} = 1.3$ GHz. Applying these frequencies f_{p1} or f_{p4} into equation (4.7) or (4.10), f_{p2} or f_{p3} into equation (4.8) or (4.9), $f_{r1,e}$ into equation (4.18), and $f_{r2,e}$ into equation (4.19), the characteristic impedances of the ring resonator are, thus obtained. In this design, a commercial software was employed to automatically solve in equations (4.7) through (4.11), (4.18), (4.19), (4.23), and (4.24) for the characteristic impedances of Z_{T1}, Z_{T2}, Z_{0e}, and Z_{0o} (only values amenable to practical realization were selected): $Z_{T1} = 105.6\ \Omega$, $Z_{T2} = 13.2\ \Omega$, $Z_{0e} = 133.27\ \Omega$, and $Z_{0o} = 59.7\ \Omega$. With the center frequency of the passband at 1 GHz, the simulated insertion loss, S_{21} of the proposed resonator based bandpass filter, is shown in Figure 4. 7. As observed in the figure, four attenuation poles can be found at 0.7, 0.82, 1.18, and 1.3 GHz, respectively.

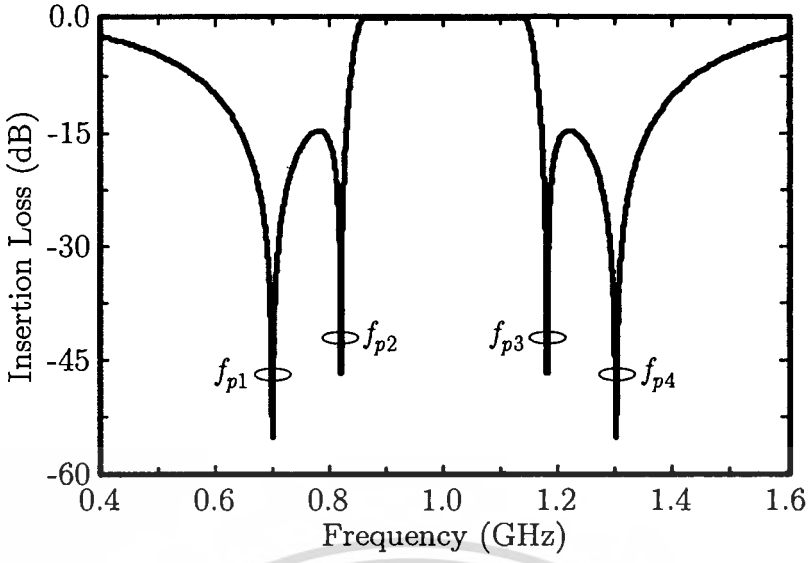

Figure 4.7 Simulated insertion loss of the ring bandpass filter designed at 1 GHz center frequency.

The attenuation level between f_{p1} and f_{p2} and/or f_{p3} and f_{p4} is more than -15 dB.

Subsequently, the initial characteristic impedances were then refined to obtain realistic filter dimensions. This was based on a practical FR-4 substrate with the help of Agilent–ADS [72]. Figure 4.8(a) shows the layout of a single square-ring bandpass filter. The dimensions (in millimeters) are summarized as follows: $w_1 = 0.3$, $\ell_1 = 85.3$, $w_2 = 5.4$, $\ell_2 = 38.2$, $w_C = 0.3$, $\ell_C = 43.2$, and $s = 0.25$. A photograph of the filter is shown in Figure 4.8(b). The dimensions, excluding two SMA connectors are approximately 67 mm × 78 mm. The measurement was performed with an Agilent N5230A vector network analyzer test system, which utilized the SOLT (Short-Open-Load-Thru) calibration.

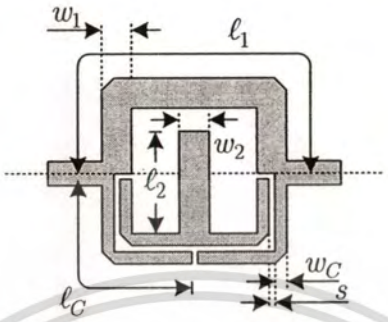

(a)

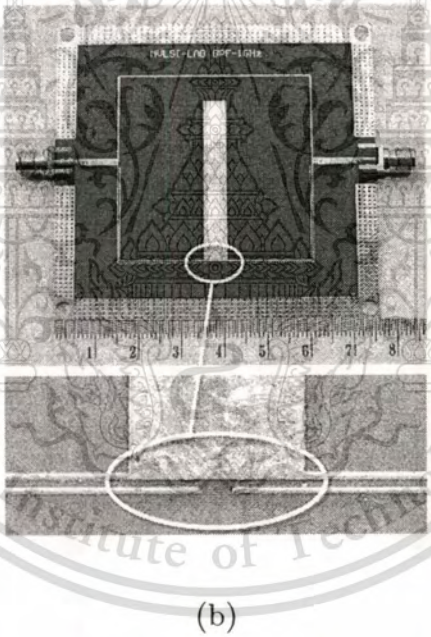

(b)

Figure 4.8 A single ring bandpass filter. (a) Layout. (b) Photograph of the fabricated filter on an FR-4 substrate.

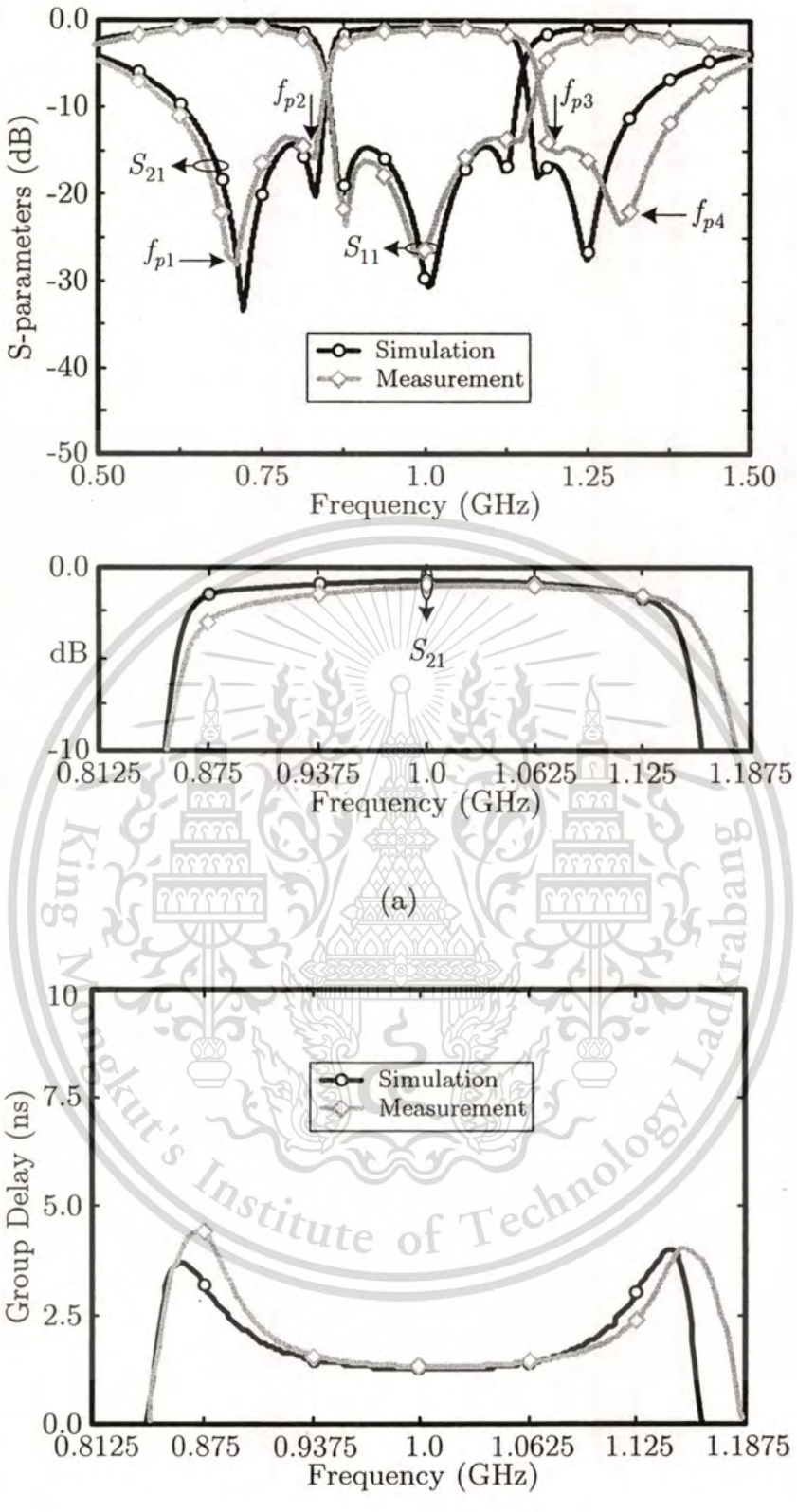

Figure 4.9 Measured and simulated results of triple-mode single ring bandpass filter. (a) Magnitude response of S_{11} and S_{21}. (b) Group delay.

The measured results of *S*-parameters are depicted in Figure 4.9(a) (*top row*), where they are in good agreement with the simulated results. The measured center frequency is at 1.02 GHz and the 3-dB fractional bandwidth is 29.36 %. The measured insertion loss, including the material losses and two SMA connectors, is better than -0.8 dB (*bottom row*), whereas the in-band reflection coefficient is greater than -13.6 dB within 0.865-1.157 GHz. The filter exhibits four attenuation poles, two on each side of the passband at 0.72, 0.83, 1.21 and 1.305 GHz, respectively. These attenuation pole frequencies are noticeable in both simulated and measured results. Moreover, a -13.5 dB attenuation level between neighboring attenuation poles can be obtained. An attenuation slope for the sharp rejection responses is calculated at 244.6 dB/GHz (calculated from 0.83 GHz with -15.13 dB to 0.88 GHz with -2.9 dB), and 227.6 dB/GHz (calculated from 1.16 GHz with -3.62 dB to 1.21 GHz with -15 dB). The group delay over the passband is less than 1.6 ns, as shown in Figure 4.9(b).

4.7.2 Cascaded Single-Ring Resonator Filter

To achieve a higher out-of-band attenuation, a cascaded version of the single square-ring resonator in Figure 4.8(a) is depicted in Figure 4.10(a), where the resonators are connected through the normal transmission line with $\ell_t = \lambda_g / 4$ and the characteristic impedance is Z_0. The dimensions of this line on an FR-4 are $w_t = 1.47$ mm and $\ell_t = 40.9$ mm. It is anticipated that the cascaded structure can provide a quadratic improvement in the attenuation performance. Figure 4.10(b) shows a photograph of the fabricated double ring filter. The circuit size of the filter occupies an area about 67 mm $\times$ 162 mm.

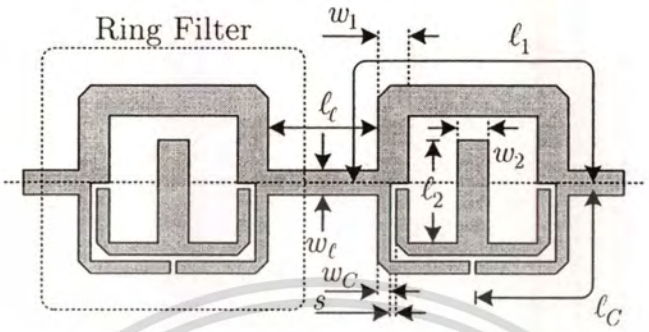

(a)

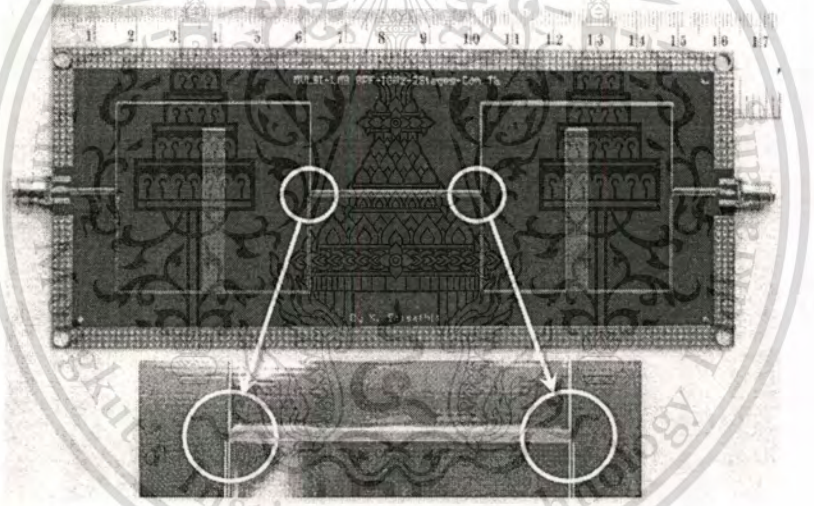

(b)

Figure 4.10 A double ring bandpass filter. (a) Layout. (b) Photograph of the fabricated filter on an FR-4 substrate.

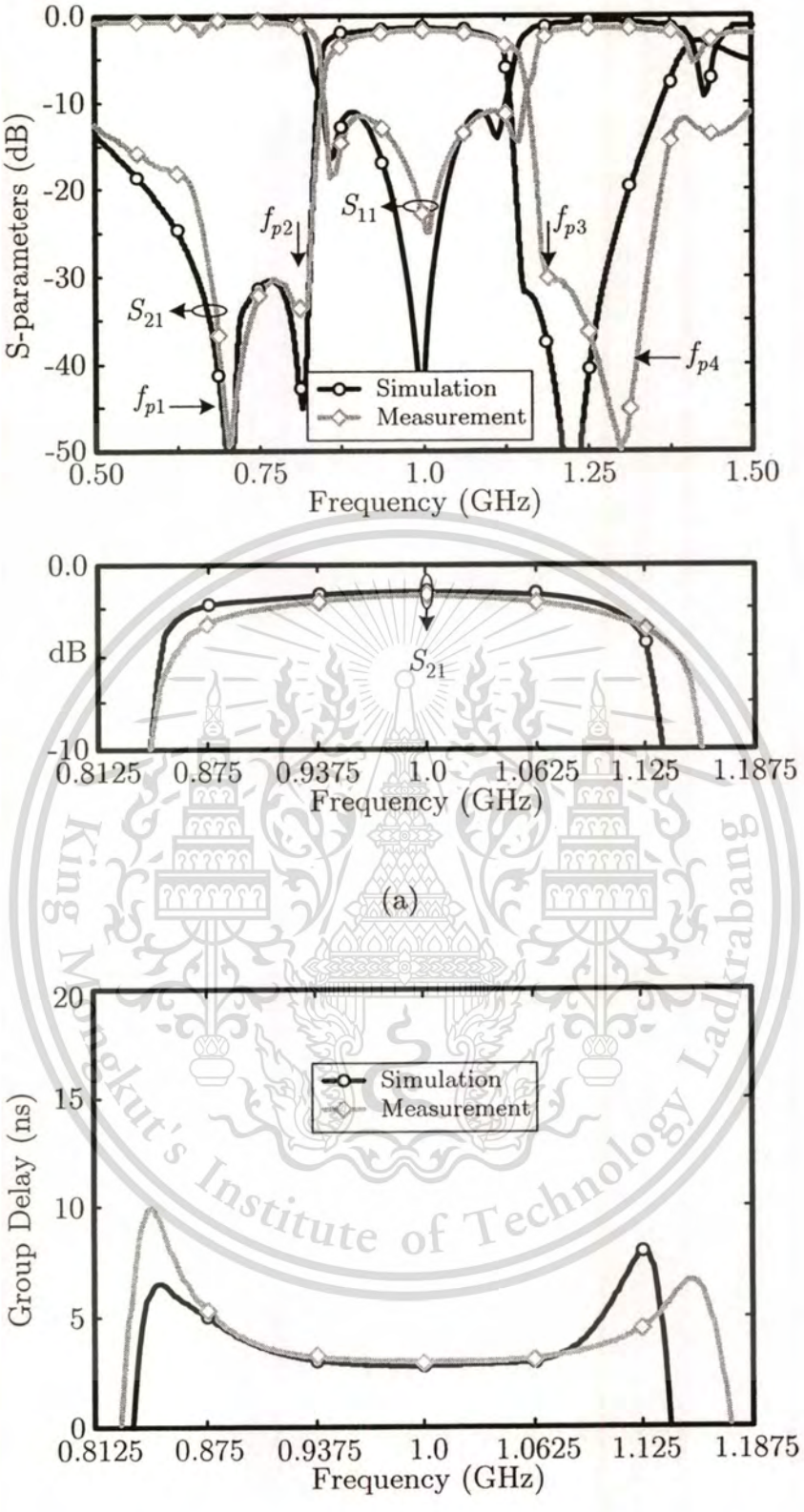

Figure 4.11 Measured and simulated results of triple-mode double ring bandpass filter. (a) Magnitude response of S_{11} and S_{21}. (b) Group delay.

Table 4.1 Comparison of specifications and measured performances of the proposed filter with other ring filters.

Specifications and Performances	Ref [43]	Ref [85]	This work
Number of ring resonator	3	2	2
Type of mode operation	Dual-mode	Dual-mode	Triple-mode
Center frequency (GHz)	5.6	2.45	1.0
Fractional bandwidth	0.493	0.37	0.272
Substrate	RT/Duroid 6010.2, Laminate	RT/Duroid 6006, Laminate	FR-4, Epoxy
Relative dielectric constant	10.2	6.15	4.55
Loss tangent	0.0023	0.0027	0.02
Passband insertion loss (dB)	-1.6	-0.84	-1.62
Reflection coefficient (dB)	-13.3	-11.4	-11.7
Group delay (ns)	< 2	Not available	< 3.2
Attenuation slope: lower, upper (dB/GHz)	99.75, 101.56	Not available	490.83, 443.33

The simulated and measured performances of this filter are superimposed as shown in Figure 4.11. As shown in Figure 4.11(a) (*top row*), the measured prototype-filter has a 3-dB fractional bandwidth of 27.2 % with the center frequency of 1.03 GHz, an insertion loss of -1.62 dB (*bottom row*) and the input/output reflection coefficients of -11.7 dB within 0.87 to 1.16 GHz. Moreover, two adjacent attenuation poles at 0.84 and 1.21 GHz, occurring near the passband, are improved at below -30 dB. The remaining attenuation poles are located at 0.72 and 1.30 GHz. A comparison between the response in Figure 4.9(a) (*top row*) and Figure 4.11(a) (*top row*) indicates that the out-band attenuation level between the adjacent attenuation poles ($f_{p1} - f_{p2}$ and $f_{p3} - f_{p4}$) is changed from -13.5 dB to -30 dB. The attenuation slope of this cascaded filter is 490.83 dB/GHz (calculated from 0.84 GHz with -32.6 dB to 0.90 GHz with -3.15 dB), and 443.33 dB/GHz (calculated from 1.15 GHz with -3.7 dB to 1.21 GHz with -30.3 dB). Furthermore, the

measured group delay over the passband as shown in Figure 4.11(b) is less than 3.2 ns. The specifications and measured performances of the proposed triple-mode bandpass filter with other dual-mode ring filters [43, 85] are compared in Table I.

4.7.3 Multi-Frequency Suppression Technique

Since the proposed ring resonator incorporates two couplers in the structure, the harmonic response is unavoidable when this resonator-based bandpass filter is fabricated in the microstrip structure. This is because of the inherently different phase velocities between even- and odd-mode in the microstrip coupler [60, 91]. In addition, theses two couplers also exhibits two resonances at the far left and right region of the response ($f_{tr,o}$ and $f_{rr,o}$) [cf. Figure 4.2] in the lower and the upper stopband, respectively.

In order to suppress the spurious response, we have introduced two T-shaped transmission lines [31], one at the input and another at the output of the double-ring filter [see Figure 4.12]. In particular, the lengths of the loaded open stubs of the T-shaped transmission lines were designed at different frequencies, i.e., at 1.7 GHz and 2.3 GHz, to overall suppress of the spurious resonant peak and coupling of the filter response. In addition, an inter-digital coupled line with two finger pairs [89-90] was inserted at the interconnecting transmission line between the two rings [see Figure 4.12(a)] and this effectively suppresses the response at the second-harmonic frequency at $2f_0 =$ 2 GHz. Note that the inter-digital coupled line also helps attenuate the additional lower stopband resonances and performs the DC blocking task for the filter. This yields the improvement of the lower and upper stopband performances.

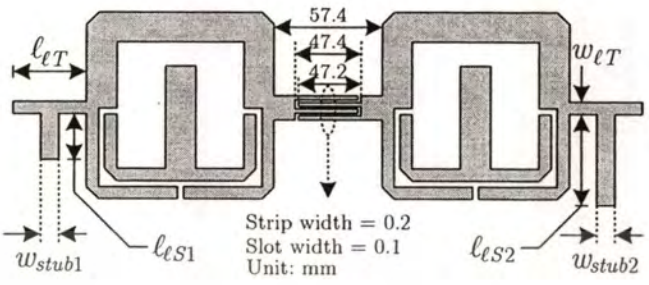

(a)

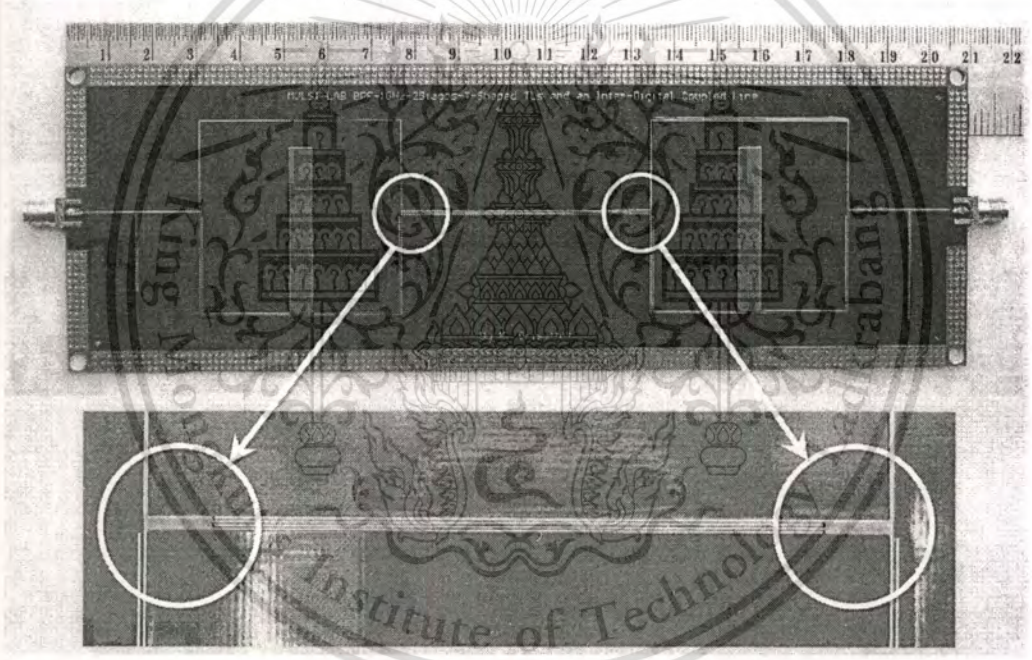

(b)

Figure 4.12 A double ring bandpass filter with T-shaped transmission lines and an inter-digital coupled line. (a) Layout. (b) Photograph of the fabricated filter on an FR-4 substrate.

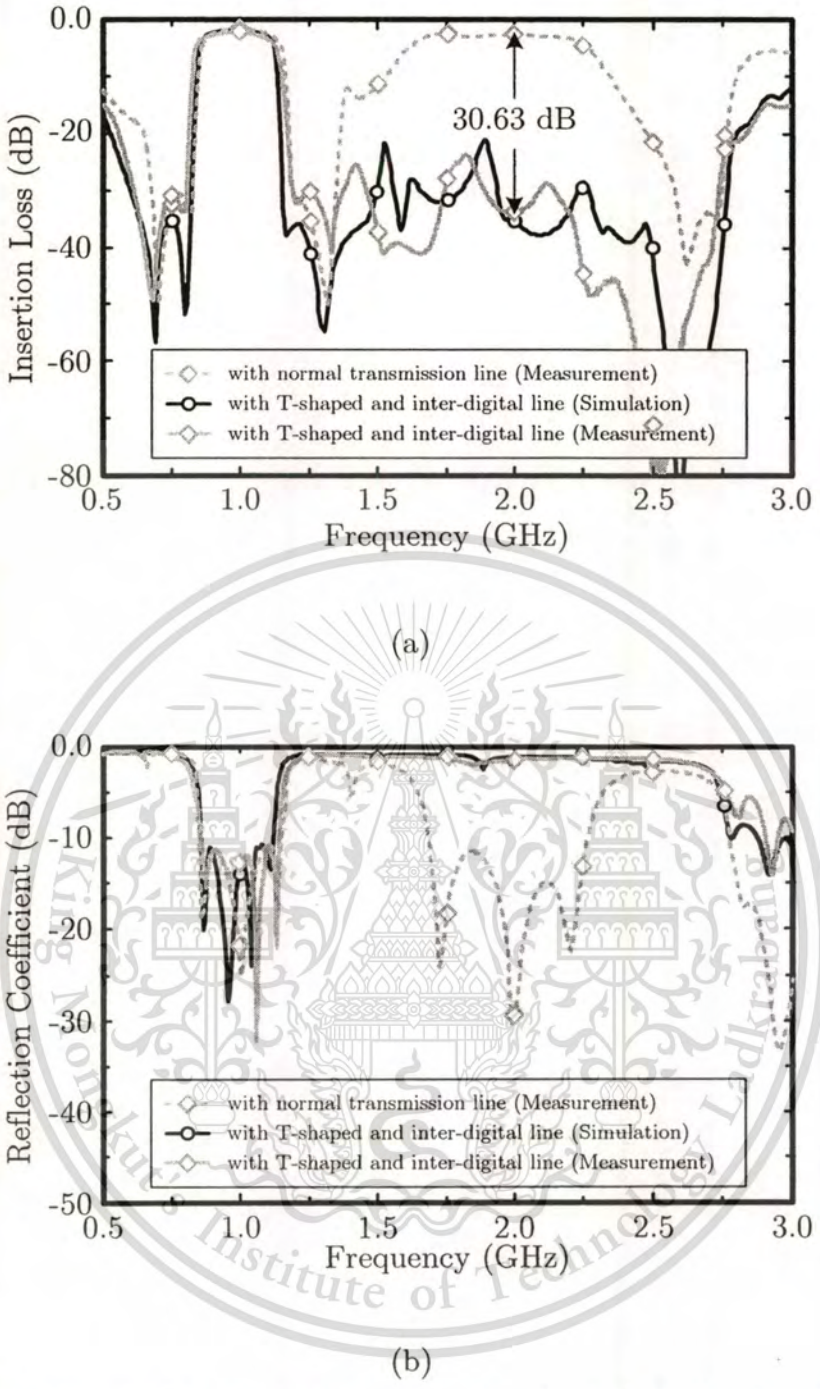

Figure 4.13 Measured and simulated results of double ring bandpass filter with T-shaped transmission lines and an inter-digital coupled line. (a) Insertion Loss and (b) Reflection coefficient.

With reference to Figure 4.12(a), each T-shaped transmission line is designed with the length ℓ_{tT} of $\lambda_g/6$; where two shunt open stubs with the length ℓ_{tS1} and ℓ_{tS2} are selected for suppression at frequencies lower and higher than second harmonic, respectively. The characteristic impedance of the transmission line is calculated at 86.6 Ω and the shunt stub at 75 Ω. Subsequently, the physical dimensions were further synthesized on an FR-4 substrate with the width ω_{tT} = 0.47 mm and the length ℓ_{tT} = 28.5 mm. Also, ℓ_{tS1} = 18.37 mm, ℓ_{tS2} = 26.25 mm, and $\omega_{stub1} = \omega_{stub2}$ = 0.67 mm. The parameters used in an inter-digital coupled line (in millimeters) are also given in Figure 4.12(a). The photograph of Figure 4.12(a) is shown in Figure 4.12(b), with the size of 67 mm × 208 mm.

Figure 4.13 shows the simulated and measured performances of the designed double ring bandpass filter in Figure 4.12(a) and (b), over a wider frequency range from 0.5 to 3 GHz. Notice that the measured magnitude responses of S_{21} and S_{11} are practically preserved, as in the case of the double ring filter with the normal transmission line. An exception is that the second-harmonic frequency at $2f_0$ = 2 GHz of the proposed double ring filter is improved, i.e., at less than -33.75 dB (over 30.63 dB improvement). Moreover, the upper stopband is also suppressed by more than -23.75 dB over the frequency range from 1.18 GHz to 2.75 GHz. A -2.1 dB measured insertion loss is obtained at the center frequency of the passband, where the reflection coefficient within the passband is kept below -11.9 dB.

4.8 Chapter Summary

A triple-mode ring resonator core and its applications to bandpass filters have been proposed and successfully fabricated in a microstrip technology. The introduction of a pair of identical open-ended coupled lines with a shunt open stub, into a transmission line branch of a conventional ring resonator, has led to the triple-mode operation. When the triple-mode resonator is employed to implement a bandpass filter, the triple passband resonance frequencies along with the two attenuation poles close to the edges of the passband on either side, essentially give rise to a flat passband and sharp rejection response. The direct feed structure with T-shaped transmission line, and the fact that the signal mainly propagates along the transmission

line path of the triple-mode resonator over the passband frequencies, also yield a low insertion loss. Detailed analysis of the resonator, including the attenuation pole and resonance frequencies, has been studied to enable analytical and systematic designs, with minimum design iterations using electromagnetic simulation. Design examples and implementations of three prototype filters have been verified through simulations and measurements. To further improve out-of-band performance, the use of an inter-digital coupled line and two T-shaped transmission lines, particularly in the cascaded filter prototype, was also successfully introduced.

CHAPTER 5

CONCLUSIONS

This chapter summarizes this work in Section 5.1 and then point out possible directions for future work in Section 5.2.

5.1 Summary

This research has focus on the analysis, and design of passive devices and filters in microwave frequency region. The emphasis of two passive devices, Wilkinson divider and Hybrid coupler, is placed on analyzing divider with harmonic suppression. In this dissertation, an equivalent T-shaped transmission line with its compact size is substituted for a conventional transmission line of such devices to create the attenuation pole at the undesired frequency while the performances at operating frequency are maintained. The T-shaped technique can also be applied to other passive devices for harmonic suppression with simultaneously compact size. This technique is a direct extension of [31].

This dissertation also includes the design and implementation of two ring resonator bandpass filters. These ring filters are based on the dual-mode and triple-mode resonators, respectively. For dual-mode ring filter, it is one of the bandpass filter implementations with the benefit of a narrowband response. With the use of an artificial transmission line, the limitation of series stub perturbation due to the requirement of a very low or high characteristic impedance, at the symmetrical plane of the ring that is difficult to realize in the conventional microstrip line, is alleviated.

In the past, when the bandpass filter with wideband response was required, many filter design approaches were suggested [43-45, 89-90] and implemented in several communication systems. The triple-mode ring resonator core is *first* developed based on the planar ring resonator and is *newly proposed* in this dissertation as a better solution for enabling inherently sharp rejection and constant passband characteristic with low insertion loss. The analysis of the ring is based on the principle of two-port network and the even- and odd-mode excitation. The mathematical results presented in this

dissertation and employed in the design of bandpass ring filter are useful in achieving performances, which are close to the design specifications.

This dissertation also includes the implementation of the wideband bandpass filter. Since spurious response is attributed to the proposed triple-mode ring incorporating two coupled lines, some techniques have been added in the cascaded single-ring filter for multi-spurious suppression to suppress the effect of the difference between the modal phase velocities.

Therefore, this dissertation provides good practical techniques for power dividers and ring filters in microwave and millimeter-wave communication applications.

5.2 Future Work

There are various challenging issues that need exploration in future research work. Miniaturization and spurious frequency suppression have been an active research topic over the past few decades with applications in microwave and millimeter-wave communication systems. The following suggestions thus propose future research work based upon the contribution of this dissertation.

5.2.1 Wide Stopband Characteristic in Passive Device

After the miniature Wilkinson divider and Quadrature hybrid coupler with harmonic suppression were investigated in [54] by using T-shaped transmission line as discussed in Chapter 2, some research works [93-94] have been extensively analyzed for Wilkinson divider [93] and Quadrature hybrid [94], respectively, at the unwanted frequencies.

Figure 5.1 shows an equivalent E-shaped transmission line which is a cascaded configuration of two π-shaped transmission lines. The n-th harmonic frequency will be suppressed by employing the open stub with the length of $\lambda/4n$ where n is the number of harmonic at the undesired frequency. In addition, n can be positive real number which is greater than unity. As we notice in the figure, a new E-shaped transmission line has three shunt open stubs. This implies that this E-shaped transmission line will provide three attenuation poles at the undesired frequencies. By substituting Figure 5.1 for an E-shaped line in the classical Quadrature hybrid, the possible configuration

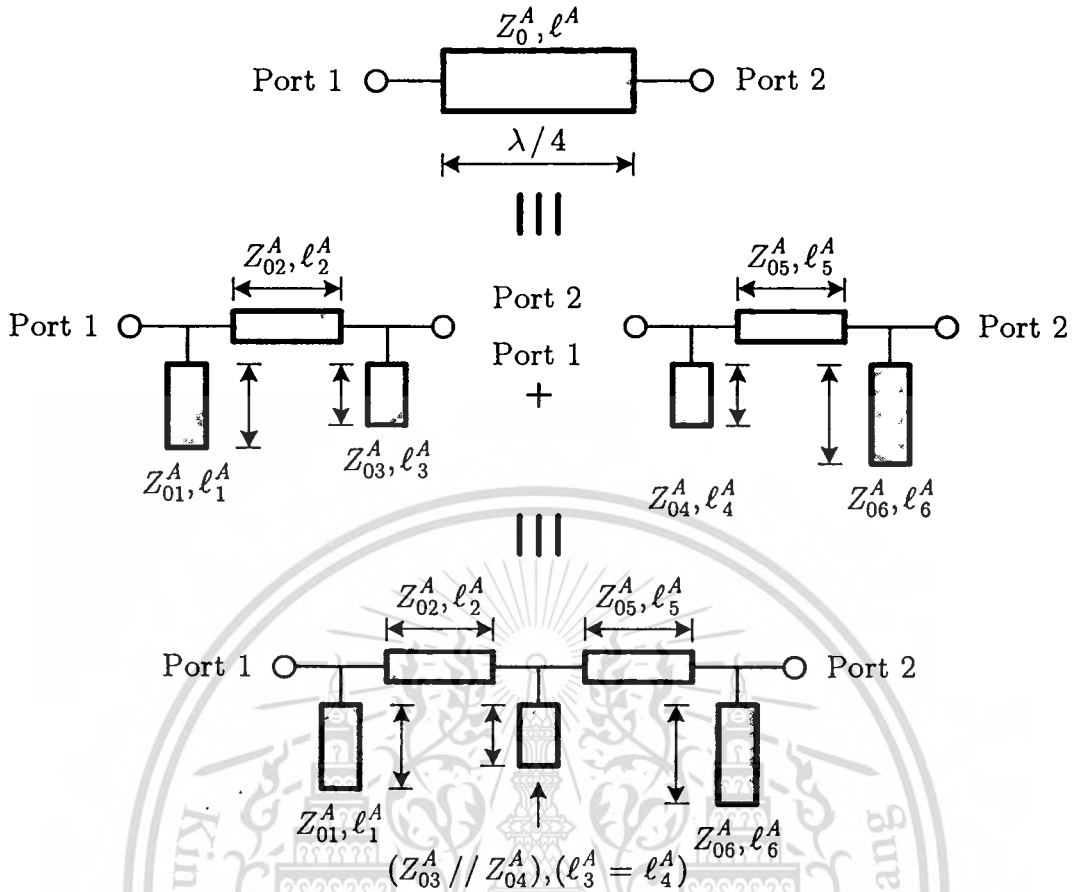

Figure 5.1 An equivalent E-shaped transmission line.

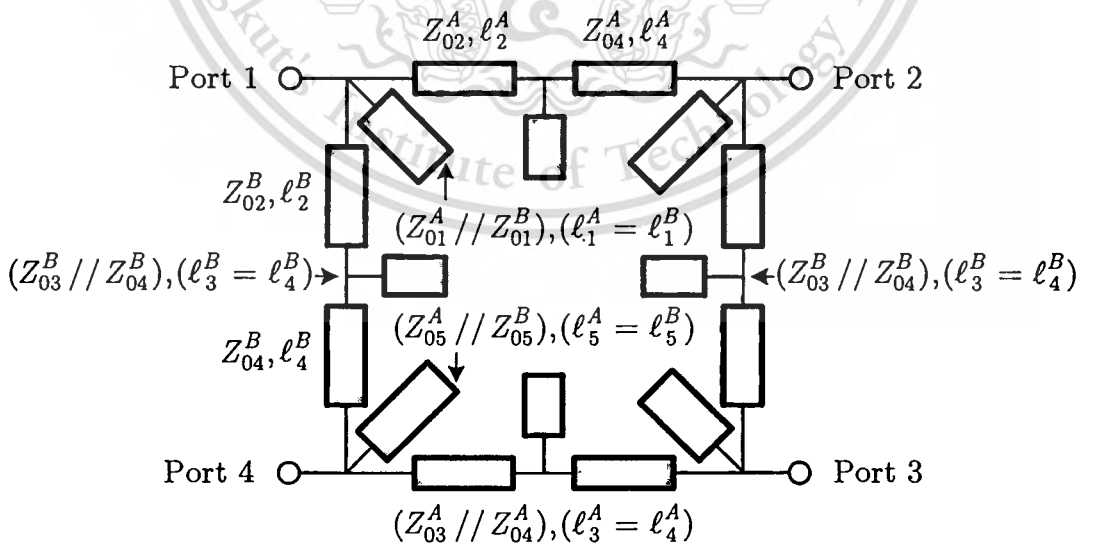

Figure 5.2 A possible configuration for Quadrature hybrid coupler.

of Quadrature hybrid coupler with simultaneously wide stopband characteristic and compact size can be displayed in Figure 5.2. By using the principle of even- and odd-mode analysis, a set of *S*-parameters will be obtained.

5.2.2 Quadruple- and Quintuple-Mode Ring Filters

As discussed in Chapter 3, the dual-mode ring bandpass filter is achieved by introducing the perturbation at the symmetrical plane of the ring. Since the symmetrical left-handed transmission line based perturbation presents highpass characteristic, the proposed filter exhibits poor out-of-band rejection. In addition, the structure needs coupling feed capacitors between two feed lines and a ring resonator for isolating the signal and any DC voltage source. Due to the limitation of self-resonant frequency of their capacitors, hence, this filter should be designed for the operating frequency only at a few gigahertz. The introduction of the inter-digital coupled line with two finger pairs [89-90] may be applied at the input and output ports. It will exhibit two extra resonant frequencies at the lower and the upper resonance in the original resonant frequency of dual-mode response. This result is called the *quadruple*-mode ring filter. Moreover, this line enables attenuation pole around twice of the fundamental frequency. This results in the rejection improvement and also suppression of spurious response, respectively.

When the inter-digital coupled lines in [89-90] are introduced at the input and output of the triple-mode ring resonator as presented in Chapter 4, the *quintuple*-mode ring can be achieved. Moreover, since two extra resonances are much closed to the original attenuation poles in the triple-mode ring, a highly steep transition characteristic will be further enhanced over the original triple-mode ring that is proposed in this dissertation [91].

REFERENCES

[1] Kenington P. B. **High-Linearity RF Amplifer Design.** Norwood, MA: Artech House, 2000.

[2] Cripps S. C. **RF Power Amplifiers for Wireless Communications.** Norwood, MA: Artech House, 2006.

[3] Pothecary N. **Feedforward Linear Power Amplifiers.** Norwood, MA: Artech House, 1999.

[4] Muhonen K. J., Kavehrad M., and Krishnamoorthy R. "Look-up table techniques for adaptive digital predistortion: A development and comparison." **IEEE Trans. Veh. Technol.,** vol. 49, no. 5, Sep. 2000. pp. 1995-2002.

[5] Kim J. and Konstantinou K. "Digital Predistortion of Wideband Signals Based on Power Amplifier Model with Memory." **Electron. Lett.,** vol. 37, no. 23, Nov. 2001. pp. 1417-1418.

[6] Woo Y., Yi J., Hong S., Kim I., Moon J., and Kim B. "Adaptive Digital Feedback Predistortion Technique for Linearizing Power Amplifier." **IEEE Trans. Microw. Theory Tech.,** vol. 55, no. 5, May. 2007. pp. 932-940.

[7] Choi J., Kim D., Kang D., and Kim B. "A Polar Transmitter with CMOS Programmable Hysteretic-Controlled Hybrid Switching Supply Modular for Multistandard Applications." **IEEE Trans. Microw. Theory Tech.,** vol. 57, no. 7, Jul. 2009. pp. 1675-1686.

[8] Pedro J. C. and Carvalho N. B. **Intermodulation in Microwave and Wireless Circuits.** Norwood, MA: Artech House, 2003.

[9] Zhang X., Larson L. E., and Asbeck P. M. **Design of Linear RF Outphasing Power Amplifers.** Norwood, MA: Artech House, 2003.

[10] Besser L., and Gilmore R. **Practical RF Circuit Design for Modern Wireless Systems: vol. I, Passive Circuits and Systems.** Boston, MA: Artech House, 2003.

[11] Mass S. A. **Microwave Mixer.** 2nd ED. Norwood, MA: Artech House, 1993.

[12] Lee Y. -T., Lee J., and Nam S. "New Planar High Q Active Resonator and Its Application to Low Phase Noise Oscillator." **Proc. IEEE-MTT-S Dig.,** Texas, Jun. 2004. pp. 2007–2010.

[13] Görür A. "A Novel Dual-Mode Bandpass Filter with Wide Stopband Using The Properties of Microstrip Open-Loop Resonator." **IEEE Microw. Wireless Compon. Lett.,** vol. 12, no. 10, Oct. 2002. pp. 386-388.

[14] Srisathit S., Patisang S., and Chongcheawchamnan M. "A Microstrip Stepped-Width Coupling Gap and Stepped-Width Ring Resonator Bandpass Filter." **Proc. ECTI-CON2005,** vol. 2, May 2005. pp. 726-729.

[15] Srisathit K. and Surakampontorn W. "Wideband Microstrip Bandpass Filter Based on Modified Parallel-Coupled Line Topology." **Proc. ISCIT.,** Dec. 2010. pp. 45-48.

[16] Nishikawa K., Tokumitsu T., and Toyada I. "Miniaturized Wilkinson power divider using three-dimensional MMIC technology." **IEEE Microw. Guided Wave Lett.,** vol. 6, no. 10, Oct. 1996. pp. 372-374.

[17] Avrillon S., Pele I., Chousseaud A., and Toutain S. "Dual-band power divider based on semiloop stepped-impedance resonators." **IEEE Trans. Microw. Theory Tech., Part 1,** vol. 51, no. 4, Apr. 2003. pp. 1269-1273.

[18] Hirota T., Minakawa A., and Muraguchi M. "Reduced-Size Branch-Line and Rat-Race Hybrids for Uniplanar MMICs." **IEEE Trans. Microw. Theory Tech.,** vol. MTT-38, no. 3, Mar. 1990. pp. 270-275.

[19] Raab F. H., Asbeck P., Cripps, S., Kenington P. B., Popovic Z. B., Pothecary N., Sevic J. F., and Sokal N. O. "Power Amplifiers and Transmitters for RF and Microwave." **IEEE Trans. Microw. Theory Tech.,** vol. 50, no. 3, Mar. 2002. pp. 814-826.

[20] Lin I.-H., Leong K. M. K. H., Caloz C., and Itoh T. "Dual-Band Sub-Harmonic Quadrature Mixer Using Composite Righ/Left-Handed Transmission Line." **IEE Proc.-Microw. Antennas Propag.,** vol. 153, no. 4, Aug. 2006. pp. 365-375.

[21] Ho T-.H. and Chung S.-J. "Design and Measurement of a Doppler Radar with New Quadrature Hybrid Mixer for Vehicle Applications." **IEEE Trans. Microw. Theory Tech.,** vol. 58, no. 1, Jan. 2010. pp. 1-8.

[22] Chiu J. C., Chang C. P., Houng M. P., and Wang Y. H. "A 12-36 GHz PHEMP MMIC Balanced Frequency Triple." **IEEE Microw. Wireless Compon. Lett.,** vol. 13, no. 5, May 2003. pp. 178-180.

[23] Yeung L. K. and Wang Y. E. "Mode-Based Beamforming Arrays for Miniaturized Platforms." **IEEE Trans. Microw. Theory Tech.,** vol. 57, no. 1, Jan. 2009. pp. 45-52.

[24] Miller R. E. and Chang K. "Integrated Active Antenna Using Annular Ring Microstrip Antenna and Gunn Diode." **Microwave Opt. Technol. Lett.,** vol. 4, no. 2, Jan. 1991. pp. 72-75.

[25] Bahl I. J. **Lumped Elements for RF and Microwave Circuit**. Boston, MA: Artech House, 2003.

[26] Lu L.-H., Bhattacharya P., Katehi L.P.B., and Ponchak G.E. "X-Band and K-Band Lumped Wilkinson Power Dividers with a Micromachined Technology." **Proc. IEEE-MTT-S Dig.,** Boston, MA, Jun. 2000. pp. 287-290.

[27] Piernas B. and Hirata M. "Enhanced miniaturized Wilkinson power divider." **Proc. IEEE-MTT-S Dig.,** Philadelphia, PA, Jun. 2003. pp. 1255-1258.

[28] Vogel R. W. "Analysis and Design of Lumped- and Lumped-Distributed Element Directional Couplers for MIC and MMIC Aapplications." **IEEE Trans. Microw. Theory Tech.,** vol. 40, Feb. 1992. pp. 253–262.

[29] Srisathit S., Chongcheawchamnan M., and Worapishet A. "Design and Realisation of Dual-Band 3 dB Power Divider Based on Two-Section Transmission-Line Topology." **Electron. Lett.,** vol. 8, no. 12, Jun. 1972. pp. 302-303.

[30] Chongcheawchamnan M., Patisang S., Krairiksh M., and Robertson, I. D. "Tri-Band Wilkinson Power Divider Using a Three-Section Transmission-Line Transformer." **IEEE Microw. Wireless Compon. Lett.,** vol. 16, no. 8, Aug 2006. pp. 452-454.

[31] Tu W.-H. and Chang K. "Compact Second Harmonic-Suppressed Bandstop and Bandpass Filters Using Open Stubs." **IEEE Trans. Microw. Theory Tech.,** vol. 54, no. 6, Jun. 2006. pp. 2497-2502.

[32] Cohn S. B. "Parallel-Coupled Transmission-Line-Resonator Filters." **IEEE Trans. Microw. Theory Tech.,** vol. 6, no. 2, Feb. 1958. pp. 223-231.

[33] Cristal E. G. and Frankel S. "Hairpin-Line and Hybrid Hairpin-Line/Half-Wave Parallel-Coupled-Line Filters." **IEEE Trans. Microw. Theory Tech.,** vol. 20, no. 11, Nov. 1972. pp. 719-728.

[34] Quendo C., Eric R., and Person C. "Narrow Bandpass Filters Using Dual-Behavior Resonator." **IEEE Trans. Microw. Theory Tech.,** vol. 51, no. 3, Mar. 2003. pp. 734-743.

[35] Wolff I. "Microstrip Bandpass Filters Using Degenerate Modes of a Microstrip Ring Resonator." **Electron. Lett.,** vol. 8, no. 12, Jun. 1972. pp. 302-303.

[36] Hong J.-S. and Lancaster M. J. "Microstrip Bandpass Filter Using Degenerate Modes of a Novel Meander Loop Resonator." **IEEE Microw. Guided Wave Lett.,** vol. 5, no. 11, Nov. 1995. pp. 371-372.

[37] Görür A., Karpuz C., and Akpinar M., "A Reduced-Size Dual-Mode Bandpass Filter with Capacitively Loaded Open-Loop Arms." **IEEE Microwave and Wireless Lett.,** vol. 13, no. 9, Sep. 2003. pp. 385-387.

[38] Hong J. S. and Lancaster M. J. "Bandpass Characteristics of New Dual-Mode Microstrip Square Loop Resonators." **Electron. Lett.,** vol. 31, no. 11, May 1995. pp. 891-892.

[39] Lugo C. and Papapolymerou J. "Bandpass Filter Design Using a Microstrip Triangular Loop Resonator with Dual-Mode Operation." **IEEE Microw. Wireless Comp. Lett.,** vol. 15, no. 7, Jul. 2005. pp. 475-477.

[40] Mao R.-J. and Tang X.-H. "Novel Dual-Mode Bandpass Filters Using Hexagonal Loop Resonators." **IEEE Trans. Microw. Theory Tech.,** vol. 54, no. 9, Sep. 2006. pp. 3526-3533.

[41] Mao R.-J., Tang X.-H., and Xiao F. "Miniaturized Dual-Mode Ring Bandpass Filters with Patterned Ground Plane." **IEEE Trans. Microw. Theory Tech.,** vol. 55, no. 7, Jul. 2007. pp. 1539-1547.

[42] Matsuo M., Yabuki H., and Makimoto M. "Dual-Mode Stepped-Impedance Ring Resonators for Bandpass Filter Applications." **IEEE Trans. Microw. Theory Tech.,** vol. 49, no. 7, Jul. 2001. pp. 1235-1240.

[43] Hsieh L.-H. and Chang K. "Compact, Low Insertion-Loss, Sharp-Rejection, and Wide-Band Microstrip Bandpass Filters." **IEEE Trans. Microw. Theory Tech.,** vol. 51, no. 4, Apr. 2003. pp. 1241-1246.

[44] Cai P., Ma Z., Guan X., Kobayashi Y., Anada T., and Hagiwara G. "Compact Millimeter-Wave Ultra-Wideband Bandpass Filter Using Dual-Mode Ring Resonator and Multiple-Mode Parallel-Coupled Line Structure." **Proc. APMC.,** Dec. 2006. pp. 163-166.

[45] Cai P., Ma Z., Guan X., Kobayashi Y., and Anada T. "Novel Compact Microstrip Dual-Mode Ring Resonator Wideband Bandpass Filter with Significantly Improved Stopband Property" **IEICE Trans. Electron.,** vol. E89-C, no. 12, Dec. 2006. pp. 1858-1864.

[46] Gilmore R. and Besser L. **Practical RF Circuit Design for Modern Wireless Systems: vol. II, Active Circuits and Systems.** Boston, MA: Artech House, 2003.

[47] Pozar D. M. **Microwave Engineering.** New York, Addison-Wesley Publishing Company, Inc. 1990.

[48] Devlin L. M. and Minnis B. J. "A Versatile Vector Modulator." **Proc. IEEE-MTT-S Dig.,** Dallas, TX, May 1990. pp. 519-521.

[49] Wilkinson E. J. "An N-way Hybrid Power Divider." **IRE Trans. Microw. Theory Tech.,** vol. MTT–8, Jan. 1960. pp. 116–118.

[50] Reed J. and Wheeler G. J. "A Method of Analysis of Symmetrical Four-Port Networks." **IRE Trans. Microw. Theory Tech.,** vol. MTT–4, no. 4, Oct. 1956. pp. 246-252.

[51] Kinayman N. and Aksun M. I. **Modern Microwave Circuit.** Norwood, MA: Artech House, 2000.

[52] Scardelletti M. C., Ponchak G. E., and Weller T. M. "Miniaturized Wilkinson Power Dividers Utilizing Capacitive loading." **IEEE Microw. Wireless Comp. Lett.,** vol. 12, no. 1, Jan. 2002. pp. 6-8.

[53] Woo D.-J. and Lee T.-K. "Suppression of Harmonics in Wilkinson Power Divider Using Dual-Band Rejection by Asymmetric DGS." **IEEE Trans. Microw. Theory Tech.,** vol. 53, no. 6, Jun. 2005. pp. 2139-2144.

[54] Srisathit K., Jadpum P., and Surakampontorn W. "Miniature Wilkinson Divider and Hybrid Coupler with Harmonic Suppression Using T-Shaped Transmission Line." **Proc. APMC.,** Dec. 2007. pp. 785-788.

[55] Sonnet Software. 2011. [Online].
Available : http://www.sonnetsoftware.com/products/lite/download.html.

[56] Ponchak G. E. "Experimental Analysis of Reduced-sized Coplanar Waveguide Transmission Lines." **Proc. IEEE-MTT-S Dig.,** Philadelphia, PA, Jun. 2003. pp. 971-974.

[57] Woo D.-J. and Lee T.-K. "Compact Planar Microstrip Branch-Line Couplers Using Quasi-Lumped Elements Approach with Nonsymmetrical and Symmetrical T-Shaped Structure." **IEEE Trans. Microw. Theory Tech.,** vol. 54, no. 9, Sep. 2006. pp. 3508-3514.

[58] Gu. J. and Sun X. "Miniaturization and Harmonic Suppression of Branch-Line and Rat-Race Hybrid Coupler Using Compensating Spiral Compact Microstrip Resonant Cell." **Proc. IEEE-MTT-S Dig.,** Long Beach, CA, Jun. 2005. pp. 1211-1214.

[59] Makimoto M. and Yamashita S. **Microwave Resonators and Filters for Wireless Communication - Theory, Design, and Application.** Berlin, Springer, 2001.

[60] Hong J.-S. and Lancaster M. J. **Microstrip Filters for RF/Microwave Applications.** New York: Wiley, 2001.

[61] Hsieh L.-H. and Chang K. **Microwave Ring Circuits and Related Structures.** 2nd ED. New Jersey: John Wiley & Sons, 2004.

[62] Awai I. "General Theory of a Circular Dual-Mode Resonator Bandpass Filter" **IEICE Trans. Electron.,** vol. E81-C, no. 1, Nov. 1988. pp. 1557-1763.

[63] Zhu L. and Wu K. "A Joint Field/Circuit Model of Line-to-Ring Coupling Structures and Its Application to the Design of Microstrip Dual-Mode Filters and Ring Resonator Circuits." **IEEE Trans. Microw. Theory Tech.,** vol. 47, no. 10, Oct. 1999. pp. 1938-1948.

[64] Sun K.-H. and Tam K.-W. "A Novel Compact Dual-Mode Bandpass Filter with Meander Open-Loop Arms." **Proc. IEEE-MTT-S Dig.,** Jun. 2004. pp. 1479-1482.

[65] Yabuki H., Sagawa M., Matsuo M., and Makimoto M. "Stripline Dual-Mode Ring Resonators and Their Application to Microwave Devices." **IEEE Trans. Microw. Theory Tech.,** vol. 44, no. 5, May 1996. pp. 723-729.

[66] Kunda A. C. and Awai I. "Control of Attenuation Pole Frequency of a Dual-Mode Microstrip Ring Resonators Bandpass Filter." **IEEE Trans. Microw. Theory Tech.,** vol. 49, no. 6, Jun. 2001. pp. 1113-1117.

[67] Tan B. T., Yu J. J., Chew S. T., Leong M.-S., and Ooi B.-L. "A Miniaturized Dual-Mode Ring Resonator Bandpass Filter with a New Perturbation." **IEEE Trans. Microw. Theory Tech.,** vol. 53, no. 1, Jan. 2005. pp. 343-348.

[68] Tan B. T., Chew S. T., Leong M. S., and Ooi B. L. "A Dual-Mode Bandpass Filter with Enhanced Capacitive Perturbation." **IEEE Trans. Microw. Theory Tech.,** vol. 51, no. 8, Aug. 2003. pp. 1906-1910.

[69] Lei M.-F. and Wang H. "An Analysis of Miniaturized Dual-Mode Bandpass Filter Structure Using Shunt-Capacitance Perturbation." **IEEE Trans. Microw. Theory Tech.,** vol. 53, no. 3, Mar. 2005. pp. 861-867.

[70] Troughton P. "Measurement Techniques in Microstrip." **Electron. Lett.,** vol. 5, no. 2, Jan 1969. pp. 25-26.

[71] Wolff I. and Knoppik N. "Microstrip Ring Resonator and Dispersion Measurement on Microstrip Lines." **Electron. Lett.,** vol. 7, no. 26, Dec. 1971. pp. 779-781.

[72] Advanced Design System (ADS) 2009. Agilent Technol., Palo Alto, CA, 2009. [Online].
Available : http://www.agilent.com/find/eesof-ads.

[73] Lai A., Itoh T., and Caloz C. "Composite Right/Left-Handed Transmission Line Metamaterials." **IEEE Microw. Mag.,** vol. 5, no. 3, Sep 2004. pp. 34-50.

[74] Mongia R. K., Bahl I. J., Bhartia P., and Hong J. **RF and Microwave Coupled-Line Circuits**. 2nd ED. Norwood, MA: Artech House, 2007.

[75] Srisathit K., Jadpum P., Bunnjaweht S., and Surakampontorn W. "New Dual-Mode Ring Bandpass Filter Using Symmetrical Left-Handed Transmission Line." **Proc. APMC.,** Dec. 2007. pp. 1015-1018.

[76] Lastoria G., Gerini G., Guglielmi M., and Emma F. "CAD of Triple-Mode Cavities in Rectangular Waveguide." **IEEE Microw. Guided Wave Lett.,** vol. 8, no. 10, Oct. 1998. pp. 339-341.

[77] Bonetti R. R. and Williams A. E. "Application of Dual TM Modes to Triple- and Quadruple-Mode Filters." **IEEE Trans. Microw. Theory Tech.,** vol. 35, no. 12, Dec. 1987. pp. 1143-1149.

[78] Chua L. H. and Syahkal D. M. "Analysis and Design of Three Transmission Zeros Band-Pass Filter Utilizing Triple-Mode Dielectric loaded Cubical Cavity." **Proc. IEEE-MTT-S Dig.,** Philadelphia, PA, Jun. 2003. pp. 937-940.

[79] Hunter I. C., Rhodes J. D., and Dassonville V. "Triple Mode Dielectric Resonator Hybrid Reflection Filters." **IEE Proc.-Microw. Antennas Propag.,** vol. 145, no. 4, Aug. 1998. pp. 337-343.

[80] Lugo C. and Papapolymerou J. "Planar Realization of a Triple-Mode Bandpass Filter Using a Multilayer Configuration." **IEEE Trans. Microw. Theory Tech., Part 1,** vol. 55, no. 2, Feb. 2007. pp. 296-301.

[81] Lugo C. A. 2006. "**Design and Synthesis Techniques for Reconfigurable Microwave Filters Using Single and Dual-Mode Resonators.**" Ph.D. dissertation, Georgia Institute of Technology, Georgia, United States, 2006.

[82] Paul D. K., Gardner P., and Tan K. P. "Suppression of Even Modes in Microstrip Ring Resonators." **Electron. Lett.,** vol. 30, no. 21, Oct. 1994. pp. 1772-1774.

[83] Jung W.-C., Park H.-J., and Lee J.-C. "Microstrip Ring Bandpass Filters with New Interdigital Side-Coupling Structure." **Proc. APMC.,** Dec. 1999. pp. 678-681.

[84] Akujuobi C. M. and Sadiku M. N. O. **Introduction of broadband communication systems.** United States: Chapman & Hall, 2007.

[85] Konpang J., Anunvrapong P., Jumniensri C., and Wongmethanukroah J. "A Compact Wide-Band Bandpass Filter Using the Microstrip Loop

Resonators with Connected Four Inner Corner Identical Braches and Outer Tuning Stubs." **Proc. IEEE–RWS Dig.,** Oct. 2006. pp. 579-582.

[86] El-Shaarawy H. B., Coccetti F., Plana R., Said M. El, and Hashish E. A. "Compact Bandpass Ring Resonator Filter with Enhanced Wide-Band Rejection Characteristics Using Defected Ground Structures." **IEEE Microw. Wireless Comp. Lett.,** vol. 18, no. 8, Aug. 2008. pp. 500-502.

[87] Ahn H.-R. and Lee K. "Ring Filters and Their Application to New Measurement Technique on Inherent-Ring-Resonance Frequency." **IEE Proc.-Microw. Antennas Propag.,** vol. 152, no. 3, Jun. 2005. pp. 161-166.

[88] Lok U.-H., Chiou Y.-C., and Kuo J.-T. "Quadruple-Mode Coupled-Ring Resonator Bandpass Filter with Quasi-Elliptic Function Passband." **IEEE Microw. Wireless Comp. Lett.,** vol. 18, no. 3, Mar. 2008. pp. 179-181.

[89] Sun S. and Zhu L. "Wideband Microstrip Ring Resonator Bandpass Filters Under Multiple Resonances." **IEEE Trans. Microw. Theory Tech.,** vol. 55, no. 10, Oct. 2007. pp. 2176-2182.

[90] Sun S. and Zhu L. "Wideband Microstrip Ring Resonator Bandpass Filter with Asymmetrically-Loads Stubs." **Proc. APMC.,** Dec. 2008, pp. 1-4.

[91] Srisathit K., Worapishet A., and Surakampontorn W. "Design of Triple-Mode Ring Resonator for Wideband Microstrip Bandpass Filetrs." **IEEE Trans. Microw. Theory Tech., Part 1,** vol. 58, no. 11, Nov. 2010. pp. 2867-2877.

[92] Zysman G. I. and Johnson A. K. "Coupled Transmission Line Networks in an Inhomogeneous Dielectric Medium." **IRE Trans. Microw. Theory Tech.,** vol. MTT-17, no. 10, Oct. 1969. pp. 753-759.

[93] Cheng K.-K. M. and Wei-Chi I. "A Novel Power Divider Design with Enhanced Spurious Suppression and Simple Structure." **IEEE Trans. Microw. Theory Tech.,** vol. 58, no. 12, Dec. 2010. pp. 3903-3908.

[94] Hazeri A. R. and Faraji T. "Miniaturisation and Harmonic Suppression of the Branch-Line Hybrid Coupler." **Int. Journal of Electronics,** vol. 98, no. 12, Dec. 2011. pp. 1699-1710.

LIST OF PUBLICATIONS

Journal

[1] Srisathit K., Worapishet A., and Surakampontorn W. "Design of Triple-Mode Ring Resonator for Wideband Microstrip Bandpass Filters." **IEEE Trans. Microw. Theory Tech.,** vol. 58, no. 11, Nov. 2010. pp. 2867-2877.

Conferences

[1] Srisathit K., Jadpum P., and Surakampontorn W. "Miniature Wilkinson Divider and Hybrid Coupler with Harmonic Suppression Using T-Shaped Transmission Line." **Proc. APMC.,** Dec. 2007. pp. 785-788.

[2] Srisathit K., Jadpum P., Bunnjaweht S., and Surakampontorn W. "New Dual-Mode Ring Bandpass Filter Using Symmetrical Left-Handed Transmission Line." **Proc. APMC.,** Dec. 2007. pp. 1015-1018.

IEEE TRANSACTIONS ON

MICROWAVE THEORY AND TECHNIQUES

A PUBLICATION OF THE IEEE MICROWAVE THEORY AND TECHNIQUES SOCIETY

NOVEMBER 2010 VOLUME 58 NUMBER 11 IETMAB (ISSN 0018-9480)

PART I OF TWO PARTS

PAPERS

(Contents Continued on Back Cover)

(Contents Continued from Front Cover)

Design of Triple-Mode Ring Resonator for Wideband Microstrip Bandpass Filters

Kunnthphong Srisathit, *Student Member, IEEE*, Apisak Worapishet, *Senior Member, IEEE*, and Wanlop Surakampontorn, *Senior Member, IEEE*

***Abstract*—A triple-mode microstrip ring resonator core for the design of bandpass filters is proposed in this paper. It is a modification of the conventional single-mode ring resonator with a pair of open-ended coupled lines and a shunt open stub for a transmission-line path of the ring substituted to form a triple-mode resonator. Since the triple-mode resonator possesses three resonances, one at the center frequency and the other two near the edges of the passband, a flat passband response can be achieved when it is employed to implement a bandpass filter. The resonator also exhibits attenuation poles close to the edges of the passband, thereby offering sharp rejection in the bandpass filter response. Moreover, since the signal applied at the input port is effectively forced to travel mainly through the transmission line path over the passband frequency, the loss incurred by the coupled lines is minimized. Extensive theoretical analysis of the triple-mode ring and design example of the bandpass filter prototypes based on the ring structure are given. The prototype filters's performance is validated through both simulations and experiments, where good agreement with the theoretical prediction is observed.**

***Index Terms*—Bandpass filter, harmonic suppression, ring resonator, sharp rejection, triple-mode, wideband response.**

I. Introduction

MICROWAVE bandpass filters commonly utilize a ring resonator with the benefit of small circuit size and sharp rejection response [1], [2]. The ring resonator originally proposed by Woff and Knoppik was introduced for microwave substrate measurement [3]. Subsequently, with the use of asymmetrical coupling or asymmetrical perturbation, the dual-mode ring bandpass filter was initially reported in [4]. Soon afterward, the ring resonator was established as one of the main structures for planar microwave bandpass filter implementations [5]–[14]. Many research works on the miniaturization were conducted with different perturbation schemes [6]–[11] in the symmetrical plane. In addition, the insertion loss associated with the ring is another improvement by putting the lumped capacitor [11], the edged coupling [12], [13] or the inter-digital side-coupling [10], [14] between two feed lines and the ring resonator. These structures do not, however, lend themselves to closed-form analysis and straightforward filter design. They thus require the design iterations with the help of electromagnetic simulation.

The dual-mode ring resonators, which enable closed-form analysis and systematic design methodology, were reported in [15]–[18]. Various parameters useful for filter design were investigated and derived, including the resonance frequencies, attenuation poles, and coupling constant. The dual-mode bandpass filter in [15] made use of the shunt-stub and that in [16] made use of the series-stub perturbations. To achieve better control of the coupling constant and, hence, the odd/even resonance frequency locations, the dual-mode bandpass filter in [17] utilized lumped capacitors for series perturbation. The same benefit was obtained for the shunt perturbation using lumped capacitors in [18], with the additional advantage of electronic tunability due to the use of grounded elements.

With the emerging broadband communication systems [19], the demand on the bandwidth in microwave bandpass filters has been unprecedentedly increasing. To accomplish such a wideband characteristic in the ring-based bandpass filters, the dual-mode square-ring bandpass filters and its performance enhancement were investigated [20]–[22]. In [20] and [21], the filter employed two tuning open stubs for conversion from a bandstop to a bandpass characteristic with direct-orthogonal feed lines for low insertion loss. With the addition of the four open-loop arms [21] or the patterned ground plane sometimes referred to as a defected ground structure [22], the spurious responses, particularly in the stopband, in the ring filter can be alleviated. Another wideband ring bandpass filter in [23] was obtained by applying two short outer-tuning stubs and a resistor at the symmetrical plane of the ring. However, the need for outer-tuning stubs entails a major drawback in terms of compactness, particularly when connected in cascade to form a higher order bandpass filter.

To achieve further improvement in the passband flatness and sharp rejection in the bandpass filter characteristic, the quadruple-mode [24] and quintuple-mode [25], [26] ring bandpass filters were developed in microstrip forms. In fact, the quintuple-mode bandpass filter in [25] and [26] essentially relies upon the triple-mode resonator core using two equal [25] and unequal [26] stub perturbation lengths, with lumped capacitors feed lines. Though the triple-mode resonator resulted in lower insertion loss and better flatness in the passband response than the dual-mode counterparts, the improvements concerning sharp rejection and out-of-band attenuation were rather modest.

Manuscript received March 23, 2010; revised July 24, 2010; accepted July 27, 2010. Date of publication October 21, 2010; date of current version November 12, 2010. This work was supported by the Thailand Research Fund (TRF) through the Royal Golden Jubilee Ph.D. Program under Grant PHD/0010/2550.

K. Srisathit and W. Surakampontorn are with the Department of Electronics, Faculty of Engineering, King Mongkut's Institute of Technology Ladkrabang (KMITL), Ladkrabang District, Bangkok 10520, Thailand. (e-mail: kunnthph@mut.ac.th and kswanlop@kmitl.ac.th).

A. Worapishet is with the Mahanakorn Microeletronic Research Center and Department of Telecommunication Engineering, Mahanakorn University of Technology, Nong-Chok District, Bangkok 10530, Thailand (e-mail: apisak@mut.ac.th).

Color versions of one or more of the figures in this paper are available online at http://ieeexplore.ieee.org.

Digital Object Identifier 10.1109/TMTT.2010.2078295

As proposed in [25] and [26], by replacing the lumped feed lines with the inter-digital coupled lines, two additional resonances were created *close* to the original attenuation poles on both sides of the edges of the passband, thus yielding sharper rejection and high-stopband-attenuation quintuple-mode bandpass filter. It is the use of the inter-digital coupling, however, that makes it difficult for a systematic filter design. As evident in [25] and [26], whereas the analytical treatment could be developed for the triple-mode resonator core, design iterations based on extensive electromagnetic simulations must be carried out to find appropriate parameters of the inter-digital feed lines in the quintuple-mode filter.

In this paper, we present the design and analysis of a triple-mode ring resonator core that enables inherent sharp rejection with excellent gain flatness and good insertion loss in the passband, while offering a systematic analytical design. The ring structure relies upon the use of cascaded coupled lines with a shunt open stub in between to form half of the total ring path, with the direct feed lines as in [20]. The shunt stub, along the coupled lines' path, generates triple passband resonance frequencies which results in a good passband flatness. The structure also introduces two attenuation poles close to the two resonances located on both sides of the edges of the passband, thereby achieving inherent sharp rejection. The shunt stub also forces the signal to propagate along the transmission line path of the ring within the passband frequencies, thus minimizing the insertion loss along the coupled lines. Finally, the direct feed structure further maintains a low insertion loss.

This paper starts with a detailed description of the proposed ring resonator to understand the phenomenon of its structure. Extensive analysis of a simplified circuit model of the ring resonator is then derived to use for subsequent filter designs. This includes the resonance frequencies, attenuation poles, and coupling constants. To verify the design equations, systematic design examples and practical implementations of the bandpass filters using the single-ring and cascaded-ring resonators are introduced. Following that, to demonstrate its feasibility, a simulation and measurement of single and cascaded bandpass filter implementations centered at 1.0 GHz, along with techniques for spurious suppression using two T-shaped transmission lines at the input and output ports and an inter-digital coupled line between identical ring resonators, are also demonstrated.

II. Proposed Triple-Mode Ring Resonator

Fig. 1(a) shows the primitive single-mode ring resonator in the form of a square ring transmission line at one wavelength λ_g. It provides the resonance frequencies at nf_{r0}, where n is an integer number; $f_{r0} = c/\lambda_g\sqrt{\varepsilon_{\text{eff}}}$ is the center frequency of the resonator, where c and ε_{eff} are the velocity of light in free space and the effective dielectric constant, respectively. Note that the term $c/\sqrt{\varepsilon_{\text{eff}}}$ is the guided wave's velocity along the medium that forms the transmission lines. Based on the primitive structure, Fig. 1(b) shows the proposed ring resonator where one half of the transmission line's square ring (lower half of the figure) is replaced by a pair of $\lambda_g/4$ open-ended coupled lines connected in cascade with a $\lambda_g/4$ shunt open stub inserted in between. The length of the transmission line in the other half of the ring is at a half wavelength $\lambda_g/2$.

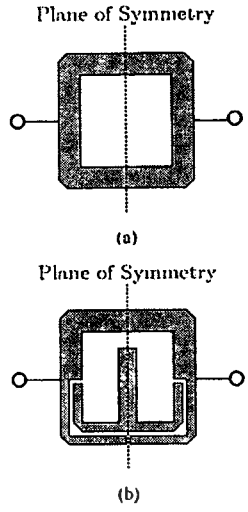

Fig. 1. Configuration of: (a) the preliminary single-mode ring and (b) the proposed triple-mode ring resonator.

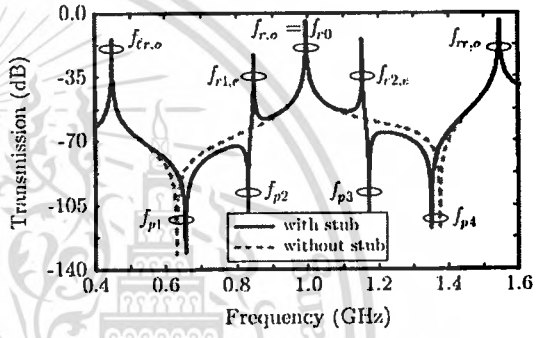

Fig. 2. Characteristic of the proposed triple-mode ring resonator in Fig. 1(b) with shunt stub (solid response) and without stub (dashed response).

Using ideal transmission-line models, Fig. 2 depicts typical *resonance* characteristics of the proposed resonator structure under weak coupling condition. Let us first consider the case without the shunt stub (dashed response). As shown in the dashed response of Fig. 2, the resonator without the shunt stub exhibits one resonance at the center frequency $f_{r,o}$; the other two resonances are at $f_{tr,o}$ and $f_{rr,o}$, located away from $f_{r,o}$ at the far left and right regions of the response. On both sides of the center frequency $f_{r,o}$, there are two attenuation poles at f_{p1} and f_{p4}. Consider now the case with the inclusion of the shunt stub. It is seen from the solid response in Fig. 2 that the resonance characteristic, particularly around $f_{r,o}$, is degenerated. In particular, there are two more resonance frequencies at $f_{r1,e}$ and $f_{r2,e}$, near the original resonance at $f_{r,o}$. Also shown in the solid response is that each side of $f_{r1,e}$ and $f_{r2,e}$ is accompanied by an additional attenuation pole, which appears very close to the resonance frequency (f_{p2} close to $f_{r1,e}$, and f_{p3} close to $f_{r2,e}$). It should be noted that, as will be shown in the analysis of Section III, the resonance frequencies $f_{r,o}$, $f_{tr,o}$, and $f_{rr,o}$ correspond to odd-mode excitation, and $f_{r1,e}$ and $f_{r2,e}$ correspond to even-mode excitation.

It is the locations of the resonance and attenuation pole frequencies at the central frequency region in Fig. 2 that underly the major advantages of the proposed resonator of Fig. 1(b).

Since there are as many as three passband resonance frequencies ($f_{r,o}$, $f_{r1,e}$, and $f_{r2,e}$), the bandpass filter based on the resonator exhibits a triple-mode response with a broad bandwidth while still maintaining a good flatness within the passband. In addition, the presence of the attenuation poles f_{p2} and f_{p3}, adjacent to $f_{r1,e}$ and $f_{r2,e}$, respectively, provides a highly steep transition characteristic. This practically yields the edges of the passband of the filter at $f_{r1,e}$ and $f_{r2,e}$. Thus, the bandwidth of the bandpass filter can be approximated from $f_{r1,e}$ to $f_{r2,e}$, whereas the center frequency is located at about $f_{r,o}$.

It is important to note that the typically high loss associated with the coupled lines in most practical realizations has practically no impact on the passband insertion loss of the filter based on the proposed resonator. This is because the shunt open stub inserted between the cascaded coupled lines acts as a series resonance to ground at the center frequency $f_{r,o}$ of the passband; this introduces a total reflection and, hence, a transmission notch of the incident wave along the coupled lines' path. As a consequence, the wave applied at the input port is effectively forced to travel mainly through the transmission line over the passband frequency; the loss incurred by the wave traveling via the coupled lines is, therefore, minimized. This, combined with the direct feed structure of the proposed resonator, results in a low-insertion-loss filter.

III. Analysis of the Proposed Ring Resonator

Here, we present the analysis method of the proposed resonator in Fig. 1(b) by using the two-port network theorem for computing the attenuation pole frequencies. Subsequently, the even- and odd-mode analyses will be performed to determine the resonance frequencies and coupling constants. For simplicity, the quasi-static TEM mode of operation is assumed. Also, the losses and discontinuity effects of the transmission lines and coupled lines are not taken into account.

A. Attenuation Pole Frequencies

The circuit model corresponding to the proposed triple-mode ring resonator in Fig. 1(b) is shown in Fig. 3(a). A simplified two-port network, depicted in Fig. 3(b), comprises the upper and lower halves of the model. The upper half is formed by the transmission line with the characteristic impedance of Z_{T1} and the electrical length of θ_1. For the lower half, there are two identical open-ended coupled lines in cascade and a shunt open stub connected in between. The even- and odd-mode impedances of the coupled lines are represented by Z_{0e} and Z_{0o}, respectively. Also, the even- and odd-mode electrical lengths are given by θ_e and θ_o, respectively. The shunt stub has the characteristic impedance of Z_{T2} and the electrical length of θ_2.

From the transmission line in the upper half of the circuit model in Fig. 3(a), the admittance matrix $[Y_{\text{upper}}]$ of the two-port network in Fig. 3(b) can be written as follows:

$$[Y_{\text{upper}}] = \begin{bmatrix} -jY_{T1}\cot(\theta_1) & jY_{T1}\csc(\theta_1) \\ jY_{T1}\csc(\theta_1) & -jY_{T1}\cot(\theta_1) \end{bmatrix} \quad (1)$$

where $Y_{T1} = 1/Z_{T1}$ is the characteristic admittance of the transmission line.

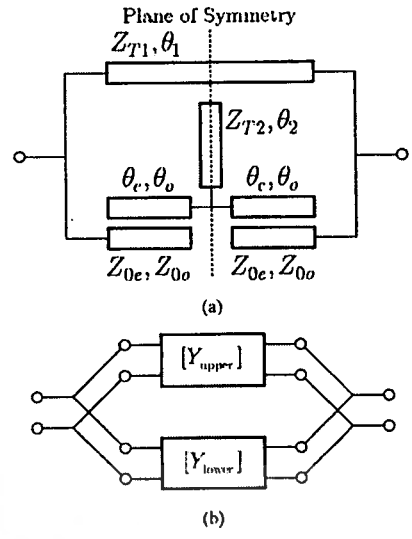

Fig. 3. Model of Fig. 1(b) for analyzing attenuation poles. (a) Circuit detail. (b) Simplified two-port network.

Considering the lower half in Fig. 3(a), the $ABCD$ matrix of the open-ended coupled line is given as follows [27]:

$$[M_{C1}] = \begin{bmatrix} A_{C1} & B_{C1} \\ C_{C1} & D_{C1} \end{bmatrix} \quad (2)$$

where

$$A_{C1} = \frac{Z_{0e}\cot\theta_e + Z_{0o}\cot\theta_o}{Z_{0e}\csc\theta_e - Z_{0o}\csc\theta_o} = D_{C1} \quad (3a)$$

$$B_{C1} = \frac{j}{2}\left(\frac{Z_{0e}^2 + Z_{0o}^2 - 2Z_{0e}Z_{0o}(\cot\theta_e\cot\theta_o + \csc\theta_e\csc\theta_o)}{Z_{0e}\csc\theta_e - Z_{0o}\csc\theta_o}\right) \quad (3b)$$

$$C_{C1} = \frac{2j}{Z_{0e}\csc\theta_e - Z_{0o}\csc\theta_o}. \quad (3c)$$

For the shunt open stub, the $ABCD$ matrix is given by

$$[M_2] = \begin{bmatrix} 1 & 0 \\ jY_{T2}\tan\theta_2 & 1 \end{bmatrix} \quad (4)$$

where $Y_{T2} = 1/Z_{T2}$ is the characteristic admittance of the shunt stub. With reference to Fig. 3(a), the overall $ABCD$ matrix of the lower half can be calculated by multiplying $[M_{C1}]$, $[M_2]$, and $[M_{C1}]$, respectively, as follows:

$$[M_{\text{lower}}] = [M_{C1}][M_2][M_{C1}]. \quad (5)$$

The admittance matrix of the lower half $[Y_{\text{lower}}]$ can then be calculated by performing a conversion of the $ABCD$ matrix $[M_{\text{lower}}]$ in (5) to $[Y_{\text{lower}}]$.

Based on the reciprocal property of the passive network, the attenuation pole is located at the frequency where the eigenimpedances of both the even- and odd-mode are equal [16]. Thus, the attenuation pole frequencies can be obtained under the condition

$$Y_{21,\text{upper}} + Y_{21,\text{lower}} = 0. \quad (6)$$

It should be noted that such a condition is equivalent to $|S_{21}| = 0$ for the two ports terminated with 50 Ω. Under the assigned characteristic impedances and electrical lengths in Fig. 3(a), and based on the condition in (6), we then obtain four attenuation pole frequencies at f_{p1}, f_{p2}, f_{p3}, and f_{p4}. With reference to the response in Fig. 2, where $f_{p1} < f_{p2} < f_{p3} < f_{p4}$, these attenuation poles are given as follows:

$$f_{p1} = \frac{2f_{r0}\tan^{-1}\left\{\frac{\sqrt{2}}{(Z_{0e}-Z_{0o})}\sqrt{\frac{G_n - F_n(Z_{0e}-Z_{0o})^2}{E_d+2F_d}}\right\}}{\pi} \tag{7}$$

$$f_{p2} = \frac{2f_{r0}\tan^{-1}\left\{\frac{\sqrt{2}}{(Z_{0e}-Z_{0o})}\sqrt{\frac{G_n + F_n(Z_{0e}-Z_{0o})^2}{E_d-2F_d}}\right\}}{\pi} \tag{8}$$

$$f_{p3} = 2f_{r0} - f_{p2} = \frac{2\pi f_{r0} - 2f_{r0}\tan^{-1}\left\{\frac{\sqrt{2}}{(Z_{0e}-Z_{0o})}\sqrt{\frac{G_n + F_n(Z_{0e}-Z_{0o})^2}{E_d-2F_d}}\right\}}{\pi} \tag{9}$$

$$f_{p4} = 2f_{r0} - f_{p1} = \frac{2\pi f_{r0} - 2f_{r0}\tan^{-1}\left\{\frac{\sqrt{2}}{(Z_{0e}-Z_{0o})}\sqrt{\frac{G_n - F_n(Z_{0e}-Z_{0o})^2}{E_d+2F_d}}\right\}}{\pi} \tag{10}$$

where

$$E_d = Y_{T1}(Z_{0e}+Z_{0o})\{Y_{T2}(Z_{0e}+Z_{0o})+2\}+4 \tag{11a}$$

$$F_d = F_n = \sqrt{\{Y_{T1}(Z_{0e}+Z_{0o})\}^2 + 4Y_{T1}\{Z_{0e}(2Y_{T2}Z_{0o}+1)+Z_{0o}\}+4} \tag{11b}$$

$$G_n = Y_{T1}\left(Z_{0e}^3+Z_{0o}^3\right)+2(Y_{T1}Y_{T2}Z_{0e}Z_{0o}+1)\left(Z_{0e}^2+Z_{0o}^2\right) + \{7Y_{T1}(Z_{0e}+Z_{0o})+4(Y_{T1}Y_{T2}Z_{0e}Z_{0o}-1)\}Z_{0e}Z_{0o}. \tag{11c}$$

Note that the subscripts n and d represent the nominator and denominator in (7)–(11), respectively.

B. Even-Mode Analysis

To determine the resonance frequencies of the ring resonator, we use the circuit model in Fig. 3(a) and apply the even- and odd-mode analysis methods along the symmetry plane. At the resonance frequencies, the *input* admittance of each mode will be equal to zero when the resonator is assumed lossless. Hence, the *input* admittance of the even-mode Y_e is given by

$$Y_e = Y_{\text{upper,e}} + Y_{\text{lower,e}} = 0. \tag{12}$$

By exciting the equivalent circuit in the even-mode, it appears that the symmetry plane acts as a perfect magnetic wall so that this plane represents the open circuit, as shown in Fig. 4. This divides the length of the upper transmission line with Z_{T1} into one half, i.e., $\theta = \theta_1/2$. The width of the shunt stub Z_{T2} in the lower half is also separated into one half, yielding twice in the equivalent characteristic impedance, i.e., $2Z_{T2}$. The upper-half *input* admittance $Y_{\text{upper,e}}$, calculated from $[Y_{\text{upper}}]$, is then given by

$$Y_{\text{upper,e}} = jY_{T1}\tan\theta = jY_{T1}\tan(\theta_1/2). \tag{13}$$

A convenient method to determine the lower *input* admittance $Y_{\text{lower,e}}$ is to consider the cascading $ABCD$ matrices of the coupler in (2) and (3) and the shunt stub $2Z_{T2}$. The $ABCD$ matrix of this stub is

$$[M_{T2}] = \begin{bmatrix} \cos\theta_2 & j2Z_{T2}\sin\theta_2 \\ j\frac{Y_{T2}\sin\theta_2}{2} & \cos\theta_2 \end{bmatrix}. \tag{14}$$

The resulting $ABCD$ matrix in the lower half can be obtained from

$$[M_{\text{lower,e}}] = [M_{C1}][M_{T2}] = \begin{bmatrix} A_{\text{lower,e}} & B_{\text{lower,e}} \\ C_{\text{lower,e}} & D_{\text{lower,e}} \end{bmatrix}. \tag{15}$$

Subsequently, the lower-half *input* admittance $Y_{\text{lower,e}}$ is calculated from $[M_{\text{lower,e}}]$ as

$$Y_{\text{lower,e}} = \frac{P}{Q} \tag{16}$$

where

$$P = 2j\begin{bmatrix} 4Z_{T2}\cos\theta_2\sin\theta_e\sin\theta_o + Z_{0e}\sin\theta_2\cos\theta_e\sin\theta_o \\ +Z_{0o}\sin\theta_2\cos\theta_o\sin\theta_o \end{bmatrix} \tag{17a}$$

$$Q = \begin{bmatrix} 2Z_{0e}Z_{0o}\sin\theta_2(\cos\theta_e\cos\theta_o+1) \\ +4Z_{T2}\cos\theta_2(Z_{0e}\cos\theta_e\sin\theta_o + Z_{0o}\cos\theta_o\sin.\theta_e) \\ -\sin\theta_2\sin\theta_e\sin\theta_o\left(Z_{0e}^2+Z_{0o}^2\right) \end{bmatrix}. \tag{17b}$$

Therefore, the resonance frequencies (see Fig. 2) can be solved by substituting (13), (16), and (17) into (12). After rearrangement, the first even-mode frequency $f_{r1,e}$ can be given by (18), shown at the bottom of this page, and the second even-mode frequency $f_{r2,e}$ can be given by

$$f_{r2,e} = 2f_{r0} - f_{r1,e}. \tag{19}$$

$$f_{r1,e} = \frac{2f_{r0}}{\pi}\tan^{-1}\frac{\sqrt{8Z_{T1}Z_{T2}+4Z_{0e}Z_{0o}+2(Z_{T1}+2Z_{T2})(Z_{0e}+Z_{0o})}}{(Z_{0e}-Z_{0o})} \tag{18}$$

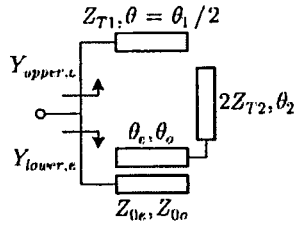

Fig. 4. Even-mode equivalent circuit of the proposed ring resonator in Fig. 3(a).

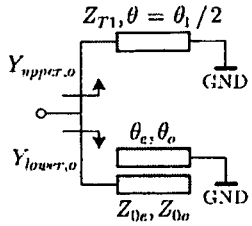

Fig. 5. Odd-mode equivalent circuit of the proposed ring resonator in Fig. 3(a).

C. Odd-Mode Analysis

The odd-mode analysis is considered to have a perfect electric wall along the plane of symmetry, so that the electrical equivalent circuit at this plane behaves as a short circuit as shown in Fig. 5. Hence, the *input* admittance in this mode at resonance frequency can be expressed as

$$Y_o = Y_{\text{upper,o}} + Y_{\text{lower,o}} = 0. \tag{20}$$

With reference to Fig. 5, the *input* admittances of the short-circuited transmission line in the upper half $Y_{\text{upper,o}}$, also calculated from $[Y_{\text{upper}}]$, and that of the coupled line in the lower half $Y_{\text{lower,o}}$, based on the calculation similar to $Y_{\text{lower,e}}$, are given by

$$Y_{\text{upper,o}} = -jY_{T1}\cot\theta = -jY_{T1}\cot(\theta_1/2) \tag{21}$$

and (22), shown at the bottom of this page. By using (20)–(22), the odd-mode resonance frequencies can be derived in a similar fashion. There are three odd-mode resonance frequencies as indicated in Fig. 2. The first two resonances are addressed in the far left and right regions at $f_{tr,o}$ and $f_{rr,o}$, respectively. These are given by

$$f_{tr,o} = \frac{2f_{r0}\tan^{-1}\left\{2\sqrt{\frac{Z_{0e}Z_{0o}}{(Z_{0e}-Z_{0o})^2+2Z_{T1}(Z_{0e}-Z_{0o})}}\right\}}{\pi} \tag{23}$$

and

$$f_{rr,o} = 2f_{r0} - f_{tr,o} = \frac{2\pi f_{r0} - 2f_{r0}\tan^{-1}\left\{2\sqrt{\frac{Z_{0e}Z_{0o}}{(Z_{0e}-Z_{0o})^2+2Z_{T1}(Z_{0e}-Z_{0o})}}\right\}}{\pi}. \tag{24}$$

Another resonance is located at $f_{r,o}$, which is the resonance of the basic ring resonator f_{r0}, i.e., $f_{r,o} = f_{r0}$. As indicated by the attenuation poles in (7)–(11) and resonances in (18) and (19), we have four unknown parameters. These are Z_{T1}, Z_{T2}, Z_{0e}, and Z_{0o}. The equations require the preassigned locations of the attenuation poles and resonances to solve these parameters, which can be obtained from the specified stopband characteristics and the edges of the passband.

The effects of the shunt stub impedance and even- and odd-mode impedances on the resonance and attenuation pole frequencies are investigated as follows. In this study, the transmission line in the upper half ring is considered as a constant parameter, where $Z_{T1} = 50\ \Omega$.

Fig. 6(a) shows the calculated location of the poles and resonance frequencies *normalized* with $f_{r,o}$ *versus* the *normalized* impedance of the shunt stub Z_{T2} with Z_0 under the condition $Z_{0e} = 150\ \Omega$ and $Z_{0o} = 50\ \Omega$. As shown in Fig. 6(a), the normalized odd-mode frequencies $f'_{tr,o}$, $f'_{r,o}$, and $f'_{rr,o}$ are independent of Z'_{T2}, as the shunt stub does not exist in the equivalent circuit due to odd-mode excitation [see Fig. 5]. Similarly, the other two attenuation poles at f'_{p1} and f'_{p4} only slightly vary with Z'_{T2}. On the other hand, the shunt-stub impedance affects the normalized even-mode frequencies $f'_{r1,e}$ and $f'_{r2,e}$. In particular, when Z'_{T2} is increased, the two attenuation poles at f'_{p2} and f'_{p3} move closer to the low and high edges of the resonances at $f'_{r1,e}$ and $f'_{r2,e}$, respectively. A sharp transition band can be thus achieved. Eventually, these poles and resonances converge to $f'_{r,o} = f'_{r0} = 1$ for a very large Z'_{T2}. It is thus evident that these attenuation poles and resonances of the proposed resonator have symmetrical properties around $f'_{r,o}$.

Fig. 6(b) and (c) shows the normalized attenuation pole and resonance characteristics in relation to the even- and odd-mode impedances, respectively. As illustrated in Fig. 6(b), under the condition of $Z_{0o} = 50\ \Omega$ and $Z_{T2} = 10\ \Omega$, the normalized resonance frequencies $f'_{tr,o}$ and $f'_{rr,o}$ are practically constant against Z'_{0e}. On the other hand, the other resonances ($f'_{r1,e}$ and $f'_{r2,e}$) and the attenuation pole frequencies (f'_{p1}, f'_{p2}, f'_{p3}, and f'_{p4}) move apart from the center frequency $f'_{r,o}$ when Z'_{0e} increases. For Fig. 6(c), under the condition of $Z_{0e} = 150\ \Omega$ and $Z_{T2} = 10\ \Omega$, the resonance and attenuation pole frequencies move closer to $f'_{r,o}$ when Z'_{0o} increases. It is noticed that the frequencies $f'_{r1,e}$ and f'_{p2}, as well as $f'_{r2,e}$ and f'_{p3}, are always in close proximity in all of the plots. Therefore, the sharp transition band should be maintained against the impedance parameter selections.

$$Y_{\text{lower,o}} = \frac{j(Z_{0e}\cot\theta_e + Z_{0o}\cot\theta_o)}{\frac{1}{2}(Z_{0e}\csc\theta_e + Z_{0o}\csc\theta_o)^2 - \frac{1}{2}(Z_{0e}\cot\theta_e + Z_{0o}\cot\theta_o)^2} \tag{22}$$

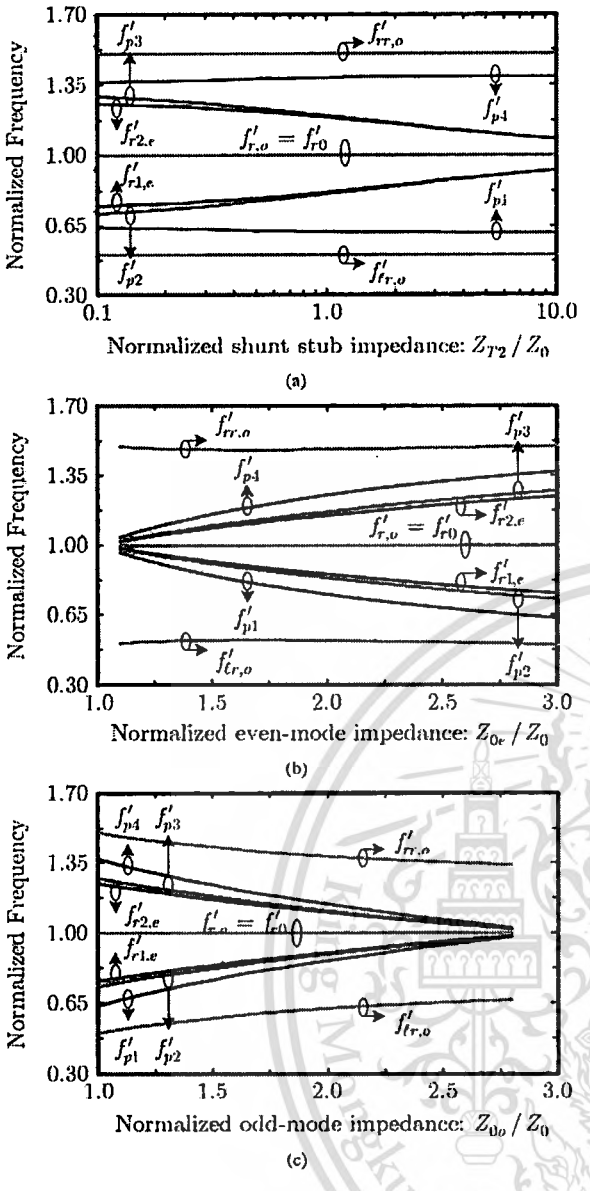

Fig. 6. Normalized attenuation pole and resonance frequencies of the triple-mode ring resonator as a function of the normalized: (a) shunt-stub impedance $Z'_{T2} = Z_{T2}/Z_0$, (b) even-mode impedance $Z'_{0e} = Z_{0e}/Z_0$, and (c) odd-mode impedance $Z'_{0o} = Z_{0o}/Z_0$.

D. Physical Interpretation

The resonances can be physically explained by virtue of the equivalent models for the even- and odd-mode models in Figs. 4 and 5. Consider first the odd-mode model in Fig. 5. It is essentially a parallel of the shorted transmission line and open-ended coupled line, both at the length of $\lambda_g/4$ (with reference to the center frequency $f_{r,o}$). At frequencies around $f_{tr,o}$, the transmission line behaves like a lumped inductor (L), whereas the coupled line behaves like a lumped capacitor (C). As a consequence, this forms a parallel LC resonator that gives rise to the resonance at $f_{tr,o}$ in the proposed ring structure. At frequencies around $f_{rr,o}$, the behaviors of the $\lambda_g/4$ shorted transmission line and coupled line are in dual fashion. Whereas the transmission line behaves like a capacitor, the coupled line behaves like an inductor. Thus, this forms a parallel LC resonator that gives rise to the resonance at $f_{rr,o}$. At around the center frequencies $f_{r,o}$, however, both the transmission line and the coupled line exhibit self-resonance, where the electric and magnetic energies are equal within their own structures. This thereby gives rise to the resonance frequency of the ring at $f_{r,o}$.

Now consider the even-mode model in Fig. 4. It is essentially a parallel of the open transmission line and open-ended coupled line at $\lambda_g/4$. At frequencies around $f_{r1,e}$, the transmission line behaves like a capacitor, whereas the coupled line behaves like an inductor, giving rise to the resonance at $f_{r1,e}$. At frequencies around $f_{r2,e}$, the transmission line and coupled line behaves in dual fashion, yielding the resonance at $f_{r2,e}$.

The physical mechanism that is attributed to the attenuation poles at f_{p1} and f_{p4} is based upon the output cancellation of the signals propagating along the upper transmission-line path and the lower open-ended coupled-line path. For the attenuation poles at f_{p2} and f_{p3}, they are attributed to the input/output characteristics of the cascaded coupled lines with $\lambda_g/4$ shunt open stub, which is effectively shorted to ground at f_{p2} and f_{p3}.

IV. Design Examples and Discussions

A. Single Ring Resonator Filter

To validate the feasibility of the proposed ring resonator, a single ring bandpass filter with a system impedance of $Z_0 = 50\ \Omega$ was designed and fabricated on an FR-4 substrate ($\varepsilon_r = 4.55$, $h = 0.8$ mm, and $\tan\delta = 0.02$) at $f_0 = 1$ GHz center frequency, with a 30% fractional bandwidth.

Based on the theoretical analysis in Section III and the required specification, we may first assume that the low edge of the resonances is at $f_{r1,e} = 0.85$ GHz, and the high edge of the resonances is at $f_{r2,e} = 2f_0 - f_{r1,e} = 1.15$ GHz. The attenuation pole f_{p2} is selected at 0.82 GHz to obtain a sharp rejection response, whereas the lower pole f_{p1} is at 0.7 GHz. This subsequently yields $f_{p3} = 1.18$ GHz and $f_{p4} = 1.3$ GHz. Applying these frequencies f_{p1} or f_{p4} into (7) or (10), f_{p2} or f_{p3} into (8) or (9), $f_{r1,e}$ into (18), and $f_{r2,e}$ into (19), the characteristic impedances of the ring resonator are thus obtained. In this design, a commercial software was employed to automatically solve in (7)–(11), (18), (19), (23), and (24) for the characteristic impedances of Z_{T1}, Z_{T2}, Z_{0e}, and Z_{0o} (only values amenable to practical realization were selected): $Z_{T1} = 105.6\ \Omega$, $Z_{T2} = 13.2\ \Omega$, $Z_{0e} = 133.27\ \Omega$, and $Z_{0o} = 59.7\ \Omega$. With the center frequency of the passband at 1 GHz, the simulated insertion loss S_{21} of the proposed resonator-based bandpass filter is shown in Fig. 7. As observed in the figure, four attenuation poles can be found at 0.7, 0.82, 1.18, and 1.3 GHz, respectively. The attenuation level between f_{p1} and f_{p2} and/or f_{p3} and f_{p4} is more than 15 dB.

Subsequently, the initial characteristic impedances were then refined to obtain realistic filter dimensions. This was based on a practical FR-4 substrate with the help of Agilent-ADS [28]. Fig. 8(a) shows the layout of a single square-ring bandpass filter. The dimensions (in millimeters) are summarized as follows: $w_1 = 0.3$, $\ell_1 = 85.3$, $w_2 = 5.4$, $\ell_2 = 38.2$, $w_C = 0.3$, $\ell_C = 43.2$, and $s = 0.25$. A photograph of the filter is shown in Fig. 8(b). The dimensions, excluding two SMA connectors, are approximately

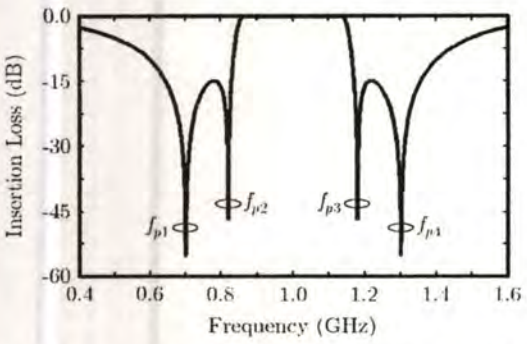

Fig. 7. Simulated insertion loss of the ring bandpass filter designed at 1 GHz.

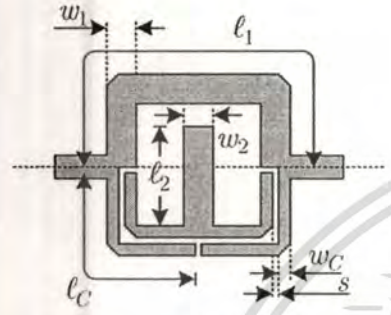

(a)

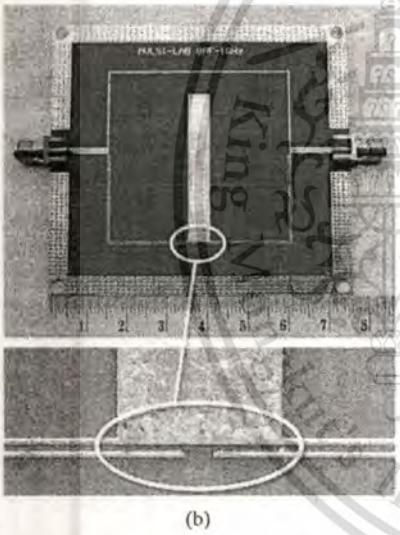

(b)

Fig. 8. Single-ring bandpass filter. (a) Layout. (b) Photograph of the fabricated filter on an FR-4 substrate.

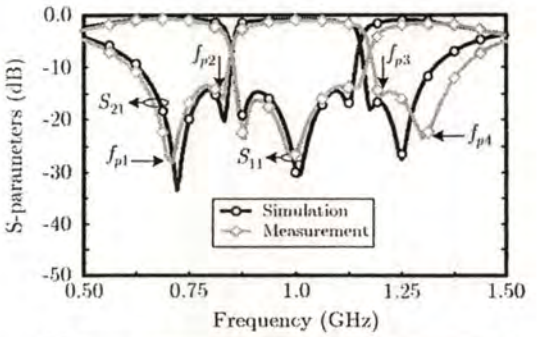

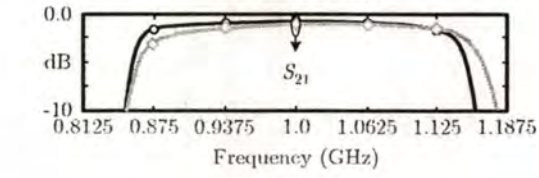

(a)

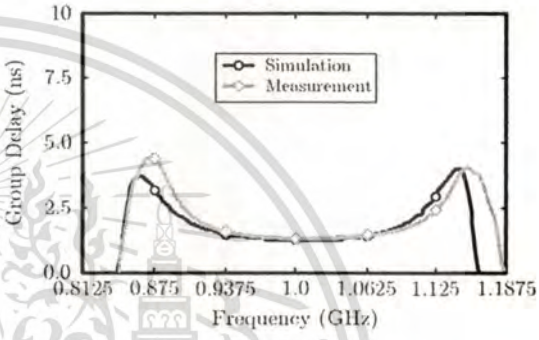

(b)

Fig. 9. Measured and simulated results of triple-mode single-ring bandpass filter. (a) Magnitude response of S_{11} and S_{21}. (b) Group delay.

67 mm × 78 mm. The measurement was performed with an Agilent N5230A vector network analyzer test system, which utilized the short-open-load-thru (SOLT) calibration.

The measured results of S-parameters are depicted in the top row of Fig. 9(a), where they are in good agreement with the simulated results. The measured center frequency is at 1.02 GHz and the 3-dB fractional bandwidth is 29.36%. The measured insertion loss, including the material losses and two SMA connectors, is better than 0.8 dB [bottom row of Fig. 9(a)], whereas the in-band return loss is greater than 13.6 dB within 0.865–1.157 GHz. The filter exhibits four attenuation poles, two on each side of the passband at 0.72, 0.83, 1.21, and 1.305 GHz, respectively. These attenuation pole frequencies are noticeable in both simulated and measured results. Moreover, a 13.5-dB attenuation level between neighboring attenuation poles can be obtained. An attenuation slope for the sharp rejection responses is calculated at 244.6 dB/GHz (calculated from 0.83 GHz with −15.13 dB to 0.88 GHz with −2.9 dB), and 227.6 dB/GHz (calculated from 1.16 GHz with −3.62 dB to 1.21 GHz with −15 dB). The group delay over the passband is less than 1.6 ns, as shown in Fig. 9(b).

B. Double-Ring Filter With Cascaded Single-Ring Resonator

To achieve a higher out-of-band attenuation, a cascaded version of the single square-ring resonator in Fig. 8(a) is depicted in Fig. 10(a), where the resonators are connected through the normal transmission line with $\ell_t = \lambda_g/4$ and the characteristic impedance is Z_0. The dimensions of this line on an FR-4 are $w_t = 1.47$ mm and $\ell_t = 40.9$ mm. It is anticipated that the cascaded structure can provide a quadratic improvement in the attenuation performance. Fig. 10(b) shows a photograph of the fabricated double-ring filter. The circuit size of the filter occupies an area about 67 mm × 162 mm.

The simulated and measured performances of this filter are superimposed as shown in Fig. 11. As shown in the top row of Fig. 11(a), the measured prototype filter has a 3-dB fractional bandwidth of 27.2% with the center frequency of 1.03 GHz, an insertion loss of 1.62 dB [bottom row of Fig. 11(a)], and the input/output return losses of 11.7 dB within 0.87–1.16 GHz.

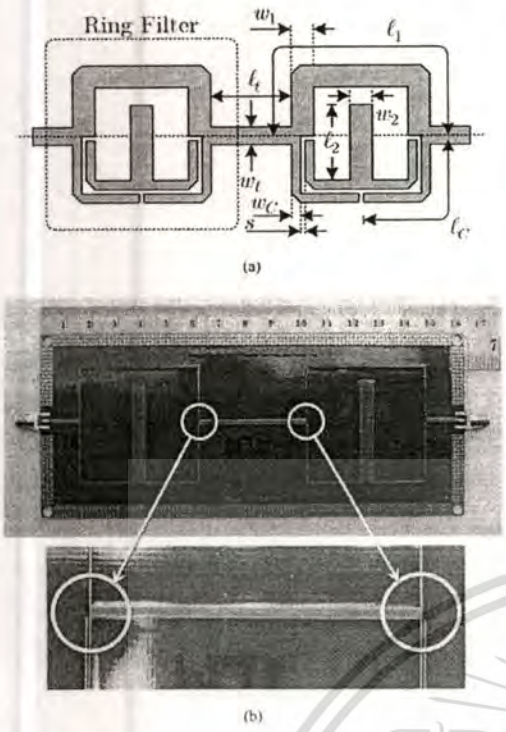

Fig. 10. Double-ring bandpass filter. (a) Layout. (b) Photograph of the fabricated filter on an FR-4 substrate.

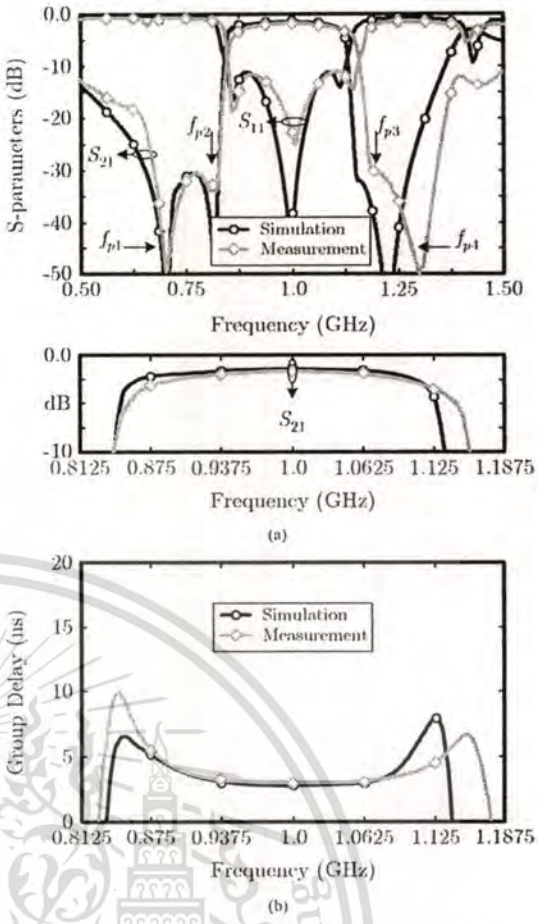

Fig. 11. Measured and simulated results of triple-mode double-ring bandpass filter. (a) Magnitude response of S_{11} and S_{21}. (b) Group delay.

Moreover, two adjacent attenuation poles at 0.84 and 1.21 GHz, occurring near the passband, are improved at below 30 dB. The remaining attenuation poles are located at 0.72 and 1.30 GHz. A comparison between the response in the top row of Fig. 9(a) and the top row of Fig. 11(a) indicates that the out-band attenuation level between the adjacent attenuation poles ($f_{p1} - f_{p2}$ and $f_{p3} - f_{p4}$) is increased from 13.5 to 30 dB. The attenuation slope of this cascaded filter is 490.83 dB/GHz (calculated from 0.84 GHz with -32.6 dB to 0.90 GHz with -3.15 dB), and 443.33 dB/GHz (calculated from 1.15 GHz with -3.7 dB to 1.21 GHz with -30.3 dB). Furthermore, the measured group delay over the passband as shown in Fig. 11(b) is less than 3.2 ns. The specifications and measured performances of the proposed triple-mode bandpass filter with other dual-mode ring filters [20], [21] are compared in Table I.

Since the proposed ring resonator incorporates two couplers in the structure, the harmonic response is unavoidable when this resonator-based bandpass filter is fabricated in the microstrip structure. This is because of the inherently different phase velocities between even- and odd-mode models in the microstrip coupler [2], [27]. In addition, theses two couplers also exhibits two resonances at the far left and right regions of the response ($f_{tr,o}$ and $f_{rr,o}$) (see Fig. 2) in the lower and upper stopbands, respectively.

In order to suppress the spurious response, we have introduced two T-shaped transmission lines [29], one at the input and another at the output of the double-ring filter (see Fig. 12). In particular, the lengths of the loaded open stubs of the T-shape transmission lines were designed at different frequencies to overall suppress of the spurious resonant peak and coupling of the filter response. In addition, an inter-digital coupled line with two finger pairs was inserted at the interconnecting transmission line between the two rings [see Fig. 12(a)], and this effectively suppresses the response at the second-harmonic frequency at $2f_0 = 2$ GHz. Note that the inter-digital coupled line also helps attenuate the additional lower stopband resonances and performs the dc blocking task for the filter. This yields the improvement of the lower and upper stopband performances.

With reference to Fig. 12(a), each T-shaped transmission line is designed with the length $\ell_{\ell T}$ of $\lambda_g/6$, where two shunt open stubs with the length $\ell_{\ell S1}$ and $\ell_{\ell S2}$ are selected for suppression at frequencies lower and higher than second harmonic, respectively. The characteristic impedance of the transmission line is calculated at 86.6 Ω and the shunt stub at 75 Ω. Subsequently, the physical dimensions were further synthesized on an FR-4 substrate with the width $w_{\ell T} = 0.47$ mm and the length $\ell_{\ell T} = 28.5$ mm. Also, $\ell_{\ell S1} = 18.37$ mm, $\ell_{\ell S2} = 26.25$ mm, and $w_{\text{stub1}} = w_{\text{stub2}} = 0.67$ mm. The parameters used in an inter-digital coupled line (in millimeters) are also given in Fig. 12(a). The photograph of Fig. 12(a) is shown in Fig. 12(b), with a size of 67 mm × 208 mm.

Fig. 13 shows the simulated and measured performances of the designed double-ring bandpass filter in Fig. 12(a) and (b) over a wider frequency range from 0.5 to 3 GHz. Notice that the measured magnitude responses of S_{21} and S_{11} are practically preserved, as in the case of the double-ring filter with the

TABLE I
COMPARISON OF SPECIFICATIONS AND MEASURED PERFORMANCES OF THE PROPOSED FILTER WITH OTHER RING FILTERS

Specifications and Performances	Ref [20]	Ref [21]	This work
Number of ring resonator	3	2	2
Type of mode operation	Dual-mode	Dual-mode	Triple-mode
Center frequency (GHz)	5.6	2.45	1.0
Fractional bandwidth	0.493	0.37	0.272
Substrate	RT/Duroid 6010.2, Laminate	RT/Duroid 6006, Laminate	FR-4, Epoxy
Relative dielectric constant	10.2	6.15	4.55
Loss tangent	0.0023	0.0027	0.02
Passband insertion loss (dB)	1.6	0.84	1.62
Return loss (dB)	13.3	11.4	11.7
Group delay (ns)	< 2	Not available	< 3.2
Attenuation slope: lower, upper (dB/GHz)	99.75, 101.56	Not available	490.83, 443.33

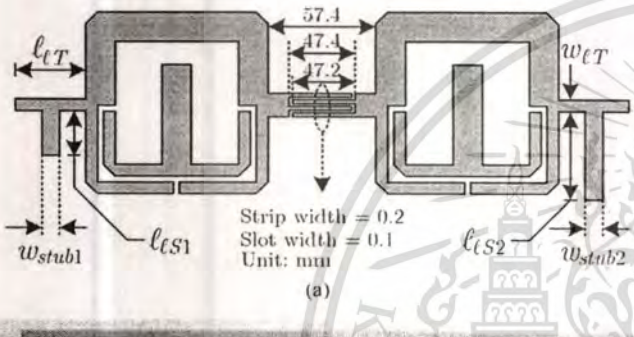

(a)

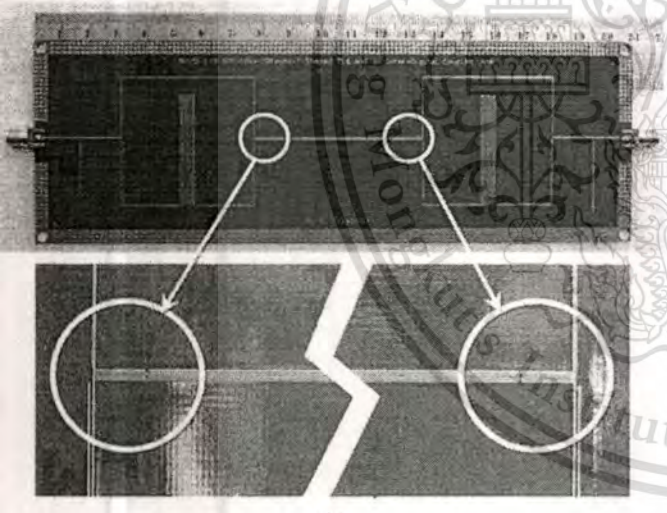

(b)

Fig. 12. Double-ring bandpass filter with T-shaped transmission lines and an inter-digital coupled line. (a) Layout. (b) Photograph of the fabricated filter on an FR-4 substrate.

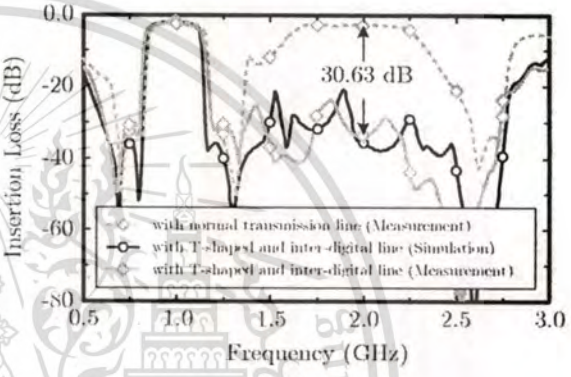

(a)

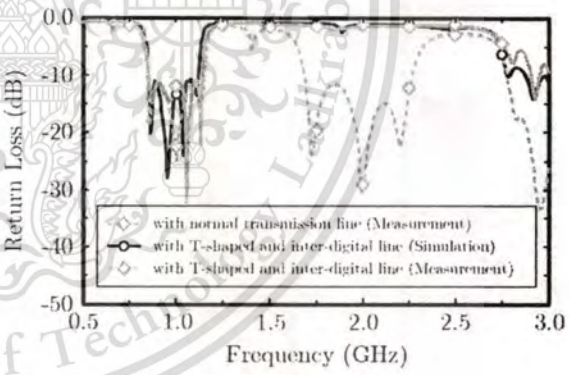

(b)

Fig. 13. Measured and simulated results of double-ring bandpass filter with T-shaped transmission lines and an inter-digital coupled line. (a) Insertion losses. (b) Return losses.

normal transmission line. An exception is that the second-harmonic frequency at $2f_0 = 2$ GHz of the proposed double-ring filter is improved, i.e., at less than 33.75 dB (over 30.63-dB improvement). Moreover, the upper stopband is also suppressed by more than 23.75 dB over the frequency range from 1.18 to 2.75 GHz. A 2.1-dB measured insertion loss is obtained at the center frequency of the passband, where the return loss within the passband is kept below 11.9 dB.

V. CONCLUSION

A triple-mode ring resonator core and its applications to bandpass filters have been proposed and successfully fabricated in a microstrip technology. The introduction of a pair of identical open-ended coupled lines with a shunt open stub, into a transmission line branch of a conventional ring resonator, has led to the triple-mode operation. When the triple-mode resonator is employed to implement a bandpass filter, the triple passband resonance frequencies along with the two attenuation poles close to the edges of the passband on either side,

essentially give rise to a flat passband and sharp rejection response. The direct feed structure with a T-shaped transmission line, and the fact that the signal mainly propagates along the transmission line path of the triple-mode resonator over the passband frequencies, also yield a low insertion loss. Detailed analysis of the resonator, including the attenuation pole and resonance frequencies, has been studied to enable analytical and systematic designs, with minimum design iterations using electromagnetic simulation. Design examples and implementations of three prototype filters have been verified through simulations and measurements. To further improve out-of-band performance, the use of an inter-digital coupled line and two T-shaped transmission lines, particularly in the cascaded filter prototype, was also successfully introduced.

ACKNOWLEDGMENT

The authors would like to thank Agilent Technology for providing access to Advanced Design System software under Agilent EESof EDA University License Agreement with Mahanakorn University of Technology. The authors would also like to thank Dr. C. Jongkunstidchai, Rajamangala University of Technology Rattanakosin, for providing the measurement equipment. The authors would also like to thank the assistant editor, associate editor, editors, and anonymous reviewers for their valuable comments and suggestions that greatly helped improve the quality of the manuscript.

REFERENCES

[1] K. Chang, *Microwave Ring Circuits and Antenna*. New York: Wiley, 1996.

[2] J.-S. Hong and M. J. Lancaster, *Microstrip Filters for RF/Microwave Applications*. New York: Wiley, 2001.

[3] I. Wolff and N. Knoppik, "Microstrip ring resonator and dispersion measurement on microstrip lines," *Electron. Lett.*, vol. 7, no. 26, pp. 779–781, Dec. 1971.

[4] I. Wolff, "Microstrip bandpass filters using degenerate modes of a microstrip ring resonator," *Electron. Lett.*, vol. 8, no. 12, pp. 302–303, Jun. 1972.

[5] D. K. Paul, P. Gardner, and K. P. Tan, "Suppression of even modes in microstrip ring resonators," *Electron. Lett.*, vol. 30, no. 21, pp. 1772–1774, Oct. 1994.

[6] J.-S. Hong and M. J. Lancaster, "Microstrip bandpass filter using degenerate modes of a novel meander loop resonator," *IEEE Microw. Guided Wave Lett.*, vol. 5, no. 11, pp. 371–372, Nov. 1995.

[7] A. Görür, C. Karpuz, and M. Akpinar, "A reduced-size dual-mode bandpass filter with capacitively loaded open-loop arms," *IEEE Microw. Wireless Compon. Lett.*, vol. 13, no. 9, pp. 385–387, Sep. 2003.

[8] K.-H. Sun and K.-W. Tam, "A novel compact dual-mode bandpass filter with meander open-loop arms," in *IEEE MTT-S Int. Microw. Symp. Dig.*, Jun. 2004, pp. 1479–1482.

[9] B. T. Tan, J. J. Yu, S. T. Chew, M.-S. Leong, and B.-L. Ooi, "A miniaturized dual-mode ring resonator bandpass filter with a new perturbation," *IEEE Trans. Microw. Theory Tech.*, vol. 53, no. 1, pp. 343–348, Jan. 2005.

[10] R.-J. Mao, X.-H. Tang, and F. Xiao, "Miniaturized dual-mode ring bandpass filters with patterned ground plane," *IEEE Trans. Microw. Theory Tech.*, vol. 55, no. 7, pp. 1539–1547, Jul. 2007.

[11] H. Yabuki, M. Sagawa, M. Matsuo, and M. Makimoto, "Stripline dual-mode ring resonators and their application to microwave devices," *IEEE Trans. Microw. Theory Tech.*, vol. 44, no. 5, pp. 723–729, May 1996.

[12] A. Görür, "A novel dual-mode bandpass filter with wide stopband using the properties of microstrip open-loop resonator," *IEEE Microw. Wireless Compon. Lett.*, vol. 12, no. 10, pp. 386–388, Oct. 2002.

[13] R.-J. Mao and X.-H. Tang, "Novel dual-mode bandpass filters using hexagonal loop resonators," *IEEE Trans. Microw. Theory Tech.*, vol. 54, no. 9, pp. 3526–3533, Sep. 2006.

[14] W.-C. Jung, H.-J. Park, and J.-C. Lee, "Microstrip ring bandpass filters with new interdigital side-coupling structure," in *Proc. Asia–Pacific Microw. Conf.*, Dec. 1999, pp. 678–681.

[15] A. C. Kunda and I. Awai, "Control of attenuation pole frequency of a dual-mode microstrip ring resonators bandpass filter," *IEEE Trans. Microw. Theory Tech.*, vol. 49, no. 6, pp. 1113–1117, Jun. 2001.

[16] M. Matsuo, H. Yabuki, and M. Makimoto, "Dual-mode stepped-impedance ring resonators for bandpass filter applications," *IEEE Trans. Microw. Theory Tech.*, vol. 49, no. 7, pp. 1235–1240, Jul. 2001.

[17] B. T. Tan, S. T. Chew, M. S. Leong, and B. L. Ooi, "A dual-mode bandpass filter with enhanced capacitive perturbation," *IEEE Trans. Microw. Theory Tech.*, vol. 51, no. 8, pp. 1906–1910, Aug. 2003.

[18] M.-F. Lei and H. Wang, "An analysis of miniaturized dual-mode bandpass filter structure using shunt-capacitance perturbation," *IEEE Trans. Microw. Theory Tech.*, vol. 53, no. 3, pp. 861–867, Mar. 2005.

[19] C. M. Akujuobi and M. N. O. Sadiku, *Introduction of Broadband Communication Systems*. London, U.K.: Chapman & Hall, 2007.

[20] L.-H. Hsieh and K. Chang, "Compact, low insertion-loss, sharp-rejection, and wideband microstrip bandpass filters," *IEEE Trans. Microw. Theory Tech.*, vol. 51, no. 4, pp. 1241–1246, Apr. 2003.

[21] J. Konpang, P. Anunvrapong, C. Jumniensri, and J. Wongmethanukroah, "A compact wideband bandpass filter using the microstrip loop resonators with connected four inner corner identical brachnes and outer tuning stubs," in *IEEE Radio Wireless Symp. Dig.*, Oct. 2006, pp. 579–582.

[22] H. B. El-Shaarawy, F. Coccetti, R. Plana, M. El Said, and E. A. Hashish, "Compact bandpass ring resonator filter with enhanced wideband rejection characteristics using defected ground structures," *IEEE Microw. Wireless Comp. Lett.*, vol. 18, no. 8, pp. 500–502, Aug. 2008.

[23] H.-R. Ahn and K. Lee, "Ring filters and their application to new measurement technique on inherent-ring-resonance frequency," *Proc. Inst. Elect. Eng. Microw. Antennas Propag.*, vol. 152, no. 3, pp. 161–166, Jun. 2005.

[24] U.-H. Lok, Y.-C. Chiou, and J.-T. Kuo, "Quadruple-mode coupled-ring resonator bandpass filter with quasi-elliptic function passband," *IEEE Microw. Wireless Compon. Lett.*, vol. 18, no. 3, pp. 179–181, Mar. 2008.

[25] S. Sun and L. Zhu, "Wideband microstrip ring resonator bandpass filters under multiple resonances," *IEEE Trans. Microw. Theory Tech.*, vol. 55, no. 10, pp. 2176–2182, Oct. 2007.

[26] S. Sun and L. Zhu, "Wideband microstrip ring resonator bandpass filter with asymmetrically-loads stubs," in *Proc. Asia–Pacific Microw. Conf.*, Dec. 2008, pp. 1–4.

[27] G. I. Zysman and A. K. Johnson, "Coupled transmission line networks in an inhomogeneous dielectric medium," *IRE Trans. Microw. Theory Tech.*, vol. MTT-17, no. 10, pp. 753–759, Oct. 1969.

[28] *Advanced Design System (ADS) 2009*. Palo Alto, CA: Agilent Technol., 2009 [Online]. Available: http://www.agilent.com/find/eesof-ads

[29] W.-H. Tu and K. Chang, "Compact second harmonic-suppressed bandstop and bandpass filters using open stubs," *IEEE Trans. Microw. Theory Tech.*, vol. 54, no. 6, pp. 2497–2502, Jun. 2006.

Kunnthphong Srisathit (S'08) was born in Khonkaen, Thailand, on July 6, 1973. He received the B.Eng. (with honors) and M.Eng. degrees from the Mahanakorn University of Technology (MUT), Nong-Chok, Bangkok, Thailand, in 1996 and 2002, respectively, both in electrical engineering. He is currently working toward the Ph.D. degree in electrical engineering at King Mongkut's Institute of Technology Ladkrabang, Ladkrabang, Bangkok, Thailand.

After completing his graduate work, he started working on the design of RF and microwave circuits for wireless communication applications. Since 2007, he has been with the Faculty of Engineering, King Mongkut's Institute of Technology Ladkrabang, Ladkrabang District, Bangkok, Thailand. His current research interests include microwave circuits and devices and wireless communication systems.

Apisak Worapishet (M'00–SM'10) received the B.Eng. degree (with first-class honors) from King Mongkut's Institute of Technology Ladkrabang, Bangkok, Thailand, in 1990, the M.Eng.Sc. degree from the University of New South Wales, Australia, in 1995, and the Ph.D. degree from Imperial College, London, U.K., in 2000, all in electrical engineering.

Since 1990, he has been with Mahanakorn University of Technology, Bangkok, Thailand, where he currently serves as the Director of the Mahanakorn Microelectronics Research Center (MMRC) and an Associate Professor with the Telecommunication Department. His current research interest includes mixed-signal CMOS analog integrated circuits, wirelined and wireless RF CMOS circuits, microwave circuits, and reconfigurable communication systems.

Dr. Worapishet is a member of the Analogue Signal Processing Technical Committee (ASPTC) of the IEEE Circuits and Systems Society (CAS) and the Institute of Electrical, Information and Communication Engineers (IEICE).

Wanlop Surakampontorn (M'79–SM'04) was born in Bangkok, Thailand. He received the B.Eng. and M.Eng. degrees in electrical engineering from the King Mongkut's Institute of Technology Ladkrabang, Bangkok, Thailand, in 1976 and 1978, respectively, and the Ph.D. degree in electronics from the University of Kent at Canterbury, Kent, U.K., in 1983.

Since 1978, he has been a Member of the Department of Electronics, Faculty of Engineering, King Mongkut's Institute of Technology Ladkrabang, Bangkok, Thailand, where he is currently a Senior Professor of Electronic Engineering. His research interests are in the areas of analog and digital integrated circuit designs, real-time application of PC computers and microprocessors, digital signal processing, electronic instrumentation, and VLSI signal processing.

Dr. Surakampontorn is a member of the Institute of Electrical, Information and Communication Engineers (IEICE). He was the recipient of the Outstanding Scientist of Thailand Award in 1996 and The National Award for Distinguished Researcher, Thailand, in 1998.

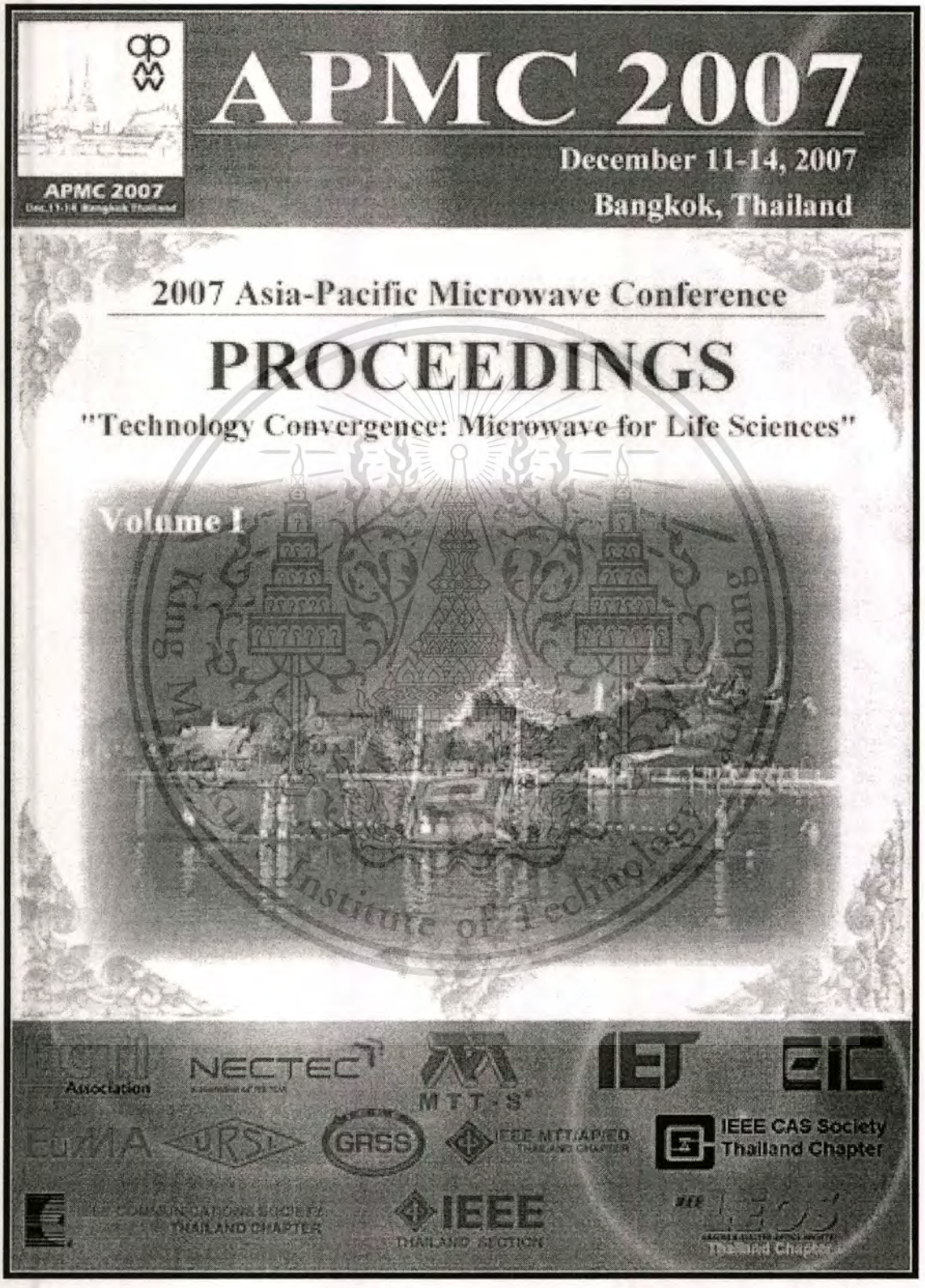

Session TH-A2-F HEMT Technology

173 76-GHz Planar Gunn VCO with Low Oscillation-FreFrequency Dright of MHz
Yoshimichi Fukasawa, Kilyoshi Kanwaguchi, Takashi Yoshida, Takahiro Sugiyama, And Atsushi Nakagawa
Gunn VCO, Temperature-competsatiob circuit; Oscillation-Freauency

174 A High Isolation 0.15 Um Depletion-Mode pHEMT SPDT Switch Using Field-Plate Technology
Chia-Shih Cheng, Shao-Wei Lin, Chien-Cheng Wei and Hsien-Chin Chiu, Rong-Jyi Yang
Field-Plate technology; High isolation; Millimeter-wave switch; pHEMT

175 Influence of Gate Head Dimensions on the Device performance of 0.12um PHEMT.
Hokyun Ahn,Jong-Won Lim, Hong-Gu Ji , Woo-Jin Chang, Jae-Kyoung Mun nad Haecheon Kim RF Circuit Group

176 High Performane inAs-Channel HEMT for Low Voltage Milimeter wave Applications
Heng-Tung Hsu, Senion Member, IEEE, Chia-Yuan Chang, Edward Yi Chang ,Senior Menber, IEEE, Chien-I Kuo, Yauyki Miyamoto

177 A Dual-Band Low Noise Amplifier in Enhancement-mode GaAs pHEMT Technology
Shih -ming-Wang, Cheng-chung Chen, and Li-Chun Yag
low noise amplifier, dual-band, Enhancement-mode Phemt

Session TH-A2-G Microwave Circuits

178 A V/UHF-Band 4-Way Power Divider
Yeo-Il Park, Jin-Hyun Ko, jae-Kwon Ha, Young-Joo Park, Dong-Chul Park
component; 4-Way Power Divider, V/UHF, Hight Power , Broadband Transmission-Line Transformer, Ferrite Toroid

179 A Wilkinson Power Divider with Different Power Rations at Different Frequencies
Sung-Hwan Ahn, Jae W.Lee Choon Sik Cho,Taek K.Lee
Wilkinson Power diider; Eve-old mode, unequal power divider; dual-band

180 Miniature Wilkinson Divider and Hybrid Coupler With Harmonic Suppression Using T-Shaped Transmission Line
K.Srisathit P.Jadpum , and W. Surakampontorn
T.shaped transmission line, quarter-wavelength transmission line, harmonic suppression, Wilkinson divider, Hybird coupler

181 Left-haveSmall Impedance Tansformers and Their Application ToArbitrary Phase Differentiated Lumped Blauns for Impedance Transforming
Hee-Ran Ahn and Bumman Kim

182 60GHz CMOS Current Reuse Cascade Amplifier
Chiaki Inui Chee Hong Lai, andMinoru Fujishima

Miniature Wilkinson Divider and Hybrid Coupler with Harmonic Suppression Using T-Shaped Transmission Line

K. Srisathit [1], P. Jadpum [2], and W. Surakampontorn [1]

[1] Faculty of Engineering and Research Center for Communications and Information Technology (ReCCIT), King Mongkut's Institute of Technology Ladkrabang (KMITL), Ladkrabang, Bangkok 10520, THAILAND.

[2] Microwave and Antenna Research Laboratory, Department of Telecommunication Engineering, Faculty of Engineering, Mahanakorn University of Technology, Bangkok 10530, THAILAND.

***Abstract*—This paper presents two microwave power splitters, utilizing equivalent T-shaped transmission line (TL) model. The advantages of the proposed over the conventional splitters are not only superior miniaturized size but also suppress harmonic response due to its' periodic structures. Both the proposed Wilkinson divider and Hybrid coupler based on the T-shaped TL are designed and fabricated on an FR-4 substrate at 1GHz and 2GHz, respectively. The measured results of the proposed structures are compared and show good agreement with the simulated results.**

***Index Terms*—T-shaped transmission line, quarter-wavelength transmission line, harmonic suppression, Wilkinson divider, Hybrid coupler**

I. Introduction

Nowadays, miniaturized and high-performance microwave circuits are in high demand for many wireless and microwave applications to bring down the system cost considerably [1]. Microwave devices based on planar microstrip structure have many advantages over the other transmission line (TL) structures because they not only can easily be designed to integrate with other planar circuits but also provide a low-cost mass product with high reliability [2].

For microwave power splitters in wireless communications, especially a Wilkinson divider or in-phase power divider [3] and Hybrid coupler or 90-Hybrid coupler [4] are used in the transmitter and receiver, which serve to combine or separate the signals. In a transmitter, there is not only need for a high power signal but also for transmitter noise rejection due to predominantly third-order distortion [5]. If these devices can suppress this intermodulation and miniaturized in size, the overall performance of the transmitting system will be improved.

With the large size of a Wilkinson divider and Hybrid coupler, in the conventional TL structure [3]-[4], previously, there has only been a need for size reduction [6]-[8]. For exam-ple, an equivalent TL section comprising a TL and shunt capacitances at either end [6], an artificial left-handed TL [7], and the lumped-elements [8] can replace the quarter-wave section in the microwave monolithic integrated circuits (MMICs) such as hybrid coupler [6], rat-race hybrid [6]-[7], and directional coupler [8].

This paper proposes the simultaneously third harmonic suppression and miniaturized size of both the Wilkinson divider and Hybrid coupler based on an equivalent T-shaped TL. Section II describes the design of an equivalent T-shaped for the conventional TL, resulting in the compact TL and the suppression of the unwanted harmonic frequency. To validate the performance, the proposed Wilkinson divider and Hybrid coupler are designed and realized at 1GHz and 2GHz, respectively. Both circuits can suppress the third harmonic frequency. The design results are presented in Section III. This is then followed by conclusion in Section IV.

II. T-Shaped Transmission Line Concepts

The conventional quarter-wavelength TL is shown in Fig. 1(a), where Z_A is the characteristic impedance and Θ_A is an electrical length of TL. Fig. 1(b) shows an equivalent T-shaped TL of conventional TL as shown in Fig. 1(a) [9]. The equivalent model is comprised of three section TLs. Two TLs —with the characteristic impedance, Z_{B1} and Z_{B2}, and the electrical length, Θ_{B1} and Θ_{B2}, —are connected in cascade. The other TL, an open-ended stub with characteristic impedance Z_C and electrical length Θ_C, is tied at the middle of the structure. It should be noted that this equivalence network is a symmetrical model.

In both the conventional TL and an equivalent T-shaped TL as shown in Fig. 1(a) and (b), respectively, for the sake of simplicity, we let $Z_{B1}=Z_{B2}=Z_B$ and $\Theta_{B1}=\Theta_{B2}=\Theta_B$. The equivalent T-shaped TL produces the upper attenuation frequency beyond the passband center frequency (f_0).

-4244-0749-4/07/$20.00 @2007 IEEE.

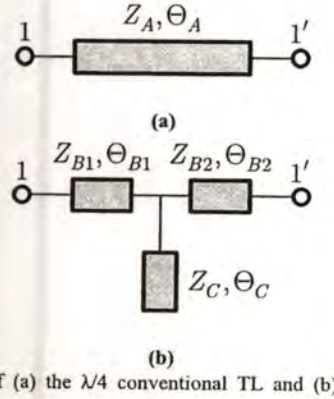

Fig. 1. Structure of (a) the λ/4 conventional TL and (b) an equivalent T-shaped TL.

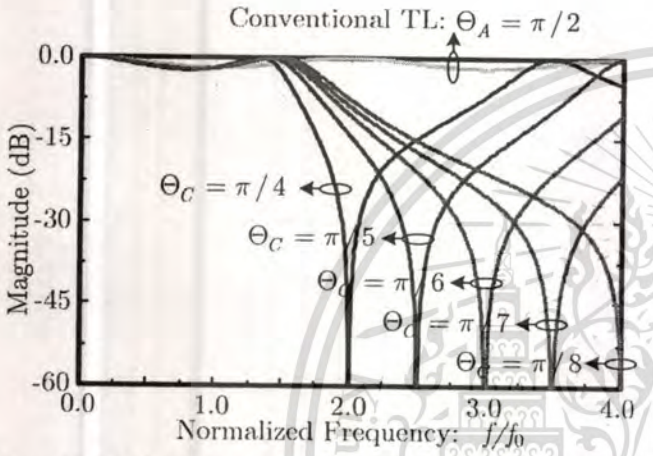

Fig. 2. Normalized arbitrary attenuation frequency with f_0 of the T-shaped TL compared with the conventional quarter-wavelength TL.

Therefore, we can express the relation of characteristic impedance Z_B and Z_C in term of Z_A as following [9]:-

$$\frac{Z_B}{Z_A} = \cot\Theta_B, \quad \text{and} \quad \frac{Z_C}{Z_A} = \frac{\cos^2\Theta_B \tan\Theta_C}{1-2\sin^2\Theta_B}, \tag{1}$$

and

$$\Theta_C = \left(\frac{\pi}{2}\right)\left(\frac{f_0}{f_i}\right). \tag{2}$$

where f_i is the frequency-suppressed location in which greater than f_0. For compact TL, the electrical length Θ_B must be less than $\pi/4$ at center frequency f_0, thus resulting in the miniaturized quarter-wavelength TL.

In order to achieve the transmission zero at frequency higher than center frequency, the electrical length of an open-ended stub (Θ_C) has been adjusted using eq. (2). Where Z_A=100Ω, an equivalent T-shaped TL can easily be calculated using eq. (1) and (2). Fig. 2 shows the simulated response of an equivalent T-shaped TL compared with the conventional quarter-wavelength TL using the calculated parameters shown in Table I. It is noted that the shorter the electrical length of the stub, the higher the attenuation frequency.

Table I Summary of the equivalent T-shaped TL parameters at differently attenuating frequency locations

Parameters		Attenuating frequency locations: Z_A=100Ω, Θ_A=π/2				
		$2.0f/f_0$	$2.5f/f_0$	$3.0f/f_0$	$3.5f/f_0$	$4.0f/f_0$
Z_B	(Ω)			173.2		
Θ_B	(rad)			π/6		
Z_C	(Ω)	150	108.98	86.60	72.23	62.13
Θ_C	(rad)	π/4	π/5	π/6	π/7	π/8

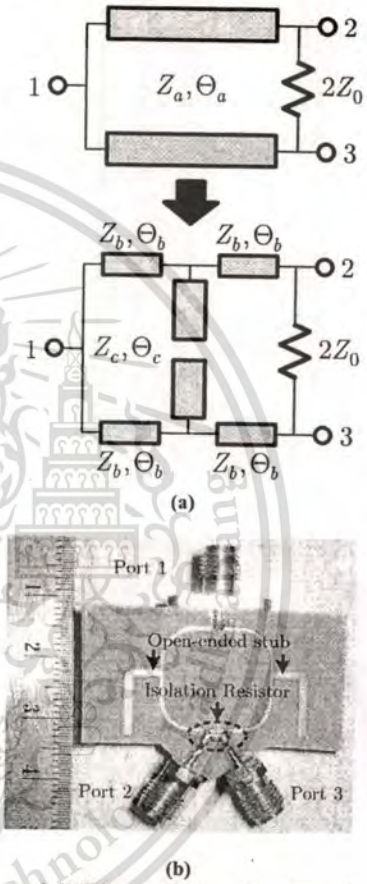

Fig. 3. The proposed Wilkinson divider with harmonic suppression (a) schematic and (b) the photograph of schematic.

III. Microwave Device Applications

As previously mentioned, two microwave circuits such as a Wilkinson divider and Hybrid coupler based on the microstrip transmission line structure are designed and fabricated for the system impedance Z_0=50Ω. Both circuits have their electrical parameters calculated, and are then synthesized and fabricated on a low-cost FR-4 board with a dielectric constant of 4.55 and thickness of 0.8mm. The designed structures are simulated using a full-wave field solver planar circuit, produced by *SONNET ™ Lite* [10]. The performance of the prototype circuits is also corroborated by the experiment results. The measurement was performed with an HP8510A vector network analyzer test system which utilized the SOLT calibration.

A. Wilkinson Divider

Fig. 3(a) shows the proposed -3dB Wilkinson divider based on an equivalent T-shaped TL, replacing the conventional quarter-wavelength TL in Fig. 1(a) with the T-shaped TL.

Typically, if all ports (Port1, Port2, and Port3) are matched with Z_0=50Ω, the characteristic impedance of TLs are Z_a=70.7Ω. Using the above equations, the initial electrical parameters based on an ideal TL are calculated. In this case, we choose $\Theta_b=\pi/6$ and $\Theta_c=\pi/6$ at f_0=1GHz for miniaturizing the Wilkinson divider and suppressing third harmonic (3GHz), respectively. Therefore, the characteristic impedance of Z_b is approximately 122.47Ω and Z_c is 61.24Ω. The 0403 SMT resistor is used as a 100Ω isolation resistor. Fig. 3(b) shows the fabricated Wilkinson divider. The circuit size is about 25×35mm.

The EM-simulated and measured results are shown in Fig. 4(a) and (b), respectively. Both the simulated and measured results are in perfect agreement. As shown in Fig. 4(a), the simulated operating frequency of the proposed Wilkinson divider is at 1.025GHz. The simulated insertion losses (s_{21} and s_{31}) are less than -3.25dB. An isolation between output ports 2 and port 3 (s_{23}) is greater than -35.83dB at center frequency and less than -10dB over 0.35 to 1.325GHz. The return loss at the input (Port1) is approximately -49.11dB, whereas both output return losses are about -35.96dB. Moreover, the amplitude imbalance and phase imbalance among the outputs are well balanced at less than 0.5dB and 1degree, respectively, over 0.1 to 4GHz. The third harmonic frequency is suppressed to below -43.7dB. In Fig. 4(b), the measured insertion losses are approximately -3.48dB at the operating frequency of 1.05GHz, owing to mainly the conductor and tangent loss. The isolation and return losses are better than -10dB at frequencies between 0.40 and 1.30GHz, and better than -27.5dB at operating frequency. Furthermore, the 3rd harmonic frequency is reduced to below -31.2dB. It can be clearly seen that the proposed structure is provided not only for a miniature Wilkinson divider but also for suppression of the third harmonic due to the periodic TL in the structure.

B. Hybrid Coupler

Here, a proposed prototype Hybrid coupler is designed and fabricated at center frequency of 2GHz with the third harmonic suppression at 6GHz using again T-shaped TL.

In the conventional Hybrid coupler as shown in Fig. 5(a) (on the top), two characteristic impedances ($Z_x=50/\sqrt{2}\Omega$ and Z_y=50Ω) with the same electrical length ($\Theta_x=\Theta_y=\pi/2$) are substituted as shown in Fig. 5(a) (on the bottom). If we let $\Theta_1=\Theta_3=\pi/6$, the over all electrical length of each T-shaped TL is about 33.3% more compact than the conventional quarter-wavelength TL. In addition, if we select $\Theta_2=\Theta_4=\pi/6$, the third harmonic suppression can also be obtained.

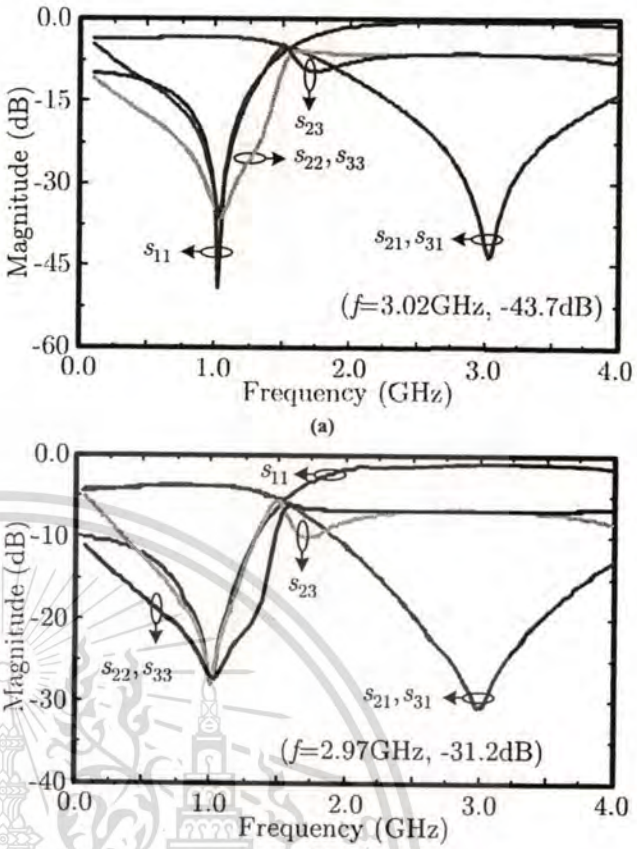

Fig. 4. Performances of the proposed microstrip Wilkinson divider (a) simulated results and (b) measured results.

Table II Calculated results for the proposed Hybrid coupler

$Z_x=50/\sqrt{2}\Omega$		$\Theta_x=\pi/2$rad		Z_y=50Ω		$\Theta_y=\pi/2$rad	
Z_1 Ω	Z_2 Ω	Θ_1 rad	Θ_2 rad	Z_3 Ω	Z_4 Ω	Θ_3 rad	Θ_4 rad
61.23	30.62	π/6	π/6	86.6	43.3	π/6	π/6

Table II shows the calculated results for the proposed Hybrid coupler in order to suppress the third harmonic frequency. Fig. 5(b) shows the fabricated Hybrid coupler, realized in the microstrip TL structure, which occupies 40×30mm of PCB area. Fig. 6(a) shows the EM-simulated results. The center operating frequency and the third harmonic frequency are inspected. It can be clearly observed that the prototype Hybrid coupler exhibits transmission notch of the incident wave along the equivalent T-shaped TL at 6GHz, thus introducing a total reflection at the input port. The center frequency is located at 2GHz with insertion losses (s_{21} and s_{31}) of -3.32dB. Inspecting at f_0, both input return loss at port 1 (s_{11}) and isolation loss between port 1 and port 4 (s_{14}) are attained below -40dB. Fig. 6(b) shows the measured results. The measured insertion losses (s_{21} and s_{31}) are about -3.6 and -3.8dB, respectively, whereas both input and isolation losses are kept below -28.5dB at center frequency of 2.025GHz.

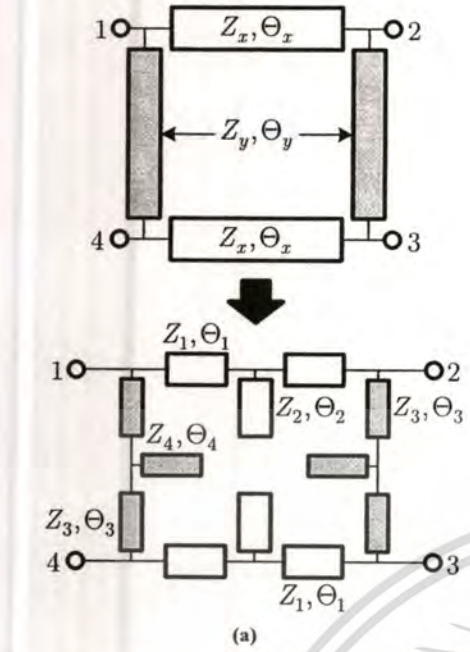

(a)

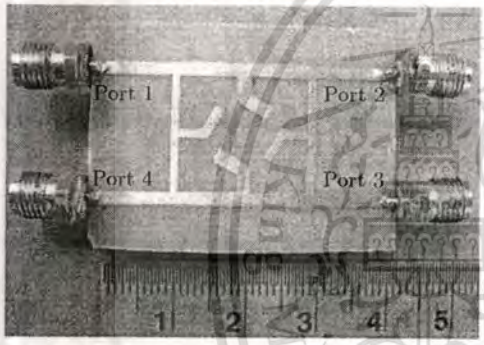

(b)

Fig. 5. The proposed Hybrid coupler with harmonic suppression (a) schematic and (b) the photograph of schematic.

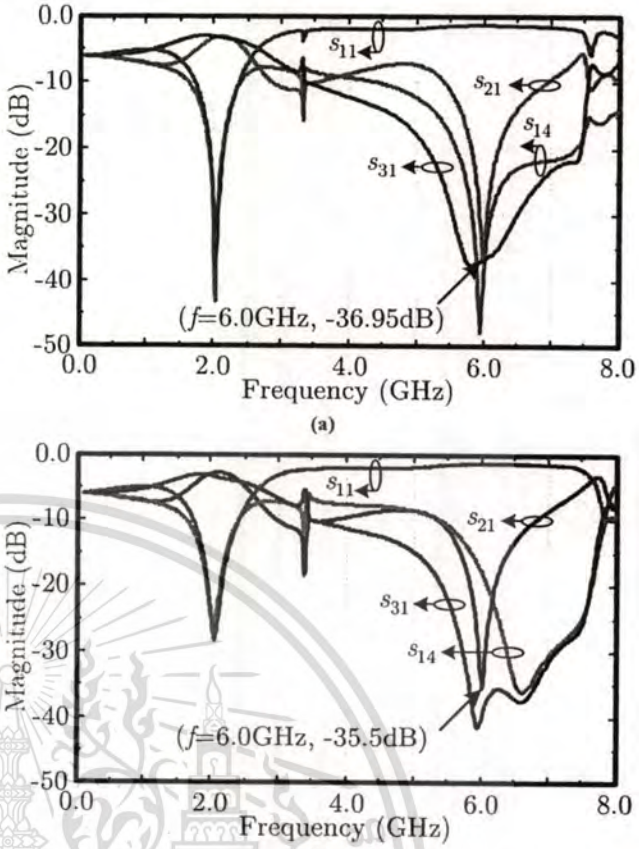

(a)

(b)

Fig. 6. Performances of the proposed microstrip Hybrid coupler (a) simulated results and (b) measured results.

IV. Conclusions

We have shown the miniaturized and third-harmonic suppression of both a Wilkinson divider and Hybrid coupler, utilizing the equivalent T-shaped transmission line. An open-ended stub acts as a series resonance at the unwanted harmonic frequency suppression. The proposed microwave circuits are very attractive to alleviate transmitter harmonic noises, occurring in the systems. The measured results prove the validity and suitability of the technique for wireless communication applications.

Acknowledgment

This work was funded by the Commission on Higher Education, Ministry of Education, Thailand, Research Group Program. The authors are grateful to Prof.Dr. Monai Krairiksh from King Mongkut's Institute of Technology Ladkrabang, Thailand, for allowing them to use the measurement systems.

References

[1] L. Besser and R. Gilmore, *Practical RF Circuit design for Modern Wireless systems: Volume I, Passive Circuits and Systems*. Boston, MA: Artech House, 2003.

[2] I. Bahl, *Lumped Elements for RF and Microwave Circuits*. Boston, MA: Artech House, 2003.

[3] E. J. Wilkinson, "An *N*-way hybrid power divider," *IRE Trans. Microw. Theory Tech.*, vol. MTT–8, pp. 116–118, Jan. 1960.

[4] J. Reed and G. J. Wheeler, "A method of analysis of symmetrical four-port networks," *IRE Trans. Microw. Theory Tech.*, vol. MTT–4, no. 4, pp. 246-252, Oct. 1956.

[5] N. Pothecary, *Feedforward Linear Power Amplifiers,* Norwood, MA: Artech House, 1999.

[6] T. Hirota, A. Minakawa, and M. Muraguchi, "Reduced-size branch-line and rat-race hybrids for uniplanar MMICs," *IEEE Trans. Microw. Theory Tech.*, vol. MTT-3851, no. 3, pp. 270-275, Mar. 1990.

[7] H. Okabe, C. Caloz, and T Itoh, "A compact enhanced-bandwidth hybrid ring using an artificial lumped-element left-handed transmission-line section," *IEEE Trans. Microw. Theory Tech.*, vol. 52, no. 3, pp. 798-804, Mar. 2004.

[8] R. W. Vogel, "Analysis and design of lumped- and lumped-distributed element directional couplers for MIC and MMIC applications," *IEEE Trans. Microw. Theory Tech.*, vol. 40, pp. 253–262, Feb. 1992.

[9] W. –H. Tu and K. Chang, "Compact second harmonic-suppressed bandstop and bandpass filters using open stubs," *IEEE Trans. Microw. Theory Tech.*, vol. 54, no. 6, pp. 2497-2502, Jun. 2006.

[10] http://www.sonnetusa.com

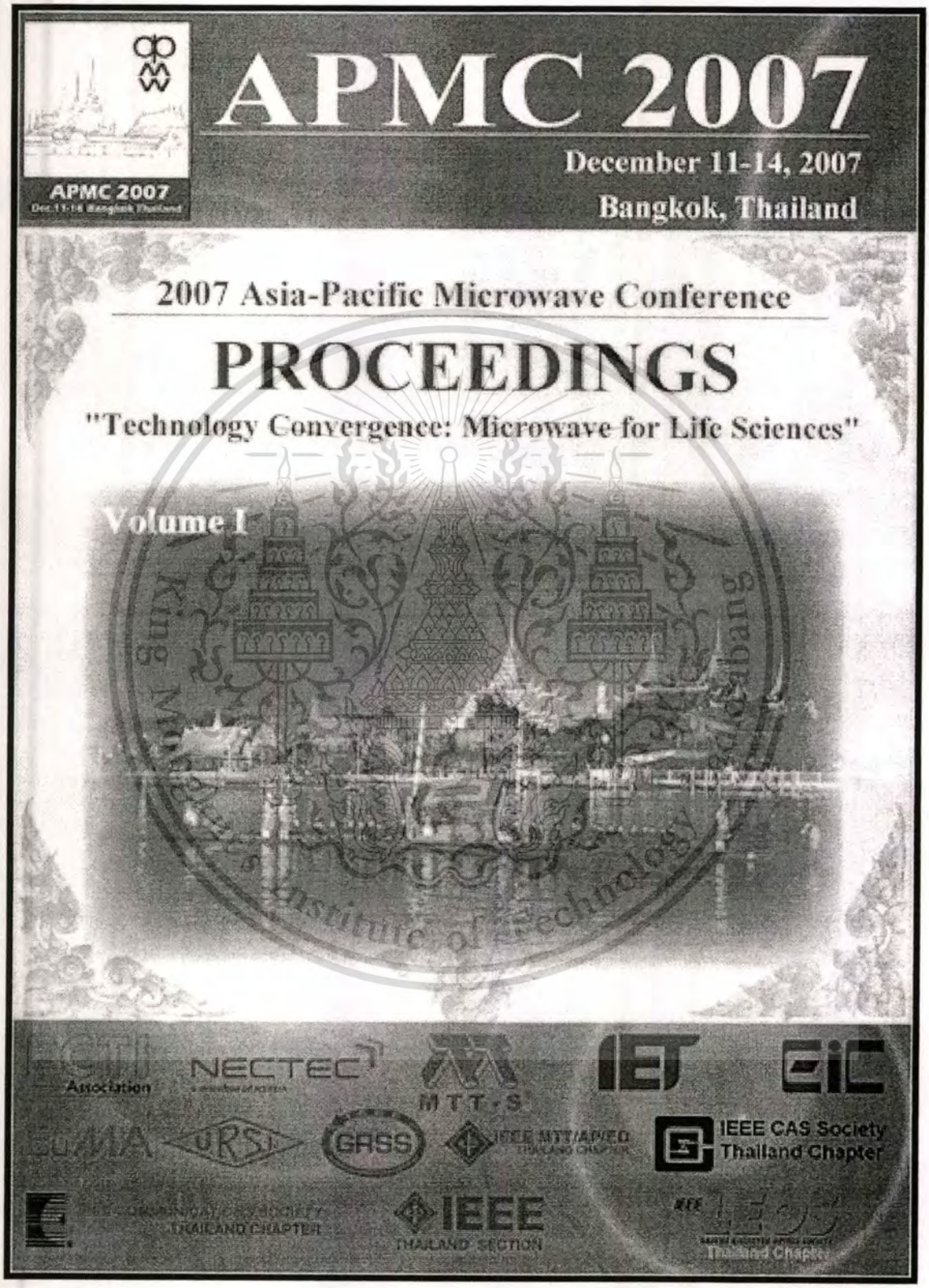

Session TH-P2-B Active Circuits I

227 A 1V Wide Tuning Range VCO for UHF DTV Tuner
Yueh-Hua Yu, Feng-Kuan Su, Yi-Jan Emery Chen and Deukhyoun Heo
VCO, CMOS, UHF, DTV Tuner, low power, low voltage

228 A Quadrature Voltage Controlled Oscillator with 9 Selective Bands for UWB Communication
Po-Yang Chang, Hui-I Wu, and Christina F. Jou
CMOS ,Quadrature voltage-controlled oscillator (QVCO), ultra-wideband (UWB)

229 Wide-Band CMOS Circuit Design Techniques for RF Amplifier and Ring VCO
Noboru Ishihara, Ryuichi Ujiie, Kenichi Shibata and Hisayasu Sato
wide-band, RF-CMOS, amplifier, ring VCO

230 94GHz Single-balanced Diode Mixer for FMCW Radar applications
Dong-Sik Ko, Mun-Kyo Lee, Dan An, Bok-Hyung Lee, Byeong-Ok Lim, Sang-Jin Lee, Sung-Woon Moon, Byoung-Chul Jun, Seok-Ho Bang, Jung-Dong Park, Wan-Joo Kim, Sam-Dong Kim and Jin-Koo Rhee

Session TH-P2-C Planar Filters IV

231 Asymmetric Dual-Mode Microstrip Filters with Adjustable Transmission Zero
Adnan Gorur, Ceyhun Karpuz, and Gokhan Murat Eryilmaz
Keywords-asymmetric frequency response; dual-mode filters; feed arrangement, positive and negative coupling coefficient

232 A New Technique to Double the Rejectband of a Low-pass Filter by Employing Coupled C-Open-Loop Resonators as Defected Ground Structure (DGS)
A. Boutejdar, A. Elsherbini, S. Amari, A. S. Omar
Micristrip LPF, DGS resonator, C-open-loop slot, cascaded DGSs, passband, bandstop

233 New Dual-Mode Ring Bandpass Filter Using Symmetrical Left-Handed Transmission Line
K. Srisathit, P. Jadpum, S. Bunniaweht, and W. Surakampontorn
Dual-mode, left-handed transmission line, ring resonator, degenerate modes

234 A Compact Low Pass Filter Design with Assigned Transmission Zeros
low-pass, C-section coupled line, transmission zero
Jan-Dong Tseng , Rong-Jie Ko

Session TH-P2-D RFID Techniques

235 Design of Pre-coding Technique for Optimal MIMO Transmission under Rician Fading Channel
P. Uthansakul and M. Uthansakul

236 An Experimental Study of Passive UHF RFID System with Longer Communication Range
Hisanori Matsumoto and Ken Takei

237 Design and Development of a Novel Paper-based Inkjet-Printed RFID-Enabled UHF (433.9 MHz) Sensor Node
Rushi Vyas, Amin Rida, Li Yang and Manos M. Tentzeris

New Dual-Mode Ring Bandpass Filter Using Symmetrical Left-Handed Transmission Line

K. Srisathit [1], P. Jadpum [2], S. Bunnjaweht [2], and W. Surakampontorn [1]

[1] Faculty of Engineering and Research Center for Communications and Information Technology (ReCCIT), King Mongkut's Institute of Technology Ladkrabang (KMITL), Ladkrabang, Bangkok 10520, THAILAND.

[2] Microwave and Antenna Research Laboratory, Department of Telecommunication Engineering, Faculty of Engineering, Mahanakorn University of Technology, Bangkok 10530, THAILAND.

***Abstract*—This paper presents a new dual-mode microstrip ring bandpass filter (BPF) based on the left-handed transmission line (LH-TL). To achieve dual-mode response, a high impedance LH-TL can easily be realized to perturb a pair of degenerate modes, which difficulty is realized in the conventional dual-mode ring filter. The proposed BPF is designed and fabricated on an FR-4 substrate to suit the 2.45GHz ISM band application with a fractional bandwidth of 16.2 percentages. Across the bandwidth, the measured insertion loss is less than 1.5dB, whereas the input and output return losses are better than 20dB from 2.37 to 2.59GHz. The measured results are in good agreement with the simulated results.**

***Index Terms*—Dual-mode, left-handed transmission line, ring resonator, degenerate modes**

I. Introduction

Microstip ring resonators are widely used applications in communication circuits such as in mixer [1], antenna [2], oscillator [3], and bandpass filter (BPF) [4]-[9]. Especially in ring BPFs, most of the designed BPFs have been realized with dual-mode response [4]-[9] due to its simple design, compact size, and narrow bandpass response, which is used to pass the wanted signal and reject the unwanted signal in the communication systems. These BPFs have been studied extensively based on microstrip TL because of its low-cost materials and easy integration with other microwave circuits.

To enhance the performances and achieve dual-mode response, various techniques are proposed. For example, a tightly coupling geometry with joint field [4] has been published to extract the model for resonator and filter design. Although, this technique can provide a new design approach for characterizing and optimizing electrical performance of line to-ring three-port coupling scheme, it has an extremely small bandwidth of BPF. The dual-mode BPF using the properties of microstrip open-loop resonator [5] and capacitively loaded open-loop arm [6] based on a modified square ring were proposed to obtain wide stopband and narrow bandwidth but they exhibit high insertion loss. Using an attachment of small triangle patch [7] at the inner-corner of the loop or the stepped-width in the coupling gap and in the ring [8] for exciting and coupling a pair of degenerate modes, a dual-mode resonator can be obtained. However, these structures are complicated and required computer iteration to carry out the desired performances [5]-[8]. In addition, the series stub perturbation has been successfully designed and realized in the microstrip TL but high technology for fabricating very high/low impedance of the stub is needed [9].

Recently, the TL approaches of left-handed (LH) structures with corresponding characteristic impedance of TL have been presented [10]-[14]. Since then, many researchers have been described and concerned with dual-frequencies [11]-[12], broad bandwidth [13], and miniaturized the circuit size [14] for modern wireless applications. As far as we know, there has not been reported the designing of a ring BPF, using the LH-TL perturbation application into the ring.

Therefore, this paper proposes the new dual-mode microstrip ring resonator utilizing artificial LH-TL. This technique is suited for realizing the high impedance stub perturbation, thus providing narrow bandpass response. In Section II, the description of an artificial LH-TL is explained in detail. After that, the principle of a dual-mode ring resonator is also described. To validate the performance, the proposed scheme is designed for the dual-mode BPF at the center frequency of 2.45GHz with a fractional bandwidth of 16.2%. The design results are presented in Section III and conclusion is given in Section IV.

II. Artificial Left-Handed Transmission Line and Dual-Mode Microstrip Ring Resonator

A. Artificial Left-Handed Transmission line

As seen in Fig. 1, the conventional TL with characteristic impedance of Z_0 and electrical length of Θ is shown in Fig. 1(a) at center frequency (f_0). Fig. 1(b) shows the unit-cell of an equivalent TL model [13] called the LH-TL as an asymmetrical network, whereas Fig. 1(c) is a proposed symmetrical network of Fig. 1(b). Moreover, the highpass characteristic can also be obtained.

-4244-0749-4/07/$20.00 @2007 IEEE.

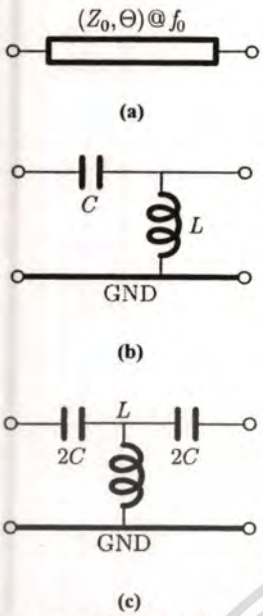

Fig. 1. Structure of (a) conventional transmission line (b) asymmetrical left-handed transmission line, and (c) symmetrical left-handed transmission line.

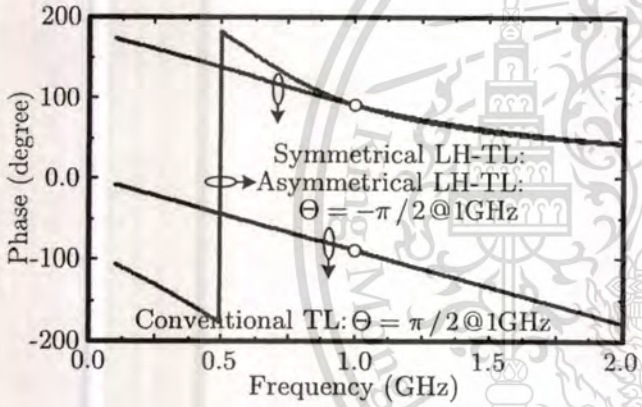

Fig. 2. Phase response of the conventional TL, asymmetrical LH-TL, and symmetrical LH-TL.

Fig. 1(b) consists of a lumped-inductor (L) and a lumped-capacitor (C). The values of both elements were calculated to introduce phase advance compared with phase response of Fig. 1(a). For lossless TL, the characteristic impedance of LH-TL at f_0 can be evaluated as following:-

$$Z_0 = \sqrt{\frac{L}{C}}, \tag{1}$$

where the insertion phase of LH-TL in Fig. 1(b) and (c) can be calculated as following [13]:-

$$\angle s_{21} = -\arctan\left(\frac{2\omega\sqrt{LC}}{1-2\omega^2 CL}\right). \tag{2}$$

The simulated phase response results of the following $\pi/2$ conventional TL, $-\pi/2$ asymmetrical LH-TL, and $-\pi/2$ symmet

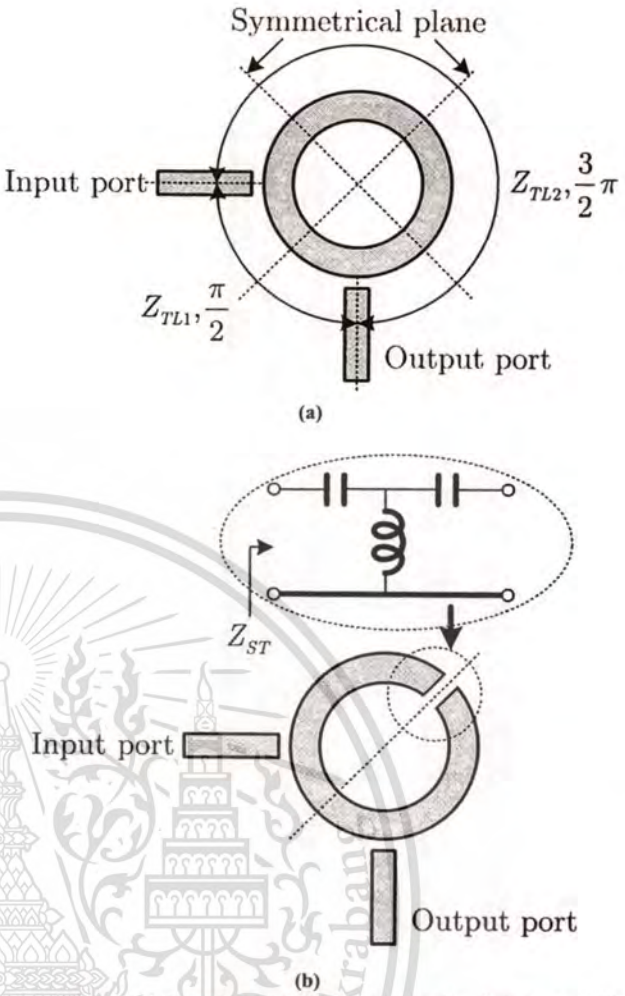

Fig. 3. Dual-mode ring resonator using (a) the conventional structure and (b) the symmetrical LH-TL perturbation.

-rical LH-TL are superimposed in Fig. 2, corresponding to the characteristic impedance of 50Ω at 1GHz. Although, both asymmetrical and symmetrical LH-TL structures can exhibit positive phase response (phase advance), the phase response of the proposed symmetry LH-TL is more linear than that of an asymmetry LH-TL around 1GHz.

B. Dual-Mode Microstrip Ring Resonator

Fig. 3(a) shows the conventional configuration of dual-mode ring resonator. This configuration consists of two conventional TLs with different electrical lengths connected in parallel. At center passband frequency, the first TL has an electrical length of $\pi/2$ and characteristic impedance of Z_{TL1}, whereas the second TL has an electrical length of $3\pi/2$ and characteristic impedance of Z_{TL2}. As a result, the total circumference should be equal to 2π at f_0. In order to achieve dual-mode response, in this paper, the symmetrical LH-TL with the characteristic impedance (Z_{ST}) and electrical length (Θ_{ST}) is inserted at the symmetrical portion as shown in Fig. 3(b). The degree of coupling modes depends on the characteristic impedance and electrical length of this LH-TL,

which in return controls the mode splitting. It is noted that the second TL's electrical length should be changed to preserve the overall electrical length of new ring resonator.

For very high or low impedance stub perturbation, it is difficult to implement the circuit due to the very small or large width in microstrip structure. In addition, the change of width in the step impedance becomes significant and the effects of the parasitic capacitance at the step can no longer be neglected [9]. In case of narrow bandwidth response, the stub's perturbation needs high characteristic impedance TL.

III. Dual-Mode Bandpass Filter Design

Here, the proposed dual-mode bandpass filter is designed at 2.45GHz with fractional bandwidth of 15% and fabricated on a low-cost FR-4 substrate with a dielectric constant of 4.55 and thickness of 0.8mm. The conductor of the PCB is copper. The designed structures have been simulated using a full-wave field solver for planar circuit, produced by *SONNET™ Lite* [15]. The prototype BPF was also corroborated by the experiment data. The measurement was performed with an HP8510A vector network analyzer test system which utilized the SOLT calibration from 0.1 to 5GHz.

First of all, the dual-mode BPF has been selected with characteristic impedances of Z_{TL1}=45Ω and Z_{TL2}=30Ω. In addition, the proposed symmetrical LH-TL parameters are calculated for the 220Ω series stub with electrical length of 15 degree by using (1) and (2), thus resulting in the capacitance (C) of 3.5pF and an inductance (L) of 17.15nH. Fig. 4 shows a photograph of the fabricated dual-mode microstrip ring BPF. The symmetrical LH-TL was realized in chip components ($2C$≈6.8pF of 0403 SMT capacitor from AVX corporation and L=17.15nH of 0603 SMT inductor from Coilcraft company). Consequently, the dual-mode ring resonator can be obtained. This structure utilizes the simple capacitive coupling using two 0403 SMT lumped-capacitors of 0.1pF. Both capacitors are placed in between the input and output feed lines to the ring resonator. The prototype size is about 4×3cm, including the SMA connectors. The simulated performances of the proposed BPF are shown in Fig. 5. As a result, the simulated insertion loss is less than 1.1dB at a center frequency of 2.43GHz, while both input and output return losses are kept below 20dB. Moreover, the prototype BPF enables two transmission zeros at 1.98GHz and 2.82GHz on either side of the center frequency.

Fig. 6 shows the measured results. The center frequency of the filter is approximately 2.48GHz with the 3-dB fractional bandwidth of 16.2%. The filter has an insertion loss better than 1.5 dB at center frequency, which is mainly due to the conductor loss of copper. In addition, the input/output return losses are greater than 20dB in the passband from 2.37 to 2.59 GHz. The transmission zeros are at the 1.97 and 2.91GHz. Furthermore, the insertion loss from 0.1GHz to the left transmission zero is attained below 16.2dB. Both simulated and measured results are in good agreement.

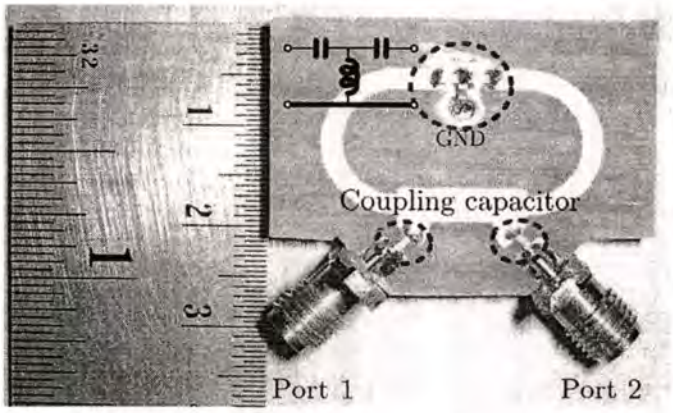

Fig. 4. The photograph of the proposed dual-mode microstrip ring BPF.

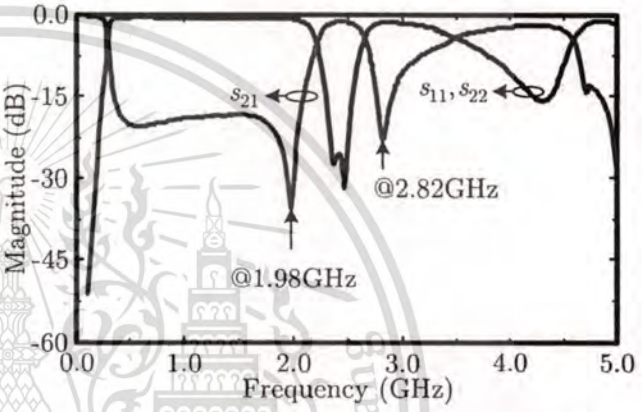

Fig. 5. Simulated performances of the proposed microstrip ring BPF.

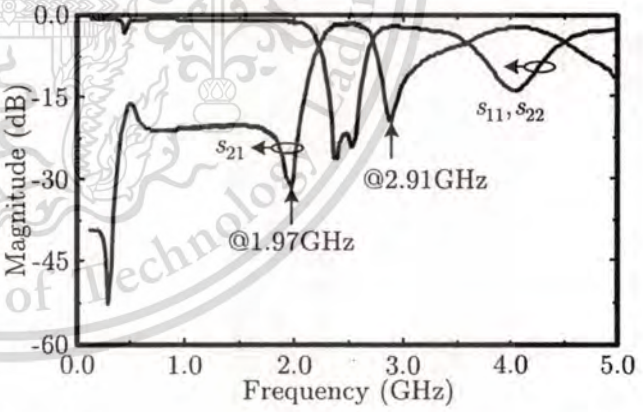

Fig. 6. Measured performances of the proposed microstrip ring BPF.

IV. Conclusions

We have shown the dual-mode microstrip ring bandpass filter employing artificial left-handed transmission line perturbation in this paper. A high impedance series stub perturbation is simply achieved by selecting the impedance and insertion phase of artificial LH-TL, preserving circumference approximately one wavelength transmission line at the center passband frequency. The proposed technique is very easy and attractive in a dual-mode microstrip bandpass

filter design. The measured results prove the technique validity and suitability for communication applications.

ACKNOWLEDGMENT

This work was funded by the Commission on Higher Education, Ministry of Education, Thailand, Research Group Program. The authors are grateful to Prof.Dr. Monai Krairiksh from King Mongkut's Institute of Technology Ladkrabang, Thailand, for allowing them to use the measurement systems.

REFERENCES

[1] K. Chang, *Microwave ring circuits and antennas*, New York: John Wiley & Sonc, Inc, 1996.

[2] R. E. Miller, and K. Chang, "Integrated active antenna using annular ring microstrip antenna and *Gunn diode," Microwave Opt. Technol. Lett.*, Vol. 4, No. 2, pp. 72-75, Jan. 1991.

[3] Y. -T. Lee, J. Lee, and S. Nam, "New planar high Q active resonator and its application to low phase noise oscillator," in *IEEE MTT-S Int. Microwave Symp. Dig.*, Texas, Jun. 2004, pp. 2007–2010.

[4] L. Zhu and K. Wu, "A joint field/circuit model of line-to-ring coupling structures and its application to the design of microstrip dual-mode filters and ring resonator circuits, " *IEEE Trans. Microw. Theory Tech.*, vol. 47, no. 10, pp. 1938-1948, Oct. 1999.

[5] A. Görür, "A novel dual-mode bandpass filter with wide stopband using the properties of microstrip open-loop resonator," *IEEE Microwave and Wireless Lett.*, vol. 12, no. 10, pp. 386-388, Oct. 2002.

[6] A. Görür, C. Karpuz, and M. Akpinar, "A reduced-size dual-mode bandpass filter with capacitively loaded open-loop arms," *IEEE Microwave and Wireless Lett.*, vol. 13, no. 9, pp. 385-387, Sep. 2003.

[7] J. S. Hong and M. J. Lancaster, "Bandpass characteristics of new dual-mode microstrip square loop resonators, " *Electron. Lett.*, vol. 31, no. 11, pp. 891-892, May 1995.

[8] S. Srisathit, S. Patisang, and M. Chongcheawchamnan, "A microstrip stepped-width coupling gap and stepped-width ring resonator bandpass filter," in *the 2nd ECTI International Conference (ECTI-CON2005)*, May 2005, vol. 2, pp. 726-729.

[9] M. Matsuo, H. Yabuki, and M. Makimoto, "Dual-mode stepped-impedance ring resonator for bandpass filter applications," *IEEE Trans. Microw. Theory Tech.*, vol. 49, no. 7, pp. 1235-1240, Jul. 2001.

[10] C. Caloz and T. Itoh, "Novel microwave devices and structures based on the transmission line approach of meta-materials," in *IEEE MTT-S Int. Microwave Symp. Dig.*, Philadelphia, PA, Jun. 2003, pp. 195–198.

[11] l. Lin, C. Caloz, and T. Itoh, "A branch-line coupler with two arbitrary operating frequencies using left-handed transmission lines," in *IEEE MTT-S Int. Microwave Symp. Dig.*, Philadelphia, PA, Jun. 2003, pp. 325–328.

[12] X. Q. Lin, R. P. Liu, X. M. Yang, J. X. Chen, X. X. Yin, Q. Cheng, and T. J. Cui, "Arbitrarily dual-band components using simplified structures of conventional CRLH TLs," *IEEE Trans. Microw. Theory Tech.*, vol. 54, no. 7, pp. 2902-2909, Jul. 2006.

[13] C. Caloz and T. Itoh, "Transmission line approach of left-handed (LH) materials and microstrip implementation of an artificial LH transmission line," *IEEE Trans. Microw. Theory Tech.*, vol. 52, no. 5, pp. 1159-1166, May 2004.

[14] H. Okabe, C. Caloz, and T Itoh, "A compact enhanced-bandwidth hybrid ring using an artificial lumped-element left-handed transmission-line section," *IEEE Trans. Microw. Theory Tech.*, vol. 52, no. 3, pp. 798-804, Mar. 2004.

[15] http://www.sonnetusa.com

LIST OF CITATIONS

[1] Shamaileh K., Qaroot A., and Dib N. "Non-Uniform Transmission Line Transformers and Their Application in The Design of Compact Multi-Band Bagley Power Dividers with Harmonics Suppression." **Prog. In Electromag Research,** vol. 113, 2011. pp. 269-284.

[2] Cheng K.-K. M. and Wei-Chi I. "A Novel Power Divider Design with Enhanced Spurious Suppression and Simple Structure." **IEEE Trans. Microw. Theory Tech.,** vol. 58, no. 12, Dec. 2010. pp. 3903-3908.

[3] Hazeri A. R. and Faraji T. "Miniaturisation and Harmonic Suppression of The Branch-Line Hybrid Coupler." **Int. Journal of Electronics,** vol. 98, no. 12, Dec. 2011. pp. 1699-1710.

[4] Hazeri A. R., Kashaninia A., Faraji T., and Arani M. F. "Miniaturization and Harmonic Suppression of The Branch-Line Coupler Based on Radial Stubs." **IEICE Electron. Exp.,** vol. 8, no. 10, Oct. 2011. pp. 736-741.

[5] Wu Y., Liu Y., Li S., and Yu C. "A Simple Microstrip Bandpass Filter with Analytical Design Theory and Sharp Skirt Selectivity." **J. Electromag. Waves App.,** vol. 25, no. 8-9, 2011. pp. 1253-1263.

[6] El-Gibari M., Averty D., Lupi C., Li H., and Toutain S. "Ultra-Wideband GCPW-MS Transitions for Characterising Microwave and Photonic Components Based on Thin Polymer." **Electron. Lett.,** vol. 47, no. 9, Apr. 2011. pp. 553-555.

[7] Wei C.-L., Jia B.-F., and Zhu Z.-J. "Design of Triple-Mode Microstrip Filter with Source-Load Coupling." **Microw. Optical Technology Lett.,** vol. 53, no. 10, Oct. 2011. pp. 2403-2406.

http://scholar.google.co.th/scholar?q=srisathit&hl=en&as_sdt=1%2C5&as_sdtp=on

AUTHOR BIOGRAPHY

Kunnthphong Srisathit was born in Khonkaen, Thailand, on July 6, 1973. He received the B.Eng. degree (with honors) in Electronic Engineering from the Mahanakorn University of Technology, Nongchok District, Bangkok, Thailand, in 1996 and the M.Eng. degree in Telecommunication Engineering at the same university in the area of broadband amplification technique and its application in CMOS technology for high-gain performance, in 2002. He is currently working toward the D.Eng. degree in Electrical Engineering in the area of novel architectures for high performance planar microwave devices and filters at the King Mongkut's Institute of Technology Ladkrabang, Ladkrabang District, Bangkok, Thailand.

After completing his graduate work, he started working on the design of Doherty Power Amplifier in CMOS technology (under Mr. Chaiwat TongChoi, Assoc. Prof. Dr. Mitchai Chongcheawchamnan, and Prof. Apisak Worapishet) and also received the honorable mention for the best performance in the 3rd National IC Design Contest (NIC2003). Hereafter, he had intensively studied on the design and analysis of RF and microwave circuits and their applications. During 2005 to 2006 he was received the grant from the CAT TELECOM-Company to design cavity duplexer for the WCDMA2000-1x (under technical supported by Assoc. Dr. Prof. Mitchai Chongcheawchamnan). In 2007, he has co-funded by Thailand Research Fund (TRF) and the Military committee to research the transceiver for Wireless Surveillances. He has worked as a research assistant in the Mixed Signal Laboratory, Faculty of Engineering, King Mongkut's Institute of Technology Ladkrabang, which was supported by the TRF through the Senior Research Scholar Program under Grant RTA4680003 during 2006 to 2007 (under managing by Prof. Wanlop Surakampontorn). During 2007 to 2008, he was a researcher in the project Microelectronic for communication which granted by CHE-RG (also under managing by Prof. Wanlop Surakampontorn). Since 2008, he has grant from the Thailand Research Fund through the Royal Golden Jubilee Ph.D. Program under Grant PHD/0010/2550.

He is a member of the IEEE Microwave Theory and Techniques society (IEEE MTT-S) and the Electrical Engineering/Electronics, Computer,

Telecommunications, and Information Technology Association (ECTI-Association). He has also a senior member of an advisory committee with the Faculty of Engineering at the Rajamangala University of Technology Rattanakosin (RMUTR), Salaya District, Nakorn Prathom, Thailand. His current research interests include microwave circuits and devices and wireless communication systems.